Charles University

Faculty of Mathematics and Physics

HABILITATION THESIS

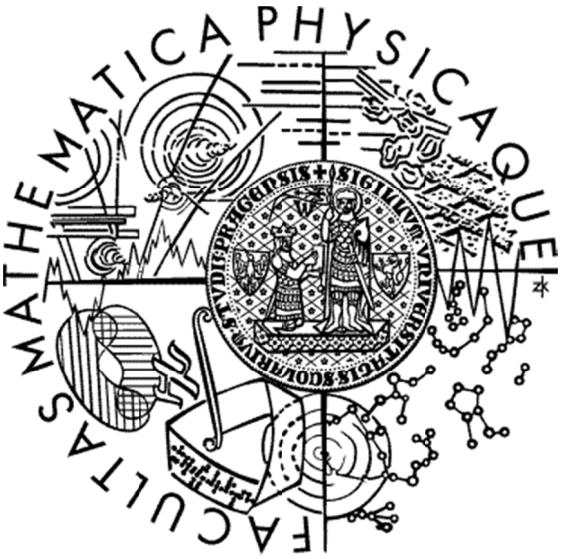

Viktor Johánek

Reactions at surfaces: from macroscopic to molecular level

Department of Surface and Plasma Science

Prague, 2018

Submitted in the field of *Physics – Physics of Surfaces and Interfaces*

Acknowledgements

Despite the commonly shared "myth of the lone scientist" (and, to be more accurate, a „mad scientist" as perceived by many outside the field) the truly innovative and efficient research requires a teamwork of, ideally, intellectually diverse groups of scientists with different backgrounds and individual skills. I had the great opportunity to be a part of several such teams during my appointments at CERN, Fritz-Haber Institute of Max-Planck Society in Berlin, University of California Irvine, University of Virginia, and Charles University in Prague. I'm indebted to all the people who inspired, motivated, educated, and supported me on my way through the world of science. The results presented in this thesis could not be accomplished without the valuable contributions of many colleagues with whom I have worked, cooperated, or discussed during the past two decades.

Financial support of the research presented in this thesis was provided by several institutions and organizations, namely by the European Union within its 7th Framework programme, COST European framework, Ministry of Education of the Czech Republic, Czech Science Foundation, National Science Foundation, U.S. Department of Energy, Deutsche Forschungsgemeinschaft, ERIC-CERIC distributed research infrastructure, Charles University, and the Czech Academy of Sciences.

Last but not least, my greatest appreciation belongs to my family for the everlasting support of their, so to speak, very own mad scientist.

"I can hardly doubt that when we have some control of the arrangement of things on a molecular scale, we will get an enormously greater range of possible properties that substances can have, and of different things that we can do."

– Richard P. Feynman, 1959

Contents

1 Introduction

Most global challenges of the current world related to science and technology are closely related to the key issues of energy, health, environment, and natural resources. Whether it is the search for clean and renewable energy sources, strategies for energy conversion and storage, efficient drug delivery, biocompatible materials, reduction of pollution, purification, water treatment, replacement of precious elements with new advanced materials, or food processing, a common denominator can be found here: **catalysis**. It is a pivotal term in chemistry and chemical physics. Moreover, because it is involved in so many things that affect all of us, it actually holds some interest for everyone (not just for chemists and other scientists), especially because the above mentioned challenges are interdependent, i.e., an improvement in one makes it easier to address others.

Indeed, the phenomenon of catalysis has enormous practical consequences in our daily lives. The contribution of catalysis to manufacturing is almost 40% of global GDP. More than 85% of the industrial chemical processes in use throughout the world utilize catalysts in some form (see Figure 1a). They play a decisive role in the production of plastics, synthetic fabrics, medicines, fuels, and many other valuable chemicals. They are also widely applied in the processing of foods or in numerous biological processes (with enzymes serving as the catalysts) – in fact, the very first use of catalysts, albeit somewhat unconscious, is dated back to 4-10 thousands years BC when natural enzymes were used in the production of fermented beer, wine, and bread. Last but not least, the utilization of renewable energy sources and purification of exhaust gases are only two of the many essential contributions of catalysis to the quality of our environment.

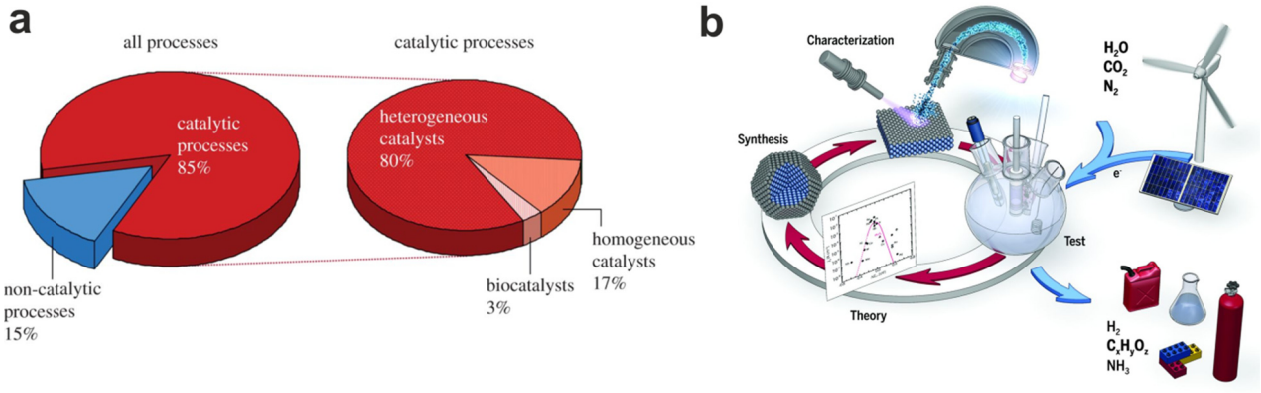

Figure 1: a) Pie charts showing the percentages of all industrial processes that entail the use of heterogeneous, homogeneous, and biocatalysis. Adapted from [1]. b) Schematic showing the combination of theoretical and experimental studies working in concert to provide us with insight into catalyzed processes (here, e.g., electrochemical conversion of water, carbon dioxide, and nitrogen into value-added products) and guides the development of the high-performance (electro)catalysts needed to enable these technologies. Adapted from [2].

Although effectively macroscopic, the origins of reactivity are of a microscopic nature. Molecular (or atomic) level of understanding of chemistry at surfaces and interfaces can be provided through a combination of insights into their structural properties and their interplay with elementary physico-chemical processes. Since the necessary technologies (regarding vacuum, electronics, materials, and others) have reached a sufficient level of maturity about 4-5 decades ago, the field of surface science has developed and expanded tremendously and became a true atomic-scale and molecular-level science. It has built a bridge between chemistry and physics by offering precise analytical tools as

well as an unprecedented control over building or modifying small structures with intricate properties.

This thesis comprises a commented collection of works aimed at exploring structure–reactivity relationships of well-defined catalysts from the surface physics perspective. It deals with metal single-crystals, thin oxide films grown on metal supports, metallic nanoparticles supported on ordered or nanostructured oxides, bimetallic compounds, and other structures used as laboratory playgrounds for various chemical processes. The central motivation behind all these studies has been the explanation and, wherever possible, optimization of the properties of the investigated catalytic systems via detailed comprehension of elementary processes taking part at their surfaces.

As will be shown in the following text, good understanding of molecular origins of reactivity on solid surfaces is crucial for rational design and tuning of catalyst composition and structure, as well as for finding optimal reaction conditions. In my contributions to this quest I have employed several advanced surface characterization techniques combined with analysis of reactants and reaction products, including various spectroscopic (XPS/SRPES/RPES, RAIRS, LEIS, TDS/TPR, AR-QMS, SIMS) [3-18] and microscopic (STM, LEEM, AFM) [10, 19-21] methods, in most cases *in-situ* ultra-high vacuum (UHV) compatible ones [22-24]. Since the prerequisite for unraveling mechanisms of catalyzed reactions is the characterization of all the relevant elementary processes, the projects I participated in were devoted to adsorption [7, 9, 10, 16, 25-33], dissociation or decomposition [4-6, 13, 19, 20, 29, 31, 33-40], co-adsorption [6, 14, 29], recombination, surface diffusion (including spillover, reverse spillover, and local fluctuation phenomena) [3, 11, 41-43], interactions between individual components of a catalyst [8, 11, 16, 17, 44-46] and other aspects of surface science and chemical physics. When classified by the type of surface, these works deal with single crystals [10, 14, 18-21, 28, 36], alloys [7-9, 16, 27, 44, 47], ordered oxides [5, 12, 32, 33, 40], nanostructured and non-continuous oxides [46, 48-52], supported nanoparticles [3, 4, 6, 9, 11-13, 15, 25-31, 33-35, 38, 39, 41-45, 53-56], and inverse catalysts [17, 51]. Several experimental works were also complemented with theoretical calculations or simulations [3, 30, 36, 40, 43, 45, 46, 53, 54, 57].

The presented research was conducted at several institutions and research infrastructures, namely Department of Chemical Physics at Fritz-Haber Institute of Max-Planck Society in Berlin, Department of Chemistry at University of California Irvine, Department of Chemistry at University of Virginia, Department of Surface and Plasma Physics at Faculty of Mathematics and Physics of Charles University, and Elettra Synchrotrone Trieste, together with other collaborating parties involved, as indicated in the respective published articles.

The following chapters and the corresponding appendices are classified topically based on the type of chemistry, rather than chronologically, by the type of catalyst used, or by the method(s) applied. It covers selected aspects of three significant areas of current heterogeneous catalysis – interaction of solid surfaces with CO_x/NO_x, with water, and with hydrocarbons.

2 Heterogeneous catalysis

A catalyst which is in a different phase than the reactants is called a **heterogeneous catalyst** [22, 58-60]. The great majority of practical applications involve solids catalysts and reactants in gas or liquid phase. From the composition and structure point of view, heterogeneous catalysts represent, in vast majority of instances, what we nowadays call **nanomaterials**. In fact, catalysis has been a nanotechnology long before this term was introduced, since efficient catalysts rely on materials with high specific areas, very complicated structures, and containing multiple finely dispersed compounds [61-64]. Materials based on oxide-supported nanometer-sized clusters find their use also beyond catalysis – for example in electronics, magnetism, biointerfaces, or energy conversion applications [65, 66].

The development of new catalytic materials relies on two main strategies which are usually combined in order to achieve desired properties – 1) increasing the active surface area (via structure of the active component and/or the support material) and 2) increasing intrinsic catalytic activity (via, e.g., a proper mixture of elements, activation of reactive sites by dopants or promotors, structural confinement etc.), as can be seen in Figure 2.

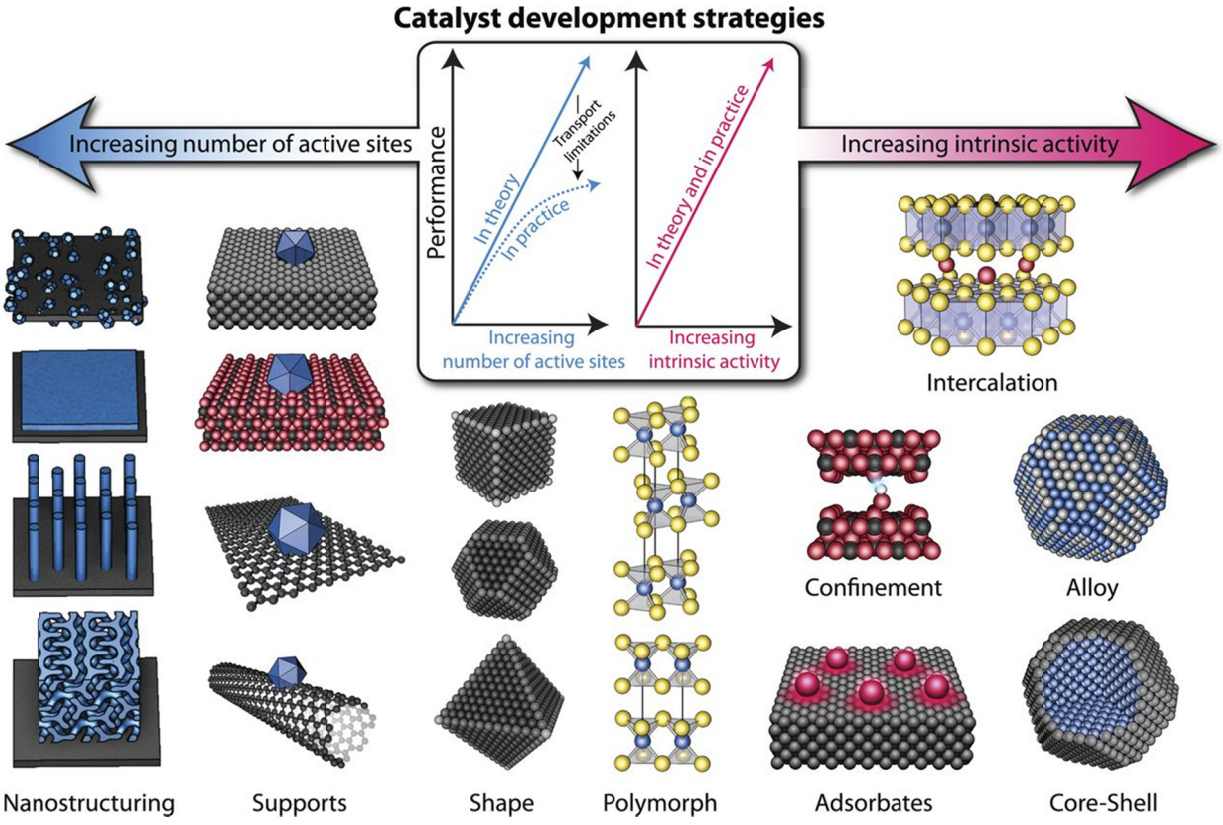

Figure 2: Schematic overview of various strategies applied in the development of new materials for heterogeneous catalysis, aimed to increase the number of active sites and/or increase the intrinsic activity of each active site. The former strategy is, however, efficient only up to a certain level of nanostructuring and catalyst loading, above which mass or charge transport limitations can hinder the reactivity. Adapted from [2].

Catalysis by metal nanoparticles perceived in more general sense (i.e., not necessarily supported on solids or purely anorganic) is also referred to as "semi-heterogeneous catalysis" [61, 67], positioned at the frontier between homogeneous and heterogeneous catalysis. In this thesis, however, we will remain in the domain of the standard heterogeneous catalysis.

Although the complexity of surfaces employed in experimental and theoretical works has increased dramatically over the last few decades and understanding basic principles of heterogeneous catalysis has been one of the main driving forces for the development of modern surface science [68], this field still remains far from becoming routine.

2.1 Common motivation and challenges

As has already been indicated in the previous chapter, chemists have been practicing nanotechnology (albeit not calling it so) for about two centuries, and for half a century by design. What modern nanotechnology and material physics has brought to chemistry was the ingenuity and the level of control in organizing atoms and molecules into ultrasmall structures with intricate properties and desired functionality.

The catalysis-related issues of carbon management and renewable energy sources received increased recognition by the worldwide scientific, industrial, and political communities. Huge demands are being placed mainly on 1) increasing the efficiency of energy production and utilization of renewable sources, 2) significantly decreasing the carbon intensity of our economy, and 3) improving our ability to capture and sequester atmospheric carbon dioxide. This is why most of the works presented in this thesis deal with carbon management in some way – from catalysis of carbon oxides, through utilization and activation of light hydrocarbons, to clean hydrogen generation, just to name the main topics.

From a practical point of view, apart from the primary motivation of using catalysts to run reactions with higher rates (and thus more affordably) there are a number of particular factors and aims driving the progress in the catalysis research, with the aforementioned environmental benignness in mind. They can be summarized as follows:

- Minimization of the noble material usage, e.g. by their replacement with other elements, structural tailoring (via morphology, crystallography, dispersion, …), change of their oxidation state, alloying with other elements, etc.;
- High efficiency per amount of the catalytic material used;
- Low energy consumption (typically implying catalysis at lower temperatures and pressures);
- Good tolerance for the presence of impurities in source chemicals;
- High purity of products, putting lower demands on post-reaction purification;
- Affordable and scalable process of the catalyst fabrication;
- Production of novel compounds not achievable otherwise (where the cost does not necessarily have to be a primary concern).

In this endeavor, the main quantitative indicators to be monitored are:

- **Activity** – this essential parameter describes the increase in rate of a chemical reaction due to the presence of a catalyst. Activity is often quantified by turnover frequency (TOF) as the number of times that a given overall catalytic reaction takes place per catalytic site per unit time for a fixed set of reaction conditions (temperature, pressure or concentration, ratio of reactants, extent of reaction) [69]. In realistic applications, the aspect of accessibility of the catalytically active surface, which is related to the factors of heat and mass transport, may also play an important role in the overall activity.
- **Selectivity** towards the desired reaction product is the single most important attribute of the catalyst quality. It determines the specific reaction pathway along which the required product is

formed, and the purity of the catalyzed reaction output; ideally 100% selectivity for the desired molecule in multipath reactions should be achieved via the energetically most facile pathway.

- **Stability** is an important practical factor. It reflects the ability of a catalytic system to sustain harsh reaction conditions and an eventual presence of foreign materials, which may lead to its deactivation (via, e.g., morphological changes or poisoning). The original activity and selectivity of a catalyst has to be maintained as long as possible or there has to exist a reasonably facile procedure of catalyst regeneration.
- Among the more practical complementary aspects to be included in the catalyst evaluation is the **availability** of source materials (considering their price, global reserve volume, or environmental burden of their extraction and processing), which possesses a strong driving force in the search of alternative materials and structures.

In order to address the above goals, there have been parallel efforts made by the heterogeneous catalysis research and development in the following directions:

- Detailed molecular-level understanding of the behavior of known (and already utilized) materials and structures;
- Optimization of parameters of traditional catalysts (with respect to the material usage effectiveness, reaction activity or selectivity, stability, etc.), as well as optimization of conditions in which they operate;
- Rational design of new structures based on traditional materials and their combinations;
- Development of completely novel systems based on materials and/or structures considered non-traditional in catalysis.

More specific backgrounds and motivations related to the particular classes of chemical processes presented in this thesis will be provided individually at the beginning of each respective chapter.

2.2 Model systems in catalysis

The conventional route towards the discovery of novel or optimized functional materials in many fields of industry consists of a number of iterative steps, which makes it rather long and expensive process. In particular, application of this concept in catalysis is largely a matter of trial and error. This time consuming procedure can be speeded up through the development of methods for rapidly synthesizing large numbers of new diverse chemical compounds, followed by a quick screening of such a set for qualitative trends in the desired properties. Such approach is the domain of combinatorial methods [70, 71], commonly applied in pharmaceutical industry, exploration of complex metal–oxide compositions for potential use in semiconductors and superconductors, synthesis of new compounds for both homogeneous and heterogeneous catalysis, etc.

Another approach is based on a bottom-up strategy of systematically unraveling fundamental origins of particular surface processes and applying this knowledge in the design of new catalytic materials or their efficacious optimization. For instance, for the class of reactions involving the dissociation of reacting molecules and the subsequent removal of the dissociation products, there exists a correlation between the reaction activation energy and the stability of reaction intermediates, leading to universal relationship between adsorption energies and catalytic activity [72-74]. Scaling relations between activation and reaction energies (such as the Brønsted relation [75, 76], the Langmuir−Hinshelwood relation [76-78], the Evans–Polanyi relations [76, 79, 80], or the Hammett equation [81]) have been identified as quantitative implementations of the classical general Sabatier principle [82, 83]. Their merit is to define relatively simple fundamental descriptors of catalytic

activity and selectivity, which can be used to pinpoint what it is that determines the best catalyst. Proper classification of materials and reactions based on available values of the activation energies of elementary reaction steps (either experimental or calculated) allows screening for optimum catalyst (or electrocatalyst) for a given reaction and resolving how some of the elements can be replaced by others or combined in a new efficient way [84-86].

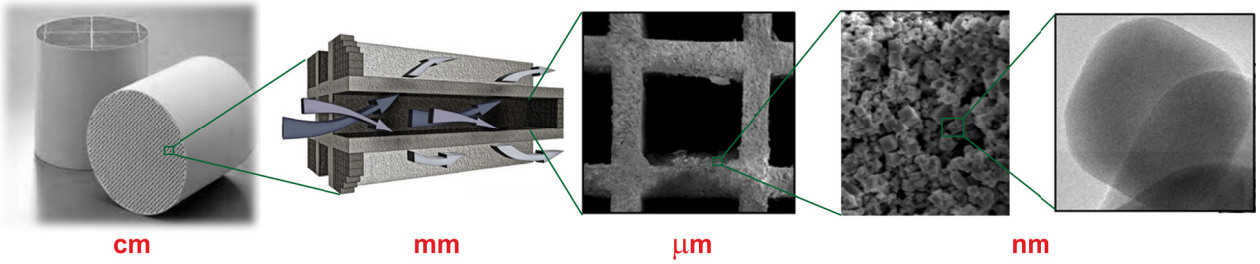

Figure 3: One of the components of a three-way catalyst (TWC) for catalytic combustion of soot in diesel engines (DPF) as an example of an industrial ("real") catalyst, demonstrating extreme complexity of such system. The actual active nanometer-sized metal nanoparticle can be seen in the rightmost image. Adapted from [87].

Unfortunately, there is a huge obstacle involved in the systematic study of the surface chemistry of industrial ("real") catalysts, already utilized in many fields of applied chemistry, which stems from their extreme complexity, both structural and compositional (see the example in Figure 3). A catalyst with high activity has to exhibit a rather large specific surface area, which is typically achieved in highly disordered multicomponent porous structures containing irregular nanoparticles at various levels of dispersion and binding to the substrate material. Moreover, under realistic reaction conditions, the catalyst can undergo dramatic changes both in microstructure and chemical composition, including encapsulation, segregation, surface diffusion, oxidation/reduction, redispersion, sintering, alloying, surface passivation, etc., being of either temporary or permanent nature.

Indeed, the inherent complexity of a real catalyst possesses its main strength as it provides ample room for optimization of its properties towards high selectivity and activity for a desired reaction. A whole variety of parameters are thus available for tuning powder or supported-nanoparticle catalysts such as effective surface area, particle size, structure, composition and dispersion, activity of the support material, presence of promotors, etc. But at the same time, it is the main reason why the detailed microscopic-scale characterization of industrially-relevant catalysts as well as the description of particular reaction mechanisms on the molecular level is often lacking and hard to be accessed by the available techniques of surface and material science.

A powerful strategy in overcoming these difficulties is a confinement to experimentally accessible planar or nearly-planar surfaces with reduced and well-defined complexity (see Figure 4), in tandem with well-controlled environments [88-90]. Such systems, capturing some of the complexities of a real catalyst, can be the means of gaining sufficiently detailed understanding of fundamental patterns of reactivity, which could be later extended to the more complex cases of porous, disordered, and more loosely-defined realistic catalytic systems. These simplified and well-defined so-called **model systems** [22, 88, 89, 91-96] comprise both model catalysts and processes in which they are involved. Moreover, model systems can also be much more intimately connected with theory via microkinetic simulations and calculations based on quantum mechanics.

The first step on the long stairway of complexity [97-100] has been paved with **single-crystal metal surfaces** [101-104] at the basic level of simplification, i.e., atomically smooth with a single low Miller

index crystallographic orientation. However, even with such nominally simple systems non-trivial structures can already be observed due to a surface reconstruction (thermally and/or chemically induced) [105-109]. An additional variety of potential structural features, along with the ordered facets, exists on high-index planes, irregular, or defective surfaces – steps, kinks, corners, and point or line defects [110, 111]. The catalytic activity of metals is known to depend substantially on the presence of structural imperfections [112-115] and there are many instances in which steps were identified as active sites as compared to planar low-index surface [15, 110, 115-121].

A partial perturbation from the ordered structure of a monocrystalline solid is represented by dislocations and grain boundaries which are usually a result of excessive strain within a crystal or of inherent polycrystallinity. These bulk imperfections induce formation of the above mentioned surface features and can result in coexistence of domains with different surface orientations.

All the above considerations are as well applicable to bulk metal **alloys** or near-surface alloys [103, 122-126], representing a simplest extension towards multi-component systems. Bimetallic catalysts often exhibit electronic and chemical properties not present on either of the parent metal surfaces. This synergistic effect is especially important when the surface alloy coverage falls into monolayer or submonolayer regime.

A similar hierarchy can be further applied to **metal oxides**, starting with ordered and stoichiometric bulk structures [95, 127-129]. The variety of oxides is tremendously rich due to the larger amount of crystallographic structures and different possible bulk terminations for the same orientation. Even for one particular chemical composition (stoichiometry) a variety of structural phases can exist, or even coexist – this is especially true for transition metals which are stable in more oxidation states [130].

A simple classification from the reactivity standpoint differentiates between inert and reducible oxides. One of the key concepts in predicting the stability and reactivity of oxide surfaces is their polarity [127, 131-134]. Most metal oxides are internally ionic (formally O^{2-} anions surrounded by metal cations) [130]. Minimization of surface energy drives the formation of a particular surface arrangement, leading to bulk terminations with different structures and polarities. Polar oxide surfaces (i.e., those with a dipole moment) are often unstable and prone to reconstructions [131, 134-136], except when present in the form of a nanostructure or stabilized by a proper modification [131, 137, 138].

Like in the case of metals, the catalytic relevance of steps on oxides has been recognized as well, e.g., on TiO_2 [139-143], CeO_2 [144-148], SnO_2 [149], Al_2O_3 [150, 151], Cu_2O [152], MgO [153, 154], ZnO [155], and many others [111, 127-129, 156]. Regarding defects on oxides [157], besides line and point defects, domain boundaries, dislocations, and cation interstitials, of special importance are oxygen vacancies [40, 143, 158-164] which are associated with a formation of metal cations with lower oxidation state. They can act as a nucleation center for nanoparticle growth (heterogeneous nucleation), adsorbate dissociation site, or anchoring site for adsorption. As one of the descriptors of reactivity, the general concept of basicity and acidity in chemistry [165, 166] can be analogically applied to heterogeneous catalysis as well (or specifically to solid oxides as in Ref. [167]). When the Brønsted and Lewis acid–base theories are related to catalyst surfaces, they lead to a definition of so-called Brønsted or Lewis surface sites: acid strength may be defined as the tendency to give up a proton, while base strength as the tendency to accept a proton. The basic or acidic character of a given surface or a type of surface site is, in general, not only determined by the composition of the material but can be strongly structurally dependent.

Ultra-thin oxides [136, 168-170] can be considered a special class of materials – well-defined systems which mimic surfaces of three-dimensionally structured oxide supports of industrial catalysts and allow to investigate metal-support interactions [171]. Thin oxides are more accessible to surface science methods as they provide the benefits of electrical conductivity (allowing, e.g., electron spectroscopies and STM, owing to the tunneling of neutralizing electrons or holes from the substrate), and good thermal conductivity (reducing temperature gradients). Moreover, the constrained dimensionality of the ultrathin oxide films (with the limit case of two-dimensional single layer [170] or even submonolayer oxides) and the proximity of the substrate may permit a production of more open or unstable (metastable) surface orientations than those achievable by cutting a single crystal, a synthesis of strongly non-stoichiometric phases, or bring a novel functionality not provided by thicker macroscopically-sized oxides [95, 132, 156, 172-175]. Discontinuous ultra-thin oxides form basis of a special type of catalytically attractive systems called inverse catalysts [156, 175-177]; see also **Appendix 11** [51] and Ref. [17]. Last but not least, thin oxides have also been used as templates for spatially controlled growth of nanoparticles [168, 172, 178, 179].

With this being said, it is evident that even the single-component systems based solely on metals or oxides provide an incredible wealth of features and phenomena with relations to heterogeneous catalysis which are worth investigating.

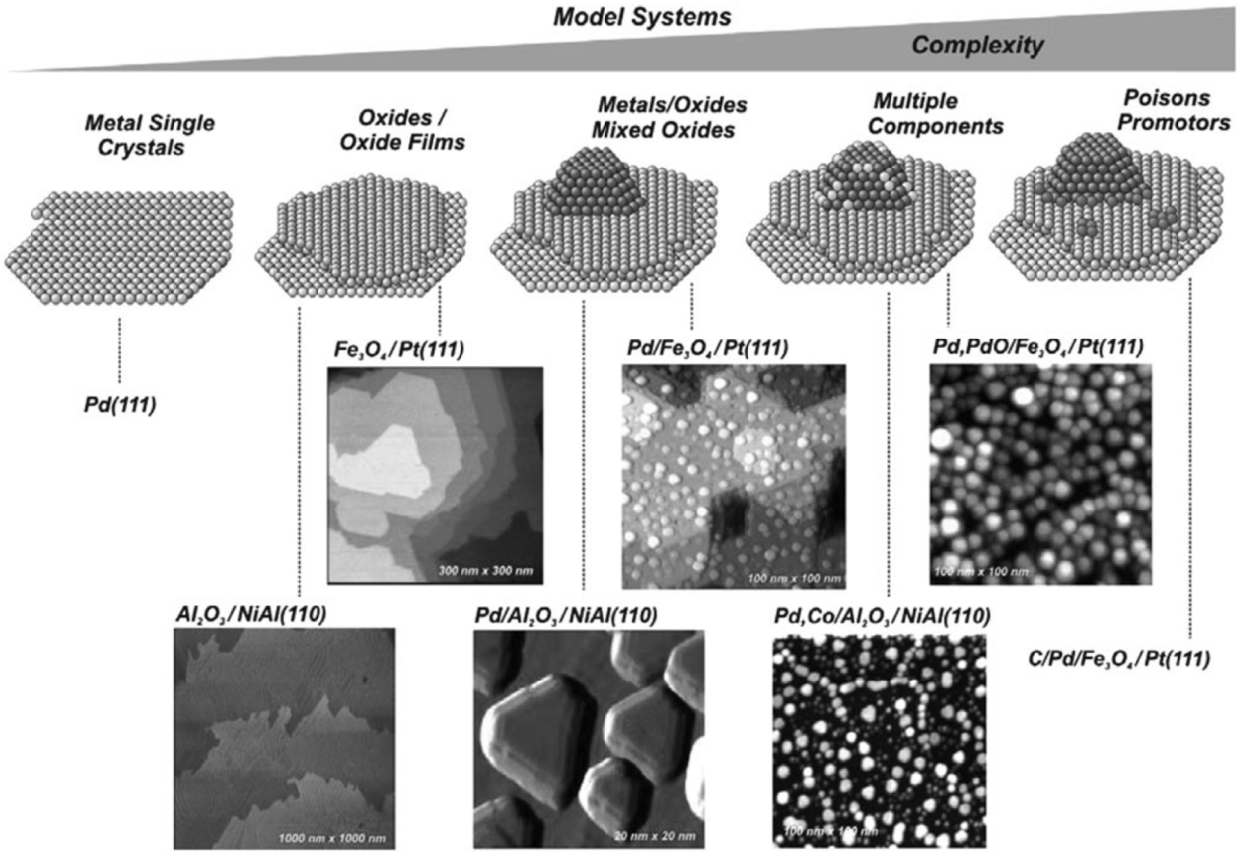

Figure 4: Schematic scale presenting model catalysts of increasing complexity which are developed in order to bridge the „materials gap" (see Section 2.3 for details) between surface science and industrial heterogeneous catalysis. The bottom panels show STM images of selected model systems with different levels of complexity. Adapted from [186].

However, in order to mimic the composition and structure of a "real" catalyst an elevated degree of complexity has to be achieved via combinations of different materials. A model catalyst based on the

conventional configuration comprises active **metal nanoparticles** (or clusters [65, 180]) supported on an oxide substrate present in the form of a bulk material or a thin film [62, 92, 94, 99, 181-185]. The potential roles of the oxide span from a mere mechanical support (inert oxides, e.g., crystalline alumina or silica) to an active participant in the reactivity (e.g., reducible oxides CeO_2, TiO_2, WO_3, Fe_2O_3, etc.). Examples from both groups are provided in Section 3.2.1 for Pd-alumina (**Appendix 1** [28]) and in Section 3.2.2 for Pt-ceria (**Appendix 3** [11] and **Appendix 4** [45]), respectively. It is shown, however, that there is no sharp borderline between the inert and the active oxides, since the above described structural variations can considerably alter the active involvement of the oxide component in the reactivity, owing to, e.g., metal–support interaction (MSI) or formation of local bimetallic phases [7-9, 11, 16, 44, 47].

A reverted metal–oxide arrangement (**i**.e., oxide nanostructures on top of a metal support) leads to an **inverse model catalyst** [156, 175-177, 187], already referred to earlier as a logical outcome of the metal-supported ultra-thin oxide system.

Because the reaction behavior and electronic structure of supported NPs is generally a function of the particle size (or even of limited dimensionality) [99, 110, 188, 189] and its shape [90, 189, 190], several related aspects need to be considered here. These include different adsorption at facets, edges, and defects, size-dependent variations of electronic structure, surface diffusion confinement, and eventual formation of surface complexes. Moreover, the chemical composition factor has to be added into the set for oxidic [156, 176, 191, 192] or bimetallic (resp. multimetallic) [159, 166, 193-196] nanoparticles. Nano-size effects associated with the ultrasmall NPs also opens pathways to synthesizing oxides with unusual stoichiometries or bimetallic particles consisting metals immiscible at the atomic level in bulk [197, 198], see the example in Figure 5.

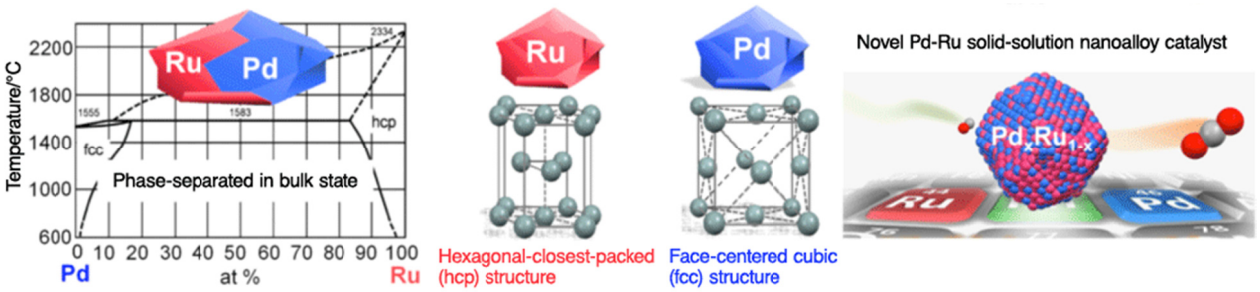

Figure 5: Pd-Ru solid-solution nanoalloy catalyst, providing high CO-oxidation activity. In these nanoparticles Pd and Ru are mixed with each other at the atomic level (as illustrated on right), although both metals are immiscible in the bulk form due to their different crystallographic structure (see the phase diagram on left). Adapted from [197].

For the purpose of model studies and, more specifically, when establishing correlations of size- and shape-dependent structural and chemical factors, it is desirable to assure the distribution of the NP properties as narrow as possible. It is because most characterization techniques provide integral information, reflecting the contributions from all parts of the analyzed area, but the observed catalytic properties may be dominated by a participation of a small subset of NPs near a specific structure or composition, or even specific reaction sites thereof. Thus, the structure–reactivity relations derived from investigations of catalysts with diverse population of particles may be misleading. The same restriction may apply to the arrangement of supported particles in the situations where surface diffusion is an important factor. It can be characterized by attributes such as particle density, spatial distribution (regular, random), orientation alignment etc.

With current modern techniques an extreme level of control can be achieved, e.g., generating monodispersed clusters with precise numbers of atoms [126, 199, 200], spatially controlled patterns [3, 201], or achieving confinement to strictly reduced dimensionality [202] (for example by creating 2D arrays of nanoparticles [203, 204], linear (1D) structures [205, 206], or isolating single atoms [99, 207-209]).

2.3 Real heterogeneous catalysis

In previous section we have shown that the key advantage of the model study approach is the possibility to identify individual factors determining the properties of catalytic systems and reactions on them via systematically increasing their complexity in highly controlled manner. However, there still remains what we call a **complexity gap** between the amount of complexity we are currently able to handle and the intricacy of the „real-world" catalytic materials (like the one shown in Figure 3). Therefore the kinetics observed in industrial catalytic reactions do not necessarily follow what we can obtain with simplified model systems. There are two aspects of the complexity gap: 1) the structural and compositional complexity of the surfaces (also denoted separately as a **materials gap**) and 2) the chemical complexity of the reaction systems.

Neverheless, this complexity gap keeps steadily closing with the growing capabilities of sample preparation and characterization methods on one side (see also Section 7) and improvement of theoretical models on the other. Several research articles and reviews have been devoted to the issue of bridging the complexity gap and correlations between models and "real-world" catalysts, see e.g. [98, 100, 181, 210-213], including the Ertl's Nobel Lecture [97].

Another serious simplification of model studies stems from the pressure restraints of the surface characterization techniques (most of them requiring UHV environment), which may lead to misleading conclusions regarding the subject of study. For example, although the CO oxidation over Ru under UHV conditions reveals the lowest catalytic activity among the late transition metals (such as Pt, Rh, and Pd), under strongly oxidizing reaction conditions (e.g., in ambient air) the CO oxidation rate on Ru turns out to be superior to the above metals [95]. This observation can be taken as a clear manifestation of the so-called **pressure gap** [214]. The transition from an inactive catalyst towards an active one turned out to be, in this case, attributed to a structural transformation of Ru to RuO_2.

Similarly, contrary to what experiments conducted with UHV equipment had led us to believe, under atmospheric pressure of reactant gases Pd or Pt metal surfaces establish PdO or PtO_2 surface phases, respectively [215], which catalyze the oxidation of CO to CO_2 via the Mars–van Krevelen mechanism [216] and not the long-assumed Langmuir–Hinshelwood one [22]. In other words this catalyzed reaction largely proceeds by utilization of lattice oxygen from oxide phase instead of direct involvement of surface chemisorbed oxygen. Hence, the reactivity is not intrinsically linked to the availability of gas-phase oxygen, but rather a certain partial O pressure is required in order to form oxide phase, igniting a reaction channel which does not participate at lower pressures. This observation, for instance, formed the basis of the work presented in **Appendix 5**.

Like in the previous issue of the complexity gap, surface science has reached a degree of maturity that allows us to cope with the pressure gap to some extent as well. An overview of efforts made towards bridging the pressure gap can be found in Refs. [211, 217, 218] (see also Section 2.5).

In any case, it should be remembered, that industrial catalysis cannot be reduced to merely describing the behavior of the active site, no matter how complex and to what level of detail. When

designing a functional chemical reactor the involvement of mass and heat transfer in the process has to be seriously taken into account, too. Moreover, it is often other factors like selectivity or secondary phenomena (such as catalyst deactivation or instability) playing decisive role rather than the catalyst activity alone.

2.4 Preparation of model catalysts

There are two fundamentally distinct strategies in the synthesis of microscopic structures. A so-called **top-down** approach was typically adopted by material physicists and engineers who developed ways to manipulate and build progressively smaller structures by the means of photolithography and other related techniques. As the size of fabricated structures gets lower (tens of nm range) this strategy becomes very challenging. The **bottom-up** route, on the other hand, which is more natural to chemists, starts from objects which are nanoscaled by their nature, such as atoms or molecules, to build up more complex and larger nanostructures (see schematic picture in Figure 6b). Although current state-of-the-art technologies from both sides has already merged in terms of the scale in which they can operate (Figure 6a), each of these two approaches carry its pros and cons and are thus being increasingly more often combined (an example is provided in **Appendix 2**, see Section 3.2.1).

From the catalysis standpoint, as was already indicated, the true nanoscale is particularly important here because nanometer-sized objects (units of nm rather than tens or hundreds) can provide characteristic structures, exhibit peculiar properties, and perform specific functions, often not achievable otherwise. The bottom-up built structures can be formed as an ensemble of relatively simple entities (such as surface structural patterns, adsorbed molecules, metal atoms, clusters, nanofibers, etc.), or have a complicated structure or chemical composition (such as molecular devices and nanomachines). The fundamental research in model catalysis is positioned around the former class of nanomaterials with the bottom-up approach as the prevailing strategy of sample preparation.

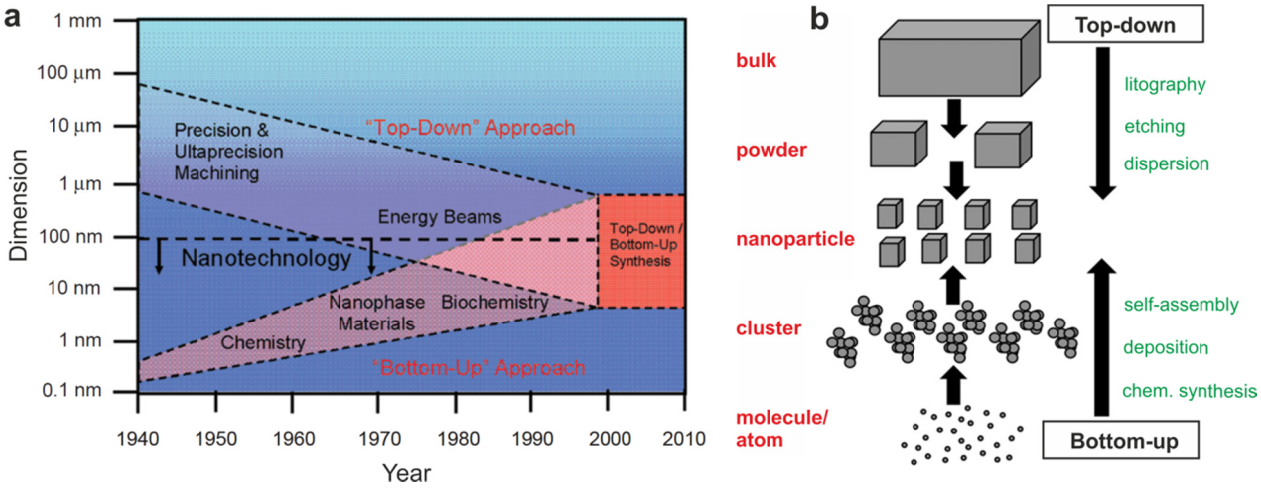

Figure 6: a) Graph illustrating the convergence of top-down and bottom-up nanotechnologies. b) Schematic diagram of the basic principles of top-down and bottom-up approaches in synthesizing nanoparticles. Partially adapted from [219].

An overview of various methods used in the preparation of catalytic materials is given in Refs. [190, 220], spanning from the traditional three-dimensional "wet" chemistry (such as precipitation or impregnation) to the "two-dimensional" methods of physical chemistry. In the following, with

regard to the topic of this thesis, we will focus on the latter class of techniques, summarized in Refs. [22, 62, 67, 221, 222], namely the preparation of well-defined solid surfaces and supported nanostructures.

Ordered metal surfaces can be prepared by cutting a single crystal along a particular crystalline orientation and subjecting to a subsequent cleaning treatment in UHV. Similarly, a fresh oriented oxide surface can be obtained by cutting or cleaving a single crystal bulk along the desired plane directly under vacuum [94], or via careful (non-reductive) surface treatment of an *ex situ* pre-cleaved single crystal in UHV. And, finally, the preparation of bimetallic surfaces can follow the same recipe as suggested for pure metals, however, the attainable compositions of such surfaces is limited to those of bimetallic systems forming stable bulk alloys. A more common and flexible way to fabricate bimetallic surfaces is via depositing one metal onto the other (usually a well-ordered single crystal), as will be briefly described below. Additional advantage of this method is that the admetal can either stay on the surface or diffuse into the subsurface region to produce surface or subsurface bimetallic layer, respectively; the particular behavior can be tuned through sample temperature during deposition.

Thin epitaxial films of a wide variety of materials (metals, oxides, semiconductors) are often grown by a precisely controllable technique of molecular beam epitaxy (MBE) [223-226], representing one of the physical vapor deposition (PVD) techniques. In this process, a nearly atomically clean surface (kept at an elevated temperature to provide sufficient thermal energy to the arriving species to readily migrate over the surface) is exposed to a beam of atoms or molecules in an UHV environment, forming a crystalline layer in registry with the substrate (epitaxial film). An eventual lattice mismatch between the support and the layer material can result in effects and structural features such as interfacial strain, periodical superstructures (superlattices, surface corrugations), rotational domains, etc. The source beam is usually realized by evaporating the deposited material from a tip or a crucible, using resistive heating or electron-beam sputtering, by ion sputtering, by cathodic arc plasma, or by pulsed laser evaporation.

For the preparation of thin oxide films or oxide nanoparticles three principle routes are at hand [92, 190, 227, 228]: 1) reactive evaporation of an oxide or a metal on a (typically inert) support in oxygen atmosphere [229, 230], 2) deposition of a metal on a suitable (typically inert) support followed by an oxidation procedure [135, 172, 231], or 3) direct oxidation of a metal, semiconductor, or metal alloy surface (usually a single crystal) [221, 232]. A large number of recipes have been developed for the preparation of various ordered oxide films including Al_2O_3, SiO_2, TiO_2, FeO or Fe_3O_4, CeO_2, MgO, NiO, ZnO, CuO or Cu_2O, Cr_2O_3, SnO_2, Co_3O_4, V_2O_5, WO_3, and many others (see, e.g., Refs. [169, 227-229] and references therein).

Apart from the above methods, other members of the PVD family are the pulsed laser deposition (PLD) [233, 234] and magnetron sputtering [235-238]. Especially magnetron sputtering has become a very popular versatile technique for preparation of new materials, allowing deposition of a very wide range of compounds and alloy thin films including oxides, nitrides, carbides, fluorides, or arsenides. It is capable of producing thin films of controllable stoichiometry and composition, including multicomponent solids with stoichiometries which would be difficult to achieve by other methods, via using composite sputtering targets or via simultaneous co-deposition from multiple targets. Contrary to conventional evaporation processes magnetron sputtering offers more flexibility and does not require heating of the source material, which has limiting consequences for the composition and morphology of the resulting layer. Direct current (DC) sputtering [239] is typically used for deposition of metals, while the radio frequency (RF) modification [240] is required for the

coating by insulating materials or for improved deposition stability; on a larger scale it is usually replaced by a pulsed sputtering [235, 238]. RF sputtering also reduces thermal load to the substrate and can provide higher deposition rates. The magnetron is operated with low pressure glow discharge of either an inert gas (e.g. argon) or a reactive gas (e.g. oxygen), which then directly participates in the growth of the thin film and can be used as one of the means of controlling its stoichiometry (referred to as the reactive sputtering [240, 241]).

In contrast to PVD, chemical vapor deposition (CVD) methods [242] are based on exposing the substrate to one or more volatile precursors, which produce a deposit with desired composition via reaction and/or decomposition on the substrate surface. It can be applied in the preparation of various thin films [243-245], metal [246] or oxide [247] clusters, nanorods [248], nanotubes [249, 250], multilayered [251, 252] or 2D [253, 254] structures, etc. In Section 5.4 of this thesis CVD method is used to grow graphene layers on a metal substrate.

Industrial **supported metal catalysts** on a large scale are typically made by wet impregnation of a porous support (usually an oxide) with a solution of a metal salt, followed by heating in air (calcining) and reduction (usually in hydrogen) [255, 256]. This procedure leads to an ensemble of metal particles non-uniform in size, shape, and spatial distribution, which can hardly be characterized systematically. Better-defined preparation protocols have been established for the systematic model studies [62, 92, 221, 222]. Physical vapor deposition (PVD) of metals [65, 92-94] (by either evaporation, magnetron sputtering or pulsed laser deposition) or direct deposition of metal clusters from the gas phase [126, 200, 257] under UHV conditions have been the preferred choice. Various aspects of NP growth, assembly, and modification has been the subject of several reviews [92, 190, 220-222].

2.5 Experimental strategies and characterization techniques

The general concepts and techniques used in catalysis, both experimental and theoretical, are inextricably mingled. Moreover, the experimental results often stimulate implementation or even development of theoretical methods and, in turn, theoretical insight naturally prompts experimental endeavor. The experimental tools of surface science can be divided into two main categories: spectroscopy and microscopy methods [23, 68, 91, 221, 258, 259]. Employing a combination of methods from both categories (multi-scale characterization [260]) and performing kinetic measurements of reactivity allows to identify the connections between structural and electronic features of the surface on one side and their role in the reaction kinetics on the other [62, 90, 110, 136, 261].

A rigorous research aiming at detailed insight into the key stages of reactions and, in particular, the modus operandi of a catalyst, requires a direct monitoring "in action" [106, 217, 260]. Even when a simultaneous characterization of the catalyst state and of the reaction processes is not feasible, the subsequent experimental procedures (including the sample preparation or high-pressure treatments) should be performed under well-controlled conditions, ideally within the same apparatus (typically a UHV system) [102]. This approach gives rise to the field of **in-situ** research methods [22-24, 221]

In contrast, the **ex-situ** methods involve sample transfer between different experimental devices (typically after sample preparation or between individual sample treatments) and thus expose the subject of study to different and less controlled environments, usually to ambient air.

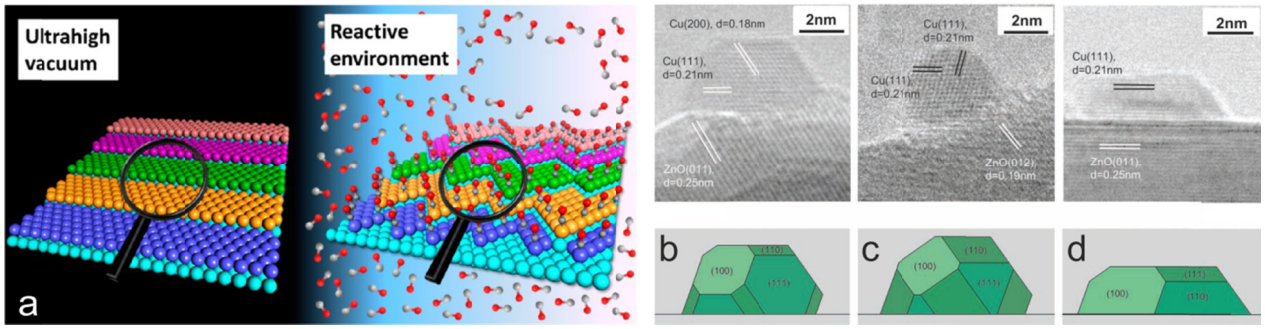

Figure 7: a) Schematic depiction of the restructuring of a stepped surface as a result of reactive environment. b)-d) In-situ TEM images and the corresponding Wulff constructions of Cu nanocrystal in Cu/ZnO catalyst in various gas environments: a) 1.5 mbar of H_2 at 220°C, b) mixture of H_2 and H_2O (53 :1 ratio at a total pressure 1.5 mbar) at 220°C, and c) gas mixture of H_2 and CO (19 :1 ratio at a total pressure 5 mbar) at 220°C. Adapted from [24] and [262].

Moreover, one should be aware of the fact that the common view of the catalyst as a physically and chemically rigid system not affected by its environment or by a running reaction is generally not valid. The active heterogeneous catalysts often restructure the metal surface around the adsorption site upon forming a bond to a molecule. This autogeneous transformation occurs to optimize the adsorbate-metal bonding and can be of temporal (ultimately limited to the site occupation period), or of permanent nature [20, 90, 106, 107, 166, 263-267]. On somewhat larger scale this restructuring can affect metal nanoparticles by changing their equilibrium shape [63, 90, 109, 184, 262, 268-271] (see the example in Figure 7b–d) or disrupting them into smaller particles [90, 272-274]. On continuous metal surfaces it can lead to a significant amount of mass transport of metal atoms over the surface, altering the whole surface landscape [106-109] (illustrated in Figure 7a), which can even inhibit the reaction, result in structural anisotropy in the reactivity [107], or induce macroscopically detectable oscillatory behavior [267, 269].

Similarly, reducible oxides can undergo chemically induced structural, morphological, or compositional changes via formation of oxygen vacancies (leading to stoichiometry variations) [109, 158, 168, 191, 275-277], rearrangement of steps or surface lattice [129, 168, 278, 279], nanoparticle reshaping [109, 280], or crystallographic transformations [191, 276, 280]. In multicomponent systems (such as, e.g., supported nanoparticles, alloys, or mixed oxides) surface segregation [125, 281, 282], encapsulation [270, 271], redispersion [99, 273, 274, 283, 284], phase separation [125, 281], sintering [270, 283, 285-288], or other phenomena involving mass transfer or material accumulation may occur as an action of temperature and reactive environment, again with potentially fundamental consequences for its catalytic properties. Sometimes, these alterations are an intentional and controlled process serving a purpose of catalyst stabilization or initial activation („induction period“). All the above reasons emphasize the importance of (whenever possible) *in-situ* sample characterization in the whole course of the scrutinized chemical process, ideally including monitoring directly under the working conditions of the catalyst.

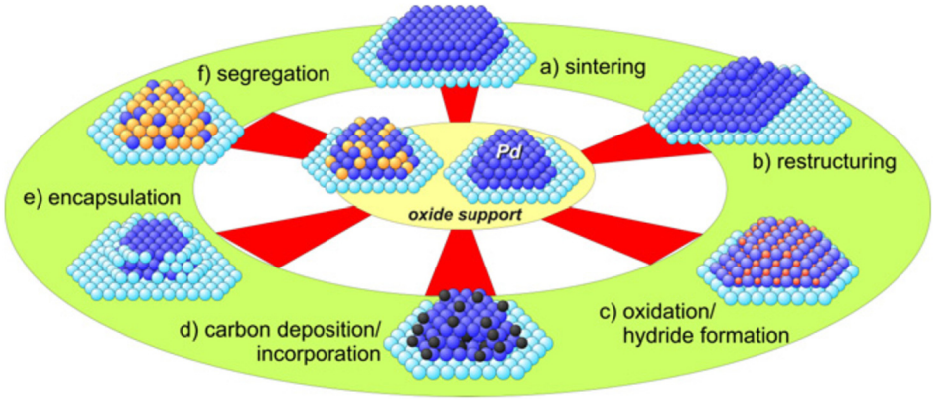

Figure 8: Illustration of structural and compositional changes that may occur during the transformation of catalysts from the "as-prepared" to the "active state": a) sintering, b) restructuring, c) oxide or hydride formation, d) coking, and e) particle encapsulation or f) surface segregation of bimetallic particles. Adapted from [196].

Nowadays, the main driving force in the development of surface science equipment for heterogeneous catalysis is the effort to bridge the pressure gap [211, 221, 289, 290], mentioned previously in Section 2.3. One of the possible approaches in achieving this goal is to build-up an experimental setup in which UHV chamber is linked to a high-pressure stage, using differential pumping. Implementing this design, XPS (or PES), TEM, SEM, or LEIS can be operated in the mbar regime [24, 217, 258, 291-295]. Another route is using a microreactor separating the UHV section of the apparatus from the high-pressure volume via electron-permeable ultrathin membrane (made from, e.g., graphene or silicon nitride) not interfering with the monitored process; this has been applied in PES, SEM, TEM, and X-ray (spectro-)microscopy setups [217, 296-305]. Some other experimental methods of surface science are intrinsically capable of working under elevated pressures (as such, or with relatively minor modifications), for example IR absorption spectroscopies (e.g., ATR-FTIR, RAIRS, or DRIFTS), Raman spectroscopy, UV/Vis and sum frequency generation laser spectroscopy (SFG), surface X-ray diffraction (SXRD), and X-ray absorption spectroscopy (XAS). These optically based techniques benefit from the low-scattering cross-sections of photons with matter, which allow deep penetration into materials and thus simplify the types of reactor designs that can be utilized for characterization under ambient or even harsh reaction conditions. Scanning probe microscopy (AFM, STM) can be operated under higher pressures as well, with certain limitations (probably more restrictive for STM).

In the following sub-sections, the major instrumentation used in the projects presented herein will be briefly described.

2.5.1 Molecular beam system at FHI-MPG

Molecular beam apparatus installed at Fritz-Haber Institute of Max-Planck Society in Berlin by workgroup of Prof. J. Libuda is an elaborate UHV system employing molecular beam techniques [96, 211, 306-310] and *in-situ* surface and gas phase detection techniques, realized by reflection absorption infrared spectroscopy (RAIRS) and quadrupole mass spectrometry (QMS), respectively. The details are provided in Ref. [311], the schematic drawing can be seen in Figure 9. The main advantage of the molecular beam approach over a simple reactor study is that the beam experiment is performed under single collision conditions [211, 308, 309], i.e., each reactant molecules undergoes only a single interaction event with the surface in an otherwise collision-free environment (UHV). Moreover, beam flux and modulation can be varied quickly and over a wide range of parameters. Implementation of the molecular beam technique allows for determination of absolute

adsorption and reaction probabilities [309, 312, 313], flexible modulation of reactant fluxes on a short timescale [306, 307], control over dynamic properties of incident molecules (kinetic energy, rotational and vibrational states), and collision-free detection of scattered and desorbing molecules.

Two types of molecular sources were installed in the apparatus: effusive and supersonic, differing in the expansion conditions, giving rise to different types of energy distribution of the molecules in the beam [90, 112, 308]. Both sources require an effective multi-stage differential pumping, and include computer-controlled shutters allowing fast beam modulation. The effusive beam uses injection of gases through parallel arrays of small channels with high Knudsen number (glass capillary arrays, GCAs). The supersonic beam operates with an injection nozzle under high pressure difference conditions, producing gas flow with molecules reaching sonic speed on exiting the nozzle and supersonic speed upon further expansion. A small solid angle is extracted from the gas plume by a skimmer. The main advantages of the supersonic beam source are narrow velocity distribution, very good collimation, widely variable kinetic energy, and a large degree of control over the internal energy of molecules.

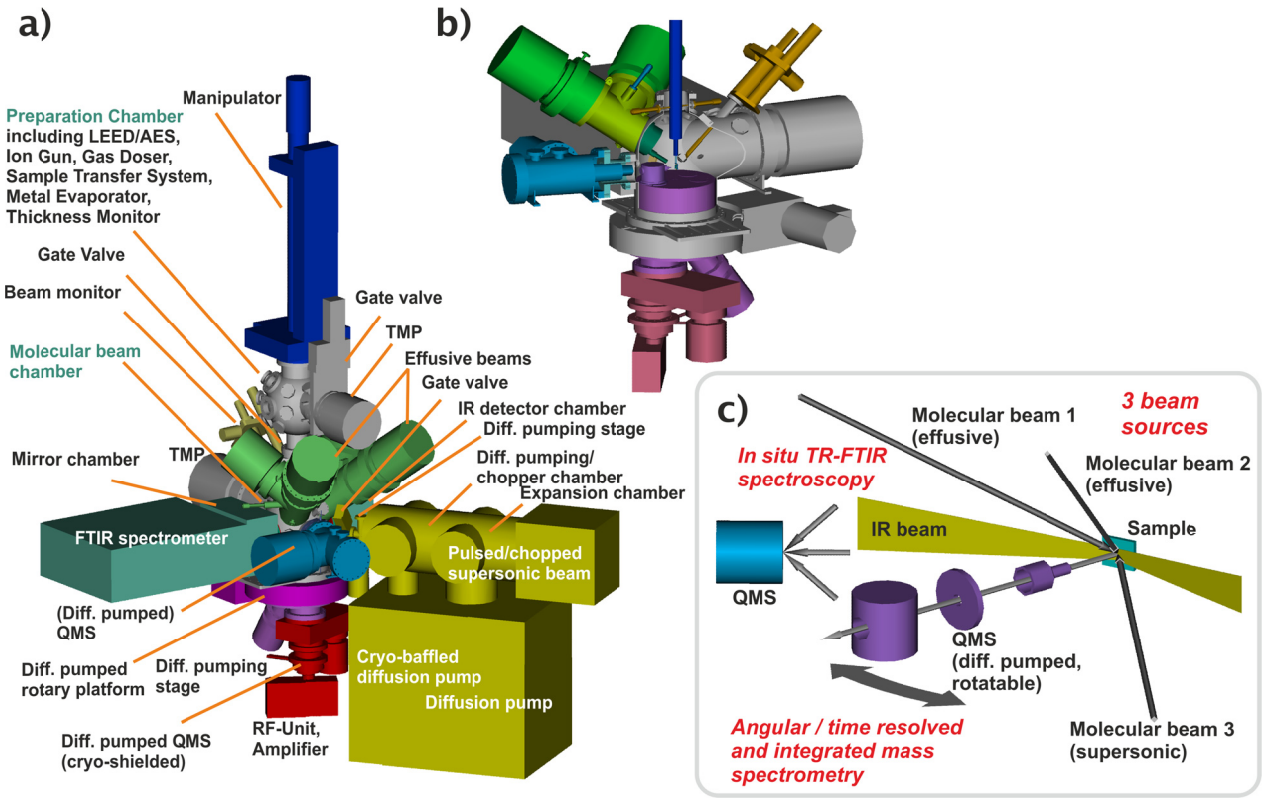

Figure 9: Molecular beam apparatus in the former Molecular beam group laboratory for combined structural and surface chemistry studies. a) Complete overview of the molecular beam UHV system, b) Detailed view of the internal parts of the main scattering chamber, c) Basic scheme describing principle and geometry of a molecular beam experiment. Adapted from [311].

Two quadrupole mass spectrometers (QMS) are used for gas phase detection. For simple reactivity experiments a QMS is placed in the scattering chamber out of the line-of-sight of the sample, providing integral rate measurements. For angular resolved studies [309, 314], differentially pumped spectrometer (AR-QMS) with liquid-nitrogen cooled ionizer housing (to reduce background pressure and thus improve the sensitivity) mounted on a motor-driven rotatable platform was employed. Detected molecules enter the QMS ionizer through an aperture tube with its axis directed at the sample. The high level of control over the thermodynamic properties of impinging molecules

and the incident geometry generated by molecular beam sources together with the AR-QMS detection opens up the possibility of studying the dynamics of gas-surface interaction [60, 307, 310, 315-319], dynamical parameters of desorbing molecules [309, 320], and experimental probing of potential energy surfaces [309, 310].

The availability of two effusive beams in the above apparatus permitted a transient isotopic exchange experiment [307, 321], which represents a route towards acquisition of transient kinetic data at constant surface coverages. It is realized via fast switching between two identically set-up molecular beams with chemically the same entities, one of them being isotopically labeled (e.g., ^{14}NO and ^{15}NO, $^{12}CH_3OH$ and $^{13}CH_3OH$, CH_3OH and CD_3OD, etc.). Such capability was utilized, e.g., in Refs.[29], [53], and [34], respectively. In some cases, isotopically labelled molecules are used only to reduce the background signal during the experiment.

UHV IR spectroscopy [322-324] operated in grazing-incidence-angle reflection mode (Reflection-Absorption IR Spectroscopy, RAIRS) [325-327] was used as a very sensitive tool to study surface adsorbates, providing very specific information on the nature of adsorbates (molecular identification, bond strength and geometry, etc.), their interaction with the substrate, properties of adsorption sites, and character and magnitude of intermolecular interactions within adsorbate layer. It can be used with any reflective surface including thin oxide films on metals. In the spectra evaluation, however, a few factors has to be taken into account, mainly the surface selection rule (limiting the sensitivity to modes with a non-zero component of the dynamic dipole moment perpendicular to the surface), and dipole coupling effects between neighboring adsorbed molecules. The spectrometer also allowed measurements in the time-resolved mode (TR-RAIRS) [328] with temporal resolution in the millisecond range.

Apart from the above described main equipment, other auxiliary devices were installed in the attached preparation chamber (separated from the main chamber by a gate valve) for the sample preparation and quality control, namely low electron energy diffraction (LEED) and Auger spectroscopy (AES) systems, differentially pumped ion sputter gun and gas doser manifold with precise leak valves for chamber back-filling with pure gases, electron beam metal evaporator, and quartz microbalance monitor for deposition rate measurements.

2.5.2 Spectro-microscopy system at Charles University

This multi-probe UHV system combining several complementary *in-situ* methods of structural and spectroscopic characterization is situated in the Surface Physics group laboratory at Charles University in Prague. It was built primarily by Dr. J. Mysliveček as a low-temperature scanning tunneling microscope (LT-STM) instrument with attached preparation and fast-entry load-lock chambers, but many additional upgrades have been made by him and coworkers over the last decade. Currently, this apparatus offers a rather unique set of surface science methods located in three main chambers (separated by gate valves), between which samples can be transferred by transfer rods without breaking vacuum. Apart from the aforementioned LT-STM (with "beetle" type head [329, 330] and liquid-nitrogen cryostat), it allows surface and near-surface structural characterization by SPA-LEED (SPECS reverse view ErLEED 150) and XPS (SPECS Phoibos 150 MDC 9 energy analyzer with a dual Al/Mg X-ray source), along with gas analysis by QMS (Pfeiffer Prisma Plus). The QMS is housed in a differentially pumped nozzle making temperature-programmed desorption (TPD) and sticking probability measurements possible. A set of back-fill dosing valves and two simple directional effusive gas beams can be employed for sample preparation

or modification and for basic molecular beam experiments on adsorption/desorption properties and surface reactivity of the investigated samples.

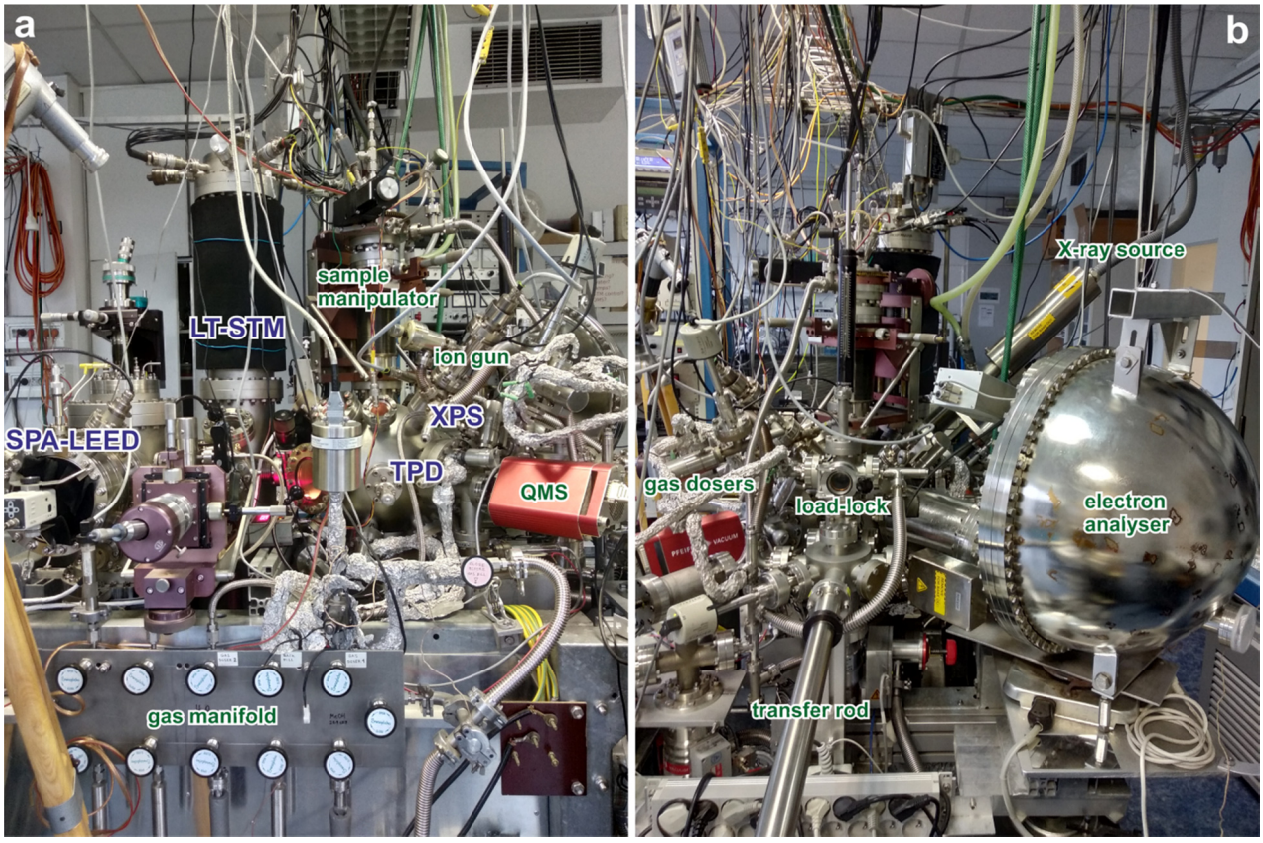

Figure 10: Experimental UHV apparatus in the Surface Physics group laboratory at Charles University in Prague for combined structural and surface chemistry studies; a) front view, b) side view (from the sample entry side). The main components of the system are marked in the photo.

The XPS/TPD chamber is also used as a preparation chamber since it is equipped with two ion sputter guns (wide beam and scanned focused beam) for substrate cleaning and controlled surface morphology modifications, two dual electron-beam evaporation sources for controlled metal or oxide deposition, quartz microbalance monitor for direct on-the-fly measurements of the amount of deposited material. The sample holder allows precise (programmed) temperature control over a broad range from approx. 85 K to 1300 K (depending on the type of sample). Five-line gas manifold is used for controlled injection of pure gases or gas mixtures into vacuum via sapphire leak valves or gas dosers.

2.5.3 Material science beamline at Elettra Synchrotrone

The Materials Science Beamline (MSB) at Elettra Synchrotrone in Trieste (Italy) is a versatile multipurpose beamline apparatus suitable for experiments in materials science, surface physics, and catalysis on various surfaces. It was installed in the frame of cooperation between the Institute of Physics of the Czech Academy of Sciences, Charles University, and Sincrotrone Trieste. The overview of the instrument and a drawing with main components is provided in Figure 11.

MSB was designed to allow surface-sensitive characterization by the means of photoemission spectroscopies with a tunable photon energy (ranging from vacuum ultraviolet to soft X-ray radiation, 22–1000 eV). The photon radiation source is realized by a bending magnet producing mostly linearly polarized light (in the horizontal direction) in tandem with a single grating

monochromator (groove density 1200 l/mm) which selects light with a desired photon energy and bandwidth [331]. The spot size on the sample has a diameter of ~100 μm. The maximum attainable light flux is approx. 2×10^{9}–6×10^{10} photons/s at the sample depending on the selected resolving power and photon energy.

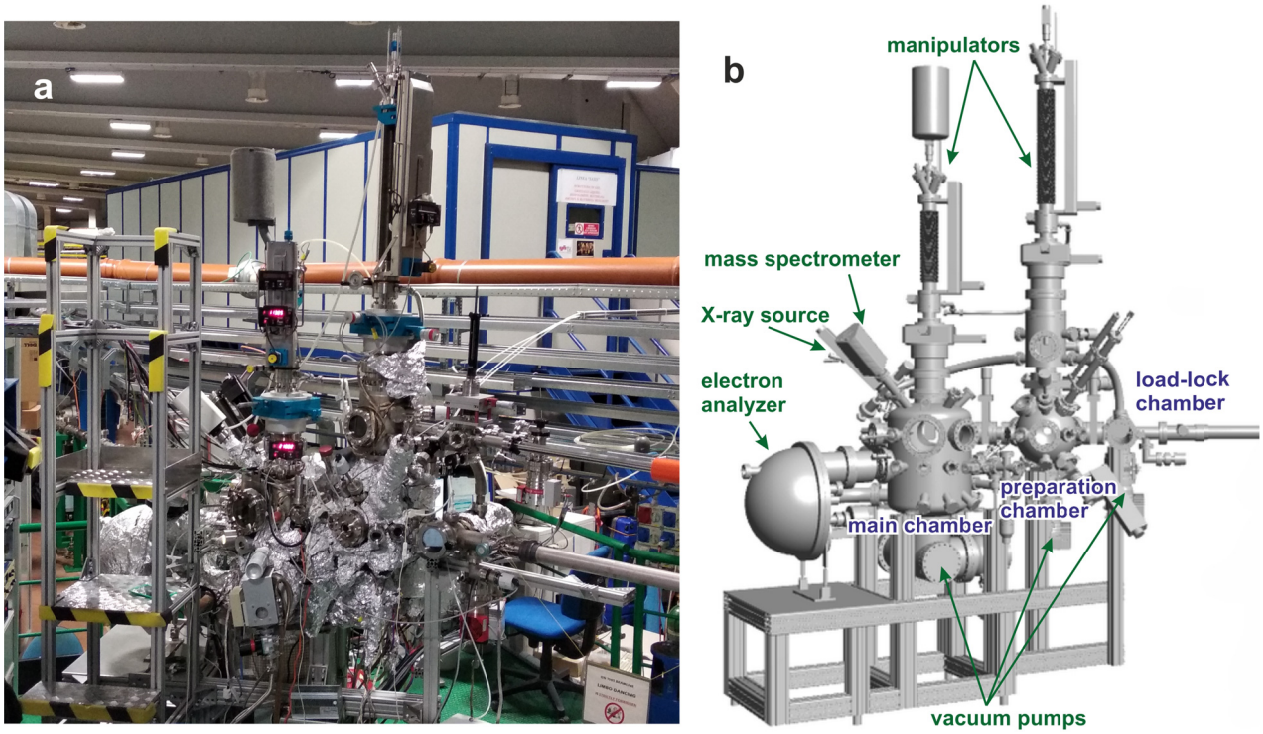

Figure 11: a) Endstation of the Material science beamline (MSB) at Elettra Synchrotrone. b) 3D model of the MSB endstation showing main components of the vaccum system. The drawing by courtesy of T. Skála.

The whole system consists of a series of UHV chambers separated by leak valves. Both main chamber and preparation chamber are pumped by a combination of turbomolecular pump and Ti sublimation pump, providing a base pressure in the low 10^{-10} mbar and 10^{-9} mbar range, respectively. Attached to the preparation chamber is a small load-lock fast entry chamber that allows the transfer of samples within 30 minutes from air to vacuum better than 10^{-8} mbar.

Gas composition in the main chamber can be monitored by a quadrupole mass spectrometer. Photoelectrons from the sample are analyzed by hemispherical electron energy analyzer (SPECS Phoibos 150 with a 100-channel detector) inclined 60° from the beamline axis. Both main and preparation chambers are equipped with Ar^{+} ion sputter guns, several gas lines with precision dosing leak valves, and a set of evaporators, allowing *in-situ* preparation of clean well-defined surfaces from various materials. The main sample manipulator allows heating and cooling of the sample (in the range of approx. 100-1200 K).

The MSB instrument offers high-resolution and high-sensitivity photoelectron spectroscopy covering range of both classical UPS and XPS spectroscopies [23, 293]. The tunable excitation energy brings the benefit of variable surface sensitivity and possibility of photoionization cross section optimization. The monochromatized variable-energy photon source also makes resonant photoemission (RPES) [230, 332, 333] and near edge X-ray absorption fine structure (NEXAFS) [334] spectroscopies possible. Moreover, the utilization of the independent sample rotation capability of the sample manipulator around azimuthal and polar axes (along with x, y and z translations) allows angular resolved photoemission studies (ARPES).

3 CO_x and NO_x surface chemistry

3.1 Motivation and background

Carbon oxide and nitrogen oxide are one of the most abundant gaseous oxides, being naturally present as well as (by-)produced by many industrial and technological processes. Along with residual hydrocarbons (including partially oxidized volatile organic compounds) they are the main constituents of exhaust gas mixture of a conventional combustion engine [335, 336], apart from harmless water vapor, indeed. Raising CO_x and NO_x levels are concern for air quality mainly in metropolitan areas and increasing CO_2 concentration in atmosphere, deemed responsible for the greenhouse effect, became a worldwide issue [337]. The reduction of nitrogen oxide emissions has become one of the greatest challenges in environment protection [335, 338].

The above implies the tremendous importance of CO oxidation and NO_x (NO and NO_2) reduction reactions. In a traditional transition-metal-based, three-way car emission control catalyst (TWC), the oxidation of CO and residual hydrocarbon fragments is performed simultaneously with the reduction of NO_x. Today modern vehicles with three-way catalysts can achieve almost complete removal of all three exhaust pollutants. TWCs are operated with air-to-fuel ratio controllers which - maintain the near-stoichiometric fuel mixture composition in order to ensure high conversion efficiency for the competing oxidation and reduction processes.

Both alumina, used as a nanoparticle support material in Section 3.2.1, and ceria, used as an active substrate in Section 3.2.2, found its extensive use in TWC [87, 339, 340]. The main role of alumina is in providing stable supporting structure with high surface area, whereas ceria possesses a dual functionality – operating as a stabilizing component and as an effective oxygen buffer enhancing oxidation activity of the catalyst. A systematic study aimed at unraveling molecular and structural origins of reactivity of metal-alumina and metal-ceria systems towards the aforementioned reactions is expected to aid in catalyst optimization with respect to high reaction yield, good fuel-stoichiometry tolerance, and resistance against deactivation (e.g., via formation of surface carbon).

3.2 CO adsorption and catalytic oxidation

Apart from the numerous practical applications, in fundamental research carbon monoxide has been used frequently as so-called surface probe molecule and CO oxidation as a prototypical reaction for heterogeneous processes at the gas-solid interfaces [341]. A probe molecule can serve as a sensitive local tool to determine, for instance, the exposed surface coverage of the active phase of a catalyst or, when handled spectroscopically, even the abundance and properties of specific adsorption sites.

The CO oxidation is one of the most extensively studied reactions also for being of extreme practical importance itself and of vital concern in environmental protection. Especially catalytic CO oxidation on surfaces consisting of or containing noble metals has attracted a considerable attention over several decades. The main focus has been progressively moving from the simpler systems of single crystal surfaces of metals towards more complex model catalysts (see also Section 2.2), hand in hand with the development of necessary instrumentation. In the following a few examples of particular achievements on this route will be presented.

3.2.1 CO oxidation on Pd/alumina

Aluminum oxide (alumina in short) is often used as a base substrate in industrially produced catalysts because of its high chemical inertness, strength, and hardness [342, 343]. There are many forms (phases) of alumina differing in crystallographic structure and purity [342, 344, 345]. Well-

ordered alumina single-crystal substrates (such as α-Al_2O_3 [344, 346-348] and γ-Al_2O_3 [344, 349, 350] have been commonly considered inert (especially the sapphire phase of α-Al_2O_3) and therefore suitable for practical catalysts in which the high chemical and thermodynamical stability is required, as well as in model systems of heterogeneous catalysis where an involvement of the substrate in reactivity is not desirable.

A series of experiments was devoted to CO interaction with alumina-supported palladium model catalysts and CO oxidation therein [9, 25-28]. Pd nanoparticles were prepared by physical vapor deposition (PVD) from a metal rod. With increasing amount of deposited Pd, both intensity of XPS signal from Pd 3d level and its binding energy change. The binding energy (BE) monotonically decreases with coverage due to electronic size effect [94, 96, 188, 351, 352] (see Figure 12a), originating in finite-size alteration of both initial state (via band structure changes induced by charge redistribution) and final state (via changes in relaxation processes due to reduced screening effects); on non-conducting or poorly conducting substrates a final state may also be affected by coulombic charging of supported particles upon rejection of photoelectron. The BE does not asymptotically approach the Pd bulk value as could be expected but rather drops to lower values, more significantly for γ-Al_2O_3 than for α-Al_2O_3. It is explained by metal–support interaction [171] between Pd and alumina involving charge transfer from substrate to NP, which is stronger on the more open crystal plane of γ-Al_2O_3 [26]. Hence, although ordered alumina surfaces were traditionally considered inert, the close examination proves that MSI can take place even on these oxides; moreover, MSI may become enhanced on defects or reduced surfaces [9, 157, 353].

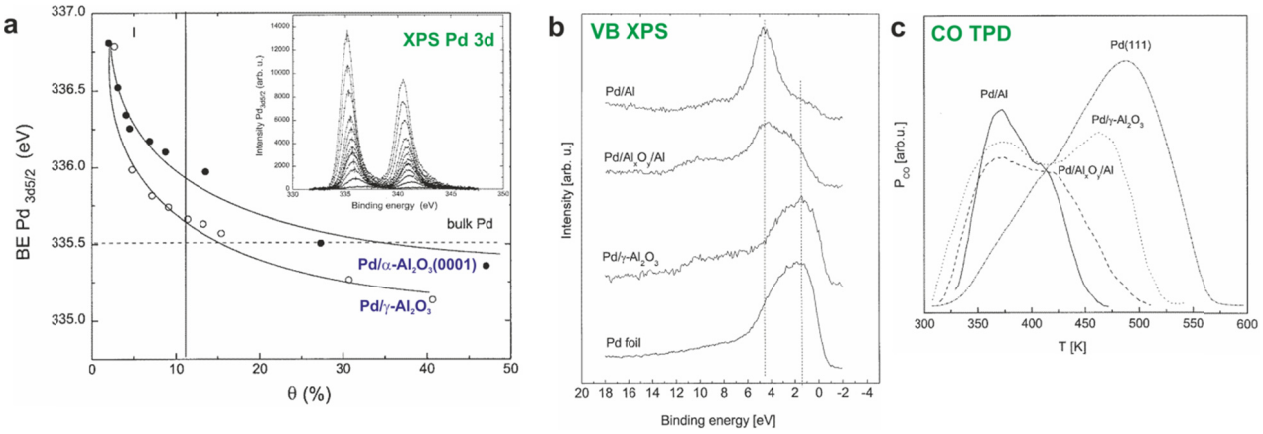

Figure 12: a) Variation of Pd $3d_{5/2}$ binding energy with relative Pd coverage upon growth on γ-Al_2O_3 (open symbols) and α-Al_2O_3 (solid symbols) substrates. The zones I and II based on FWHM analysis of Pd 3d XPS doublet denote the regions of initial growth of three-dimensional clusters (I) and their consequent lateral growth towards flat islands (II); Inset: the series of source XP spectra of Pd 3d obtained on Pd/γ-Al_2O_3 sample. b) Valence band XP spectra and c) corresponding CO TPD spectra of pristine Pd, Pd NPs on γ-Al_2O_3, Pd NPs on partially reduced aluminum oxide, and reference PdAl alloy. Adapted from [26] and [9].

The above conclusion has important consequences for reactivity of these metal–oxide catalysts, as was clearly demonstrated in **Appendix 1** (Ref. [28]). An overview of CO TPD spectra from Pt clusters (average thickness approx. 2 nm) deposited on different types of alumina substrates are compared to Pd(111) single crystal in Figure 13. The spectra exhibit maxima at approx. 450–480 K, depending on CO coverage and Pd cluster sizes (as compared to 480–530 K on Pt). In the desorption spectra of Pd NPs supported on γ-alumina prepared by thermal oxidation of Al a distinct additional peak emerges at ~360 K. It is of different origin than the low temperature shoulder seen

on Pd(111), which is a result of CO–CO repulsion within the dense adsorbate layer at higher coverages. On γ-alumina, the low temperature feature was attributed to intermetallic interaction between Pd and Al centers, present on the slightly non-stoichiometric γ-Al_2O_3 surface. The CO desorption from this surface is accompanied by CO_2 production via CO disproportionation reaction involving CO dissociation [354]. Upon repeating the adsorption–desorption cycles, partial CO dissociation is evidenced by the gradual accumulation of surface carbon (detected by XPS) and the corresponding loss of CO adsorption capacity seen in TPD [9, 25]. Electronic interaction inducing charge transfer from alumina to Pd NP was found responsible for the CO dissociation activity via the modification of back-donation of Pd 4d electrons to empty CO $2\pi^*$ orbitals [28, 355, 356].

The assumption of inertness is reasonably valid for the close-packed oxygen-terminated (0001) plane of the sapphire modification of alumina (α-Al_2O_3) [346-348, 357], which exhibits very similar shape of TPD spectra as seen on Pd(111), with only a slight shift towards lower temperature caused by finite-size effect [94, 222, 352, 358-360]. Yet on the (1-102) plane of stoichiometrically identical alumina the low temperature desorption component is evident, albeit much smaller than on γ-Al_2O_3. However, in contrast to γ-Al_2O_3, the CO dissociation was not observed on this system.

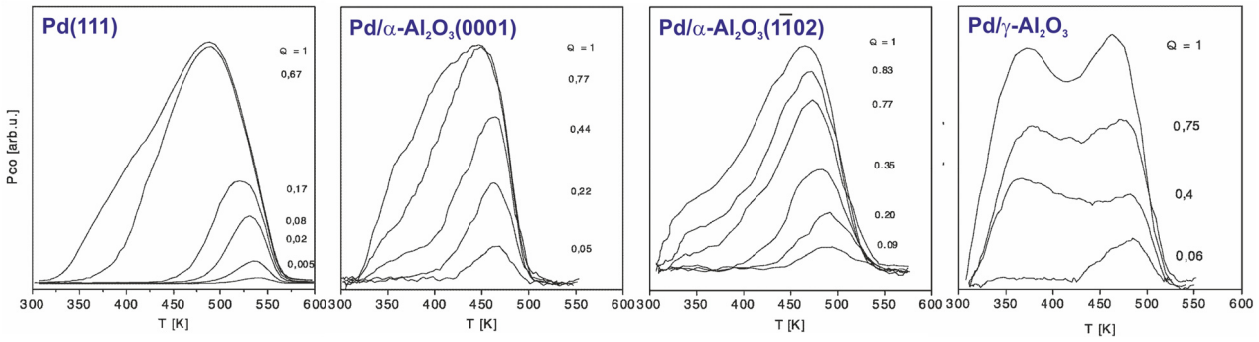

Figure 13: CO TPD spectra (left to right) on Pd(111) single crystal and Pd NPs deposited on α-Al_2O_3(0001), α-Al_2O_3(1-102), and γ-Al_2O_3, measured at different relative CO coverages (indicated in the plots). Adapted from [28].

The role of strong interaction of Pd with Al in adsorption and dissociation of CO was confirmed by intentionally introducing Pd–Al bonds to the catalytic system by 1) partial reduction of a native oxide film on pure Al by ion sputtering (yielding aluminum rich Al_xO_y thin film) or 2) preparation of stoichiometric PdAl bulk alloy to serve as a reference with maximized concentration of Pd–Al bonds [8, 9, 16]. The correlation between the valence band shape and thermal desorption spectra can be seen in Figure 12b and Figure 12c, respectively. The establishment of Pd–Al bonds affects the position of Pd 4d band shifting it to higher BE with increasing intensity of Pd–Al interaction. The formation of this noble metal-like electronic structure characterized by a lower-lying d-band and a partial depletion of density of states near Fermi level affects the CO adsorption strength via weakening of the Pd 4d—CO $2\pi^*$ bonding interaction [60, 82, 361, 362]. As a result, temperature of CO desorption on PdAl is substantially decreased and the low temperature peak near 360 K becomes the dominant component in TPD spectra.

Unlike gas-phase spectroscopies (such as QMS or TOF) applied in above studies, infrared absorption spectroscopy permits direct monitoring of the heterogeneous catalyst surface and its interactions with adsorbed molecules, including reaction intermediates [104, 322, 363], thus providing one of the most powerful tools in catalysis research. By employing *in-situ* IR reflection

absorption spectroscopy on a well morphologically characterized sample, gas-solid interactions and surface reactions can be addressed on a microscopic level. An example of such experiment is shown in Figure 14, see also Refs. [15, 35], description of the experimental system [311] and its drawing in Figure 9. The Pd nanoparticles were deposited by evaporation in UHV at room temperature onto an ordered thin aluminum oxide film grown on NiAl(110) single crystal [232, 364, 365]. Such procedure results in Pd aggregates with well-shaped crystallites (average size of approx. 6 nm), predominantly exposing facets with (111) orientation and a small fraction of (100) facets [92, 366], see the scanning tunneling microscopy (STM) image in Figure 14b and the corresponding atomic model of a single nanoparticle in Figure 14c.

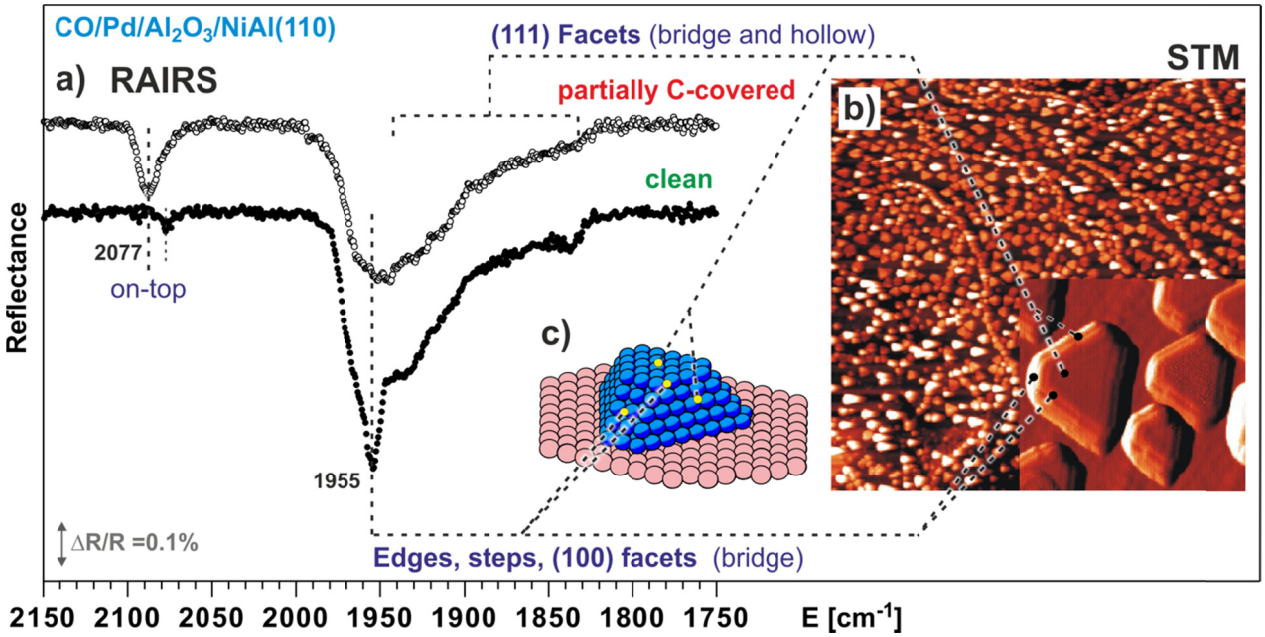

Figure 14: a) RAIR spectra of CO adsorbed at 300 K on $Pd/Al_2O_3/NiAl(110)$ obtained immediately after preparation (open symbols) and after prolonged exposure to methanol at 440 K (solid symbols), b) STM image of the as prepared sample in two magnifications (inset image size 20×20 nm^2), and c) corresponding model of a single nanoparticle. Pd coverage was $2.7x10^{15}$ cm^{-2}, sample temperature during growth 300 K. Partially adapted from [15, 311].

Linking structural and spectroscopic information allows to identify CO adsorbed at various types of surface sites and even in particular adsorption geometries. In Figure 14a, the bottom RAIR spectrum of CO-saturated surface (at room temperature) was obtained on a freshly prepared sample, where most CO adsorbs preferentially at hollow and bridge configurations on (111) facets. The sharp feature around 1955 cm^{-1} reveals additional CO binding to defect sites, mainly Pt atomic steps and particle edges. Upon selective occupation of these low-coordinated surface sites by carbon [15, 35] (as a result of prolonged exposure to methanol at elevated temperature, as will be discussed later in Section 5.2.1) a clear response is seen in the RAIR spectra as the suppression of the 1955 cm^{-1} band, in contrast to the IR band related to the (111) facet which remains nearly unaffected. The emergence of the feature at approx. 2080 cm^{-1} (only very weak on the clean sample at ~2060 cm^{-1}) was assigned to CO bonded to Pd on-top adsorption sites.

Through the combination of precise molecular-beam methods (which provide a maximum level of control over the reactants) with simultaneous RAIRS, angle-integrated and angle-resolved mass spectrometries, both global and local reaction kinetics can be probed under steady-state and

transient conditions [96, 211, 314]. The basic scheme of such experiment, realized in the former Molecular Beam group at FHI-MPG, is depicted in Figure 15e (see also [311] for technical details).

The behavior of the global (angle-integrated) steady-state reaction rate will be discussed briefly later in Section 3.3 (see also Figure 21) and as the part of the methanol oxidation description on the same model catalyst (Section 5.2.1, Figure 28b). In **Appendix 2** (Ref. [43]), the angular distribution of the steady-state production of carbon dioxide desorbing during CO oxidation from oxide-supported Pd nanoparticles has been demonstrated to be size dependent, using the above setup and the evaluation procedure illustrated in Figure 15.

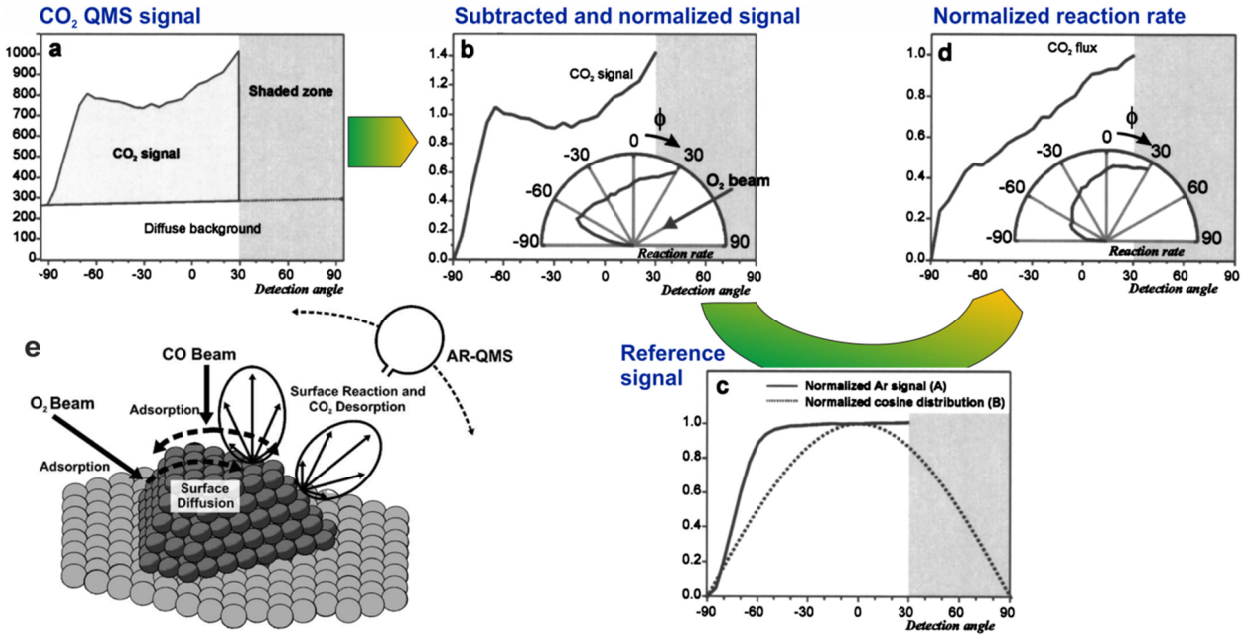

Figure 15: Steps of experimental data analysis of angle-resolved desorption mass spectrometry measurement: a) CO_2 signal measured by the angular resolved QMS between −95°-+95° during the catalytic oxidation of CO on Pd NPs (500 nm diameter) prepared by electron beam lithography on SiO_2; b) normalized signal after background subtraction (inset: polar plot of the same data); c) Ar signal backscattered from an ice covered sample at 100 K compared to theoretical cosine distribution (dotted line); d) angular distribution of the CO_2 desorption rate after correction for the experimentally derived detector function using c) (inset: polar plot of the same data). The signal was instrumentally inaccessible in the gray zone due to the shading of oxygen beam by the AR-QMS. e) Schematic representation of an angle-resolved CO oxidation experiment on a planar model catalyst with supported nanoparticles. Adapted from [43] and [96].

Particle size effects are common phenomena in heterogeneous catalysis [94, 96, 188, 189, 196, 222, 352, 367] and constitute one of the major topics of investigation at present. They are often related to the presence of specific reactive sites on clusters of particular size and structure or to the modification of their electronic or geometric properties due to the limited NP size or due to size-dependent interaction with the support. However, there are also kinetic phenomena which arise solely as result of the limited size of the reaction system like in this case, where surface diffusion on small NPs appears to be confined by their dimension. Unlike for very small NPs (units of nm), on sufficiently large particles (hundreds of nm, see also Figure 21c) regions with different local coverages (depending on the direction of the incident reactant fluxes) can thus develop on NP surface due to the limited surface mobility of adsorbed species, manifesting itself as local reaction rate variations. It result in an asymmetric angular distribution of CO_2 such as shown in Figure 15c is detected.

The variations of the CO_2 angular distribution were analyzed by applying microkinetic simulations as a function of particle size, surface temperature and reactant fluxes, which allowed quantitative calculation of the surface diffusion rates on the catalyst under reaction conditions [41]. It was further shown [43] that the two reaction regimes of the CO oxidation (CO-rich or O-rich) exhibit specific angular CO_2 distributions – while under CO rich conditions, the product distribution strongly depends on the local fluxes of the reactant molecules, under O-rich conditions nearly symmetric distributions are observed. This is in a perfect accord with the higher surface diffusivity of oxygen on Pd, mentioned earlier, as compared to CO. The residence time of oxygen was shown to depend primarily on the surface occupation by CO.

The particular reaction regime also strongly affects the global transient behavior of the supported NP catalyst as a response to abrupt changes of gas flux intensities (both at rising and leading edge of the pulse) [56]. Considering the stronger binding of CO to Pd (and its lower mobility) as compared to O, transition between the kinetic regimes is primarily driven by the surface mobility of CO. Under certain circumstances (ratio of reactant fluxes and surface temperature), a reaction bistability, i.e., spontaneous switching between the different regimes, can even be observed as a result of the coupling of the surface coverages and reaction rates over the particle surface. This extraordinary phenomenon will be described separately in Section 3.3.

3.2.2 CO oxidation on Pt/ceria and Pt–ceria EMSI

Although similar at the first sight to the previous Pd/Al_2O_3 or Pd/SiO_2 model catalysts, supported Pt nanosized particles on ceria represent a strikingly distinct physicochemical system. In contrast to the very inert and stable alumina (Al_2O_3) and silica (SiO_2), ceria (CeO_2) belongs to the class of so-called reducible oxides [368]. These materials, typically characterized by a relatively small band gap (<3 eV), can easily give away oxygen because the lowest available empty states in their conduction band consist of cation *d*-orbitals energetically located only slightly above the valance band. The removal of oxygen thus results in excess electrons which are subject of redistribution to the cationic empty levels, lowering the oxidation state (in the case of ceria from Ce^{4+} to Ce^{3+}) [157, 159, 340, 369]. The consequence to reactivity is that upon changing the oxidation state the metal cation can efficiently trap electrons from donor species adsorbed on the surface or from supported NPs, making these materials very attractive for heterogeneous catalysis [340, 370, 371].

In the article presented in **Appendix 3** (Ref. [11]) we combined several surface science methods to carefully identify adsorption sites participating in CO oxidation on Pt NPs supported on thin-film ceria, oxygen spillover [93, 96, 372] between the two components, and their mutual electronic interaction. Infrared reflection absorption spectroscopy (RAIRS) was used as a main tool in assignment of different adsorption sites. On pristine ceria CO adsorbs only weakly at structural defects (steps, edges) and Ce^{3+} centers. The occupation of these sites changes upon thermal treatment. After deposition of Pt clusters, CO primarily occupies Pt surface in 3 different configurations (on-top at particle edges and steps, on-top on Pt(111) facets, and bridge-bonded), while the bonding to defects and Ce^{3+} cations is suppressed due to preferential nucleation of Pt at these sites, making them unavailable for CO adsorption.

Upon surface exposure with CO at low temperature (150 K) followed by TPD (with a linear heating ramp 1K/s), apart from molecular desorption of adsorbed CO, a production of CO_2 can also be seen. This happens via oxygen reverse spillover [372] from the ceria support to the Pt particles at elevated temperatures and its recombination with adsorbed CO molecule. The oxygen spillover has been evidenced directly by RAIRS through an emergence of new absorption bands indicative of

metal-oxide interaction [11]. This process is thermally activated between 400–500 K, overlapping with the CO desorption temperature from Pt. As a result, part of CO desorbs whereas the remaining molecules recombine with the spilt-over oxygen to form CO_2. Both desorbing species are observed by TPD accordingly below 500 K. With the increasing number of consecutive TPD cycles the amount of CO_2 steadily decreases (see Figure 16, top), indicating the irreversible depletion of oxygen from the CeO_2 support and thus formation of oxygen vacancies [159].

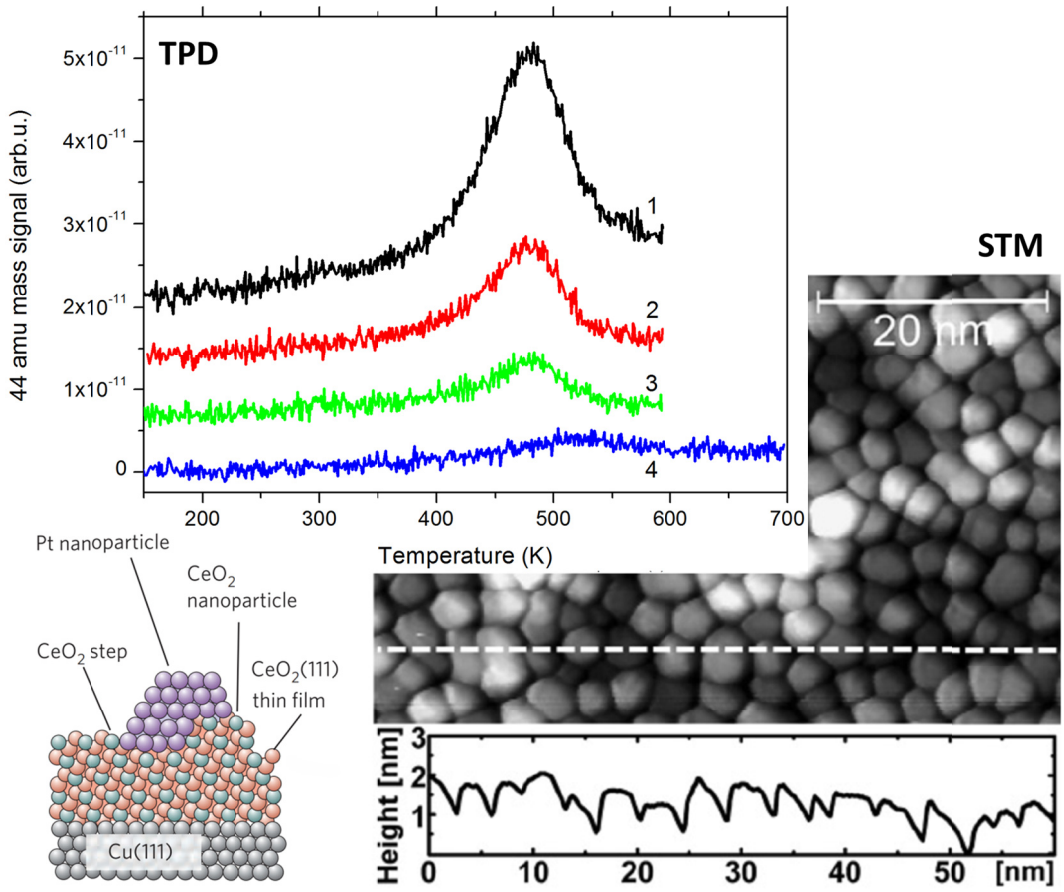

Figure 16: Four consecutive cycles of CO_2 TPD performed on Pt nanoparticles (average thickness 0.85 Å) deposited on 5 ML CeO_2(111) on Cu(111). CO exposure was 18 L at 150 K in all cases. STM image (right) shows the morphology of the as-prepared sample. The schematic representation of the sample structure (cross section through a Pt NP occupying a ceria step) is shown in the bottom left corner. Partially adapted from [11].

In principle, the intrinsic catalytic properties of a solid material are determined completely by its electronic structure which is, in turn, governed by its composition, physical structure and its flexibility. A strong metal–support interaction (SMSI) exists between late transition metal nanosized particles and ceria that can, for very small NPs, produce large electronic perturbations and significantly affect the reactivity [373-375]. In the preceding work [332] it was shown that electron transfer occurs from the Pt nanoparticles to the CeO_2 support upon Pt deposition. This effect leads to the buildup of a positive charge carried by the platinum NP and the simultaneous formation of Ce^{3+} centers in the vicinity of NP perimeter, in accord with the observed defect formation on ceria substrates due to electron localization [159].

SMSI was first termed by Tauster et al. [377] and later generalized to account for changes in catalytic activity and selectivity due to interaction of, typically, group-VIII metals with reducible oxide supports, whose surfaces can be reduced to form cations with lower valences [362, 378]. For

example, a strong enhancement in the ability of the admetal to dissociate the O–H bonds in water was demonstrated on the $Pt/CeO_2(111)$ model system, making this mixed metal–oxide an exceptionally active catalyst for the production of hydrogen [374]. SMSI is also beneficial in maintaining very fine metal dispersion and its stabilization against thermal sintering [375]. At high temperatures (and especially under oxidizing conditions), the metal adatoms or clusters become mobile and can coalesce to larger particles, which irreversibly reduces catalyst performance [287]. This sintering is often size-dependent [92, 285] and its magnitude strongly depends on the interaction strength between the metal and the support. Strongly interacting oxide such as ceria can anchor noble metal (N) clusters via forming N-O-M surface complexes (M – oxide cation), preventing the undesired sintering, as illustrated in Figure 17 [376, 379]. It can even facilitate redispersion of the metal component by emitting mobile oxidized species from the parent NP which are then effectively trapped by the support, forming stabilized single-atom active centers [380]. Ceria was found capable of stabilizing NPs in even more harsh electrochemical environments [381, 382].

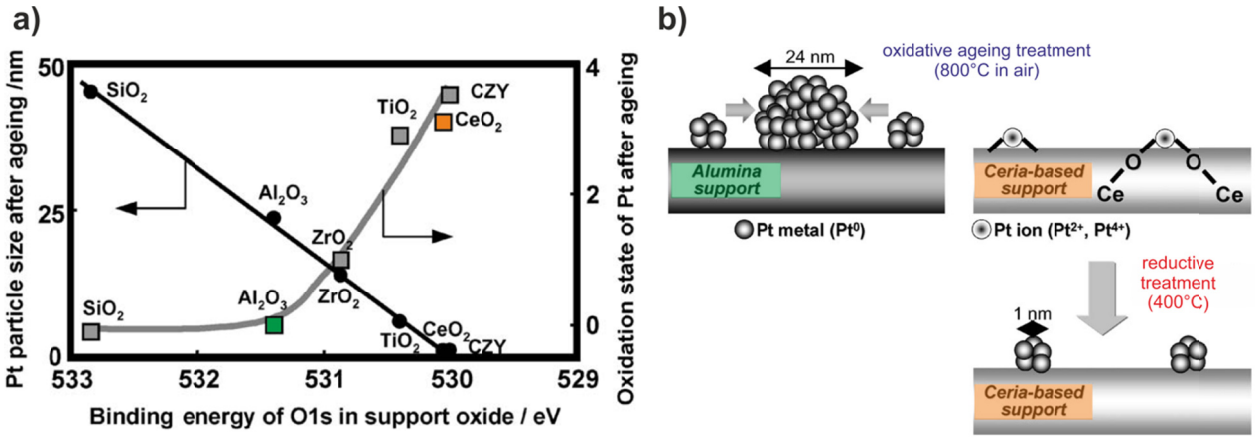

Figure 17: a) Pt–oxide-support interaction and its relation to Pt sintering in an oxidizing atmosphere (800°C in air). The binding energy of the O 1s electronic level in the oxide support (measured by XPS) reflects the interaction strength, the oxidation state of Pt after aging was quantitatively evaluated from the white line intensity of the Pt L3-edge in XANES, Pt particle size was estimated by CO titration method. b) Model illustration of the Pt sintering on a conventional Pt/Al_2O_3 catalyst and its inhibition mechanism for a Pt/ceria catalyst. Since the $Pt–Al_2O_3$ interaction is weak, Pt metal particles are formed and suffer from sintering upon heating in oxidizing atmosphere. In contrast, strong Pt–ceria interaction generating Pt–O–Ce bond prevents Pt particles from sintering during the aging treatment. After the reductive treatment, the Pt–O–Ce bond breaks, and Pt metal particles remain highly dispersed on the support. Adapted from [376].

The overall surface reactivity is, however, a complex phenomenon involving not only the electronic properties but also structural and size effects. It can be illustrated on the previous example of the Pt/CeO_2 model system – the oxygen transfer across the Pt/ceria boundary is a pure nanoscale effect, despite the fact that the electron transfer occurs both on extended ceria surfaces and on ceria nanoparticles [332]. Hence the oxygen spillover to Pt requires nanostructured ceria or ceria nanoparticles in direct contact with metal NPs. The above can be generalized to other similar systems. The vital importance of the metal–support interface in oxygen storage and release was also demonstrated for Fe_3O_4 support and Pd NPs [186, 383, 384], where the interfacial mechanism of oxygen exchange, involving formation of PdO_x interface layer, was found to be strongly NP size-dependent [186, 266, 385], with a distinct maximum of oxygen uptake for NPs around 6-7 nm in diameter [186]. Similarly, ultrasmall gold clusters (tens to hundreds of atoms) on ceria showed size-dependent structural responses to the reactant gas. Reversible transformation from ordered to disordered state with generation of low-coordinated atoms was observed under the catalytic working

condition of carbon monoxide oxidation. These dynamic low-coordinated atoms, formed via gold-carbonyl species, can act as dynamic active centers for CO oxidation, effectively boosting the reaction [386].

In the work [45] attached as **Appendix 4**, the powerful combination of microscopic (STM) and spectroscopic (SRPES, RPES) methods with theory (DFT) led to a first-ever quantification of the charge transfer (CT) between a support and nanoparticles of catalytically relevant sizes. The average size of Pt clusters was calculated from the particle density determined by STM and the total coverage derived from XP spectra, calibrated over the images of larger metal loadings providing better accuracy. Analysis of particle density and average thickness of metal deposit clearly reveals the regions of nucleation (~1 nm NPs with up to ~25 atoms/NP), particle growth (up to about 400 atoms/NP), and coalescence.

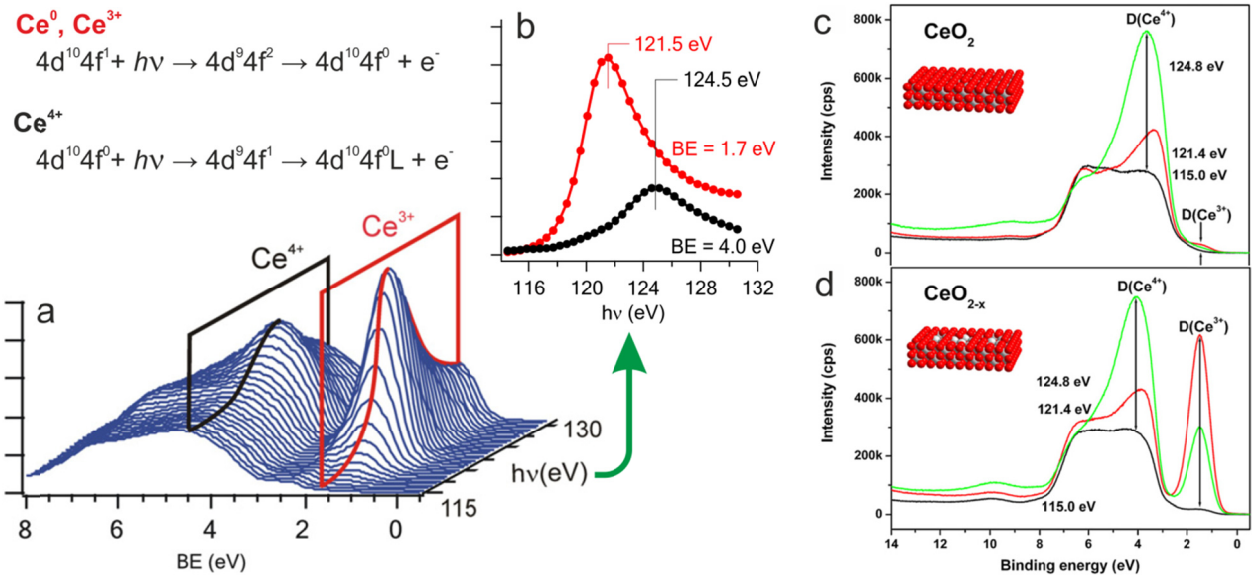

Figure 18: The principle of resonant photoemission spectroscopy (RPES) method applied to cerium oxides. It is based on selective resonant excitations 4d–4f in Ce^{3+} ($4d^{10}4f^{1}$) and Ce^{4+} ($4d^{10}4f^{0}$). The excited states ($4d^{9}4f^{2}$ and $4d^{9}4f^{1}$, respectively) decay via Super-Coster-Kronig processes, leading to a strong enhancement of certain valence band features. For Ce^{3+}, the resonance gives rise to a feature at 1.7 eV binding energy (BE), with a maximum enhancement at photon energy (PE) of 121.5 eV, whereas for Ce^{4+}, the feature appears at 4 eV BE with the maximum enhancement at 124.8 eV PE. a) Series of valence band photoelectron spectra in the Ce 4d–4f photoabsorption region of partially reduced cerium oxide, b) PE dependence of signal intensities at BE of the Ce^{4+} feature (black) and the Ce^{3+} feature (red). The level of reduction is quantified by so-called resonant enhancement ratio (RER) defined as $D(Ce^{3+})/D(Ce^{4+})$ derived from spectra measured at both resonant conditions (green and red curves) and off the resonance (black curve), as depicted in c) and d) [32, 230, 333]. Partially adapted from [333].

Since the electronic MSI (EMSI) [373] between the oxide surface and the admetal leads to electron transfer across the metal/oxide interface, reducing corresponding number of nearby Ce^{4+} cations to Ce^{3+}, it can be directly monitored by photoelectron spectroscopy. Apart from the associated changes in core level spectra of Ce 3d and 4d [230, 333, 387], which are rather complicated and difficult to be quantitatively analyzed, resonant photoemission spectroscopy (RPES) offers an extremely sensitive tool for this purpose [230, 332, 333]. The electronic structure of CeO_2 is characterized by unoccupied 4f states of Ce^{4+} ($4d^{10}4f^{0}$) while the Ce_2O_3 carries Ce^{3+} ($4d^{10}4f^{1}$) configuration [388], resulting in different structures of the valence band. The net amount of transferred charge is then derived from the enhancement of the corresponding 4d→4f resonance in the valence band photoemission spectra of Ce^{3+} ions within ceria with respect to the Ce^{4+} resonance [333] – see

Figure 18 for explanation of the experimental determination of the resonant enhancement ratio (RER).

As can be seen in Figure 19, the partial charge per Pt atom reaches a maximum for a particle consisting of approx. 30–70 atoms (yielding CT equivalent to about 1 electron transferred per 8 atoms), representing a region of the strongest EMSI. With increasing doses of platinum the total amount of charge transfer reaches saturation (at approx. 1.2×10^{18} m^{-2}, corresponding to about 17% of the surface cerium ions), denoted as the charge transfer limit.

The experimental results are complemented by theoretical models, suggesting that the charge transfer can have a profound influence on adsorption and, hence, reactivity. The adsorption energy of CO and H_2O on Pt/CeO_2 can be enhanced by as much as 0.5 eV due to charge transfer, whereas the bonding of oxygen on the same surface remains essentially invariant. With the potential relation between the electronic structure and reactivity, the above mechanism offers a straight-forward handle for effectively tuning catalytic properties of a metal-oxide system.

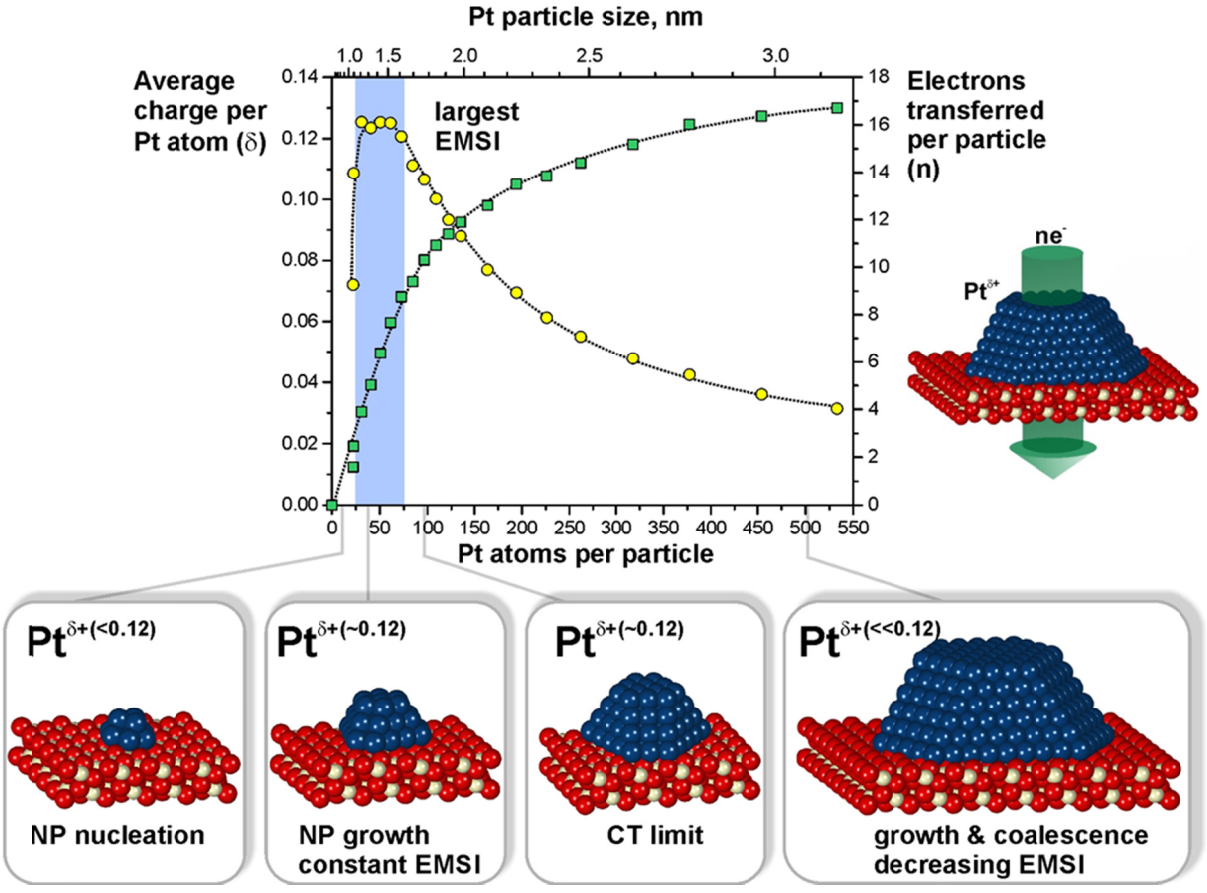

Figure 19: Charge transfer (CT) from Pt NPs to ceria support quantified in terms of electrons per Pt particle (n, green symbols) and per Pt atom (δ, yellow symbols) as a function of Pt particle size. The schematic models (bottom) represent structures in different particle size regions. Adapted from [45].

3.2.3 CO oxidation on platinum oxide

A direct implementation of platinum oxides (PtO_x) in catalysis is not very common, however, since Pt is probably the most frequently used metal catalyst, PtO_x has undoubtedly its relevance as well, because a substantial fraction of industrial catalysis is dealing with oxidation reactions or oxidative

dehydrogenation processes. Due to the oxidizing environment platinum may exist in the form of an oxide rather than metal [389]. Moreover, since the active metallic material is often deposited in highly dispersed form on an oxide support, the oxygen can also be diffusively interchanged with the substrate, especially in the case of reducible oxides such as CeO_2, TiO_2, WO_3, NiO, Fe_2O_3, Co_3O_4, etc.[157], as was thoroughly discussed and demonstrated in the previous section. Therefore, in most cases the active "live" catalyst actually comprises an oxide or a metal–oxide compound, and the reaction follows the sacrificial Mars–van Krevelen (MvK) mechanism [216] in which the oxide is directly involved in reaction via its most reactive oxygen atoms, typically those at undercoordinated defect sites or oxide–metal interfaces [111, 158, 186].

In the study presented in **Appendix 5** (Ref. [48]) platinum oxide was deposited *ex-situ* by reactive RF magnetron sputtering from a cylindrical target [236, 241] on a flat (oxidized Si wafer and polycrystalline Ta) and highly porous (multi-walled carbon nanotubes, MWCNTs) substrates [390-393]. Unlike the highly-ordered model systems described so far, such thin films, especially in the latter case, mimic the complex porous structures of real catalysts while still being accessible for reliable surface characterization. The catalytic layers were examined by X-ray photoelectron spectroscopy (XPS), scanning electron microscopy (SEM), temperature-programmed desorption (TPD), and temperature-programmed reaction (TPR) in both UHV and ambient pressure conditions. This research thus represents an example of a successful approach in, to a certain extent, bridging both materials and pressure gaps mentioned above in Section 2.3.

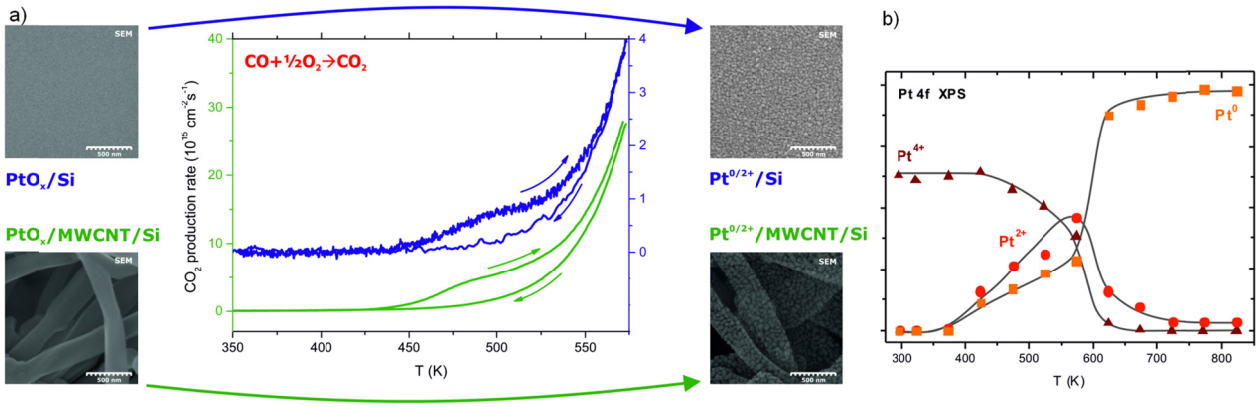

Figure 20: a) Temperature-programmed atmospheric-pressure CO oxidation, comparing reaction rates of CO_2 production on PtO_x/MWCNT/Si (green curve) and PtO_x/Si (blue). The four micrographs present SEM images of both respective samples in as-deposited form (left) and after the reaction (right); image size 1500×1500 nm^2; b) Evolution of the individual components of Pt 4f XP spectra of PtO_x thin film with temperature during annealing in vacuum. The gradual transition from fully oxidized Pt (Pt^{4+}) to metallic platinum (Pt^0) through an intermediate Pt^{2+} oxidation state is observed. Adapted from [48].

As can be seen in Figure 20a, using a highly porous but relatively inactive support such as MWCNTs can significantly enhance the overall reaction yield (owing to its high specific surface area) while following the same reactivity pattern as on a planar surface. This is what effectively diminishes the materials gap issue, because the flat samples can be much more easily characterized by standard tools of surface science.

On pure platinum, CO_2 is generated through Langmuir-Hinshelwood (LH) mechanism between adsorbed CO and O, with oxygen dissociation being the rate limiting step [115, 394, 395]; at lower temperatures the rate of this reaction route becomes very limited due to the surface blocking by adsorbed CO. On partially reduced platinum oxide, on the other hand, the CO oxidation is

governed by bifunctional mechanism where CO adsorbed on a metallic platinum site reacts with nearby oxygen bound to a cationic Pt center, which is continuously re-oxidized through Mars-van Krevelen process [216] as long as a sufficient partial pressure of oxygen is provided. This allows achieving much higher (over an order of magnitude) reaction rates at low temperatures (i.e., below ca. 475 K) as compared to pure platinum. XPS data (Figure 20b) show the co-existence of metallic and cationic Pt in this temperature region and give an evidence of the irreversible reduction of the thin film when the surface temperature is exceeded above this point.

3.3 Nonlinear reaction dynamics on nanoparticles

In the second part of Section 3.2.1 we focused mainly on angle-resolved measurements of steady state reactivity of CO oxidation on the $Pd/Al_2O_3/NiAl(110)$ model catalyst. The kinetics of this reaction was also systematically examined as a function of surface temperature, CO-to-O_2 reactant ratio, and metal particle size. Both transient and steady state behavior can be characterized by modulating the molecular beams and varying sample temperature while measuring integrated QMS signals (see Figure 27 below for an example of such experiment). By analyzing the steady-state kinetics of CO oxidation on supported Pt nanoparticles an existence of two distinct reaction regimes is revealed [396]: under CO rich conditions (i.e., high values of CO fraction in the total flux, x_{CO}), the oxidation reaction is partially inhibited due to limited oxygen adsorption on surface precovered by CO, effectively blocking most of the adsorption sites. The inhibition is stronger the lower is the surface temperature through the temperature dependence of CO desorption kinetics. In the oxygen-rich regime, on contrary, linear dependence is observed because the rate determining step of the reaction is the adsorption of CO, which is governed primarily by the O_2 flux (CO sticking coefficient is rather large under the given conditions). The typical shape of CO oxidation rate versus x_{CO} can be seen in Figure 21d for temperatures between 440–465 K (upper 3 curves).

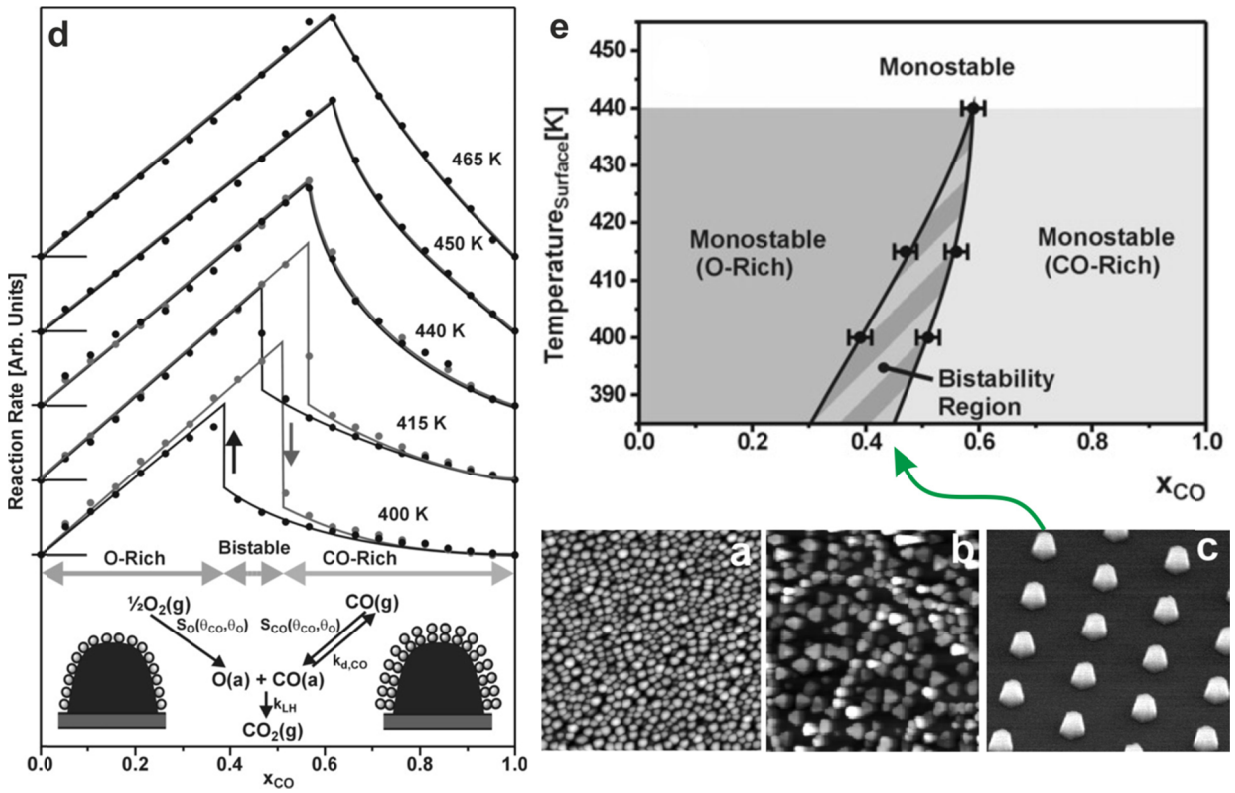

Figure 21: Three types of supported Pd model catalysts with different average particle sizes: a) 1.8 nm Pd/Al_2O_3, (prepared by vapor deposition and growth), b) 6 nm (preparation as in a)), and c) 500 nm (Pd/SiO_2, prepared by

electron beam lithography). d) Series of CO oxidation reactivity curves as a function of the CO fraction in the impinging gas flux (x_{CO}, total flux equivalent to a local pressure of 10^{-4} Pa) for five temperatures (in 400-465 K range), showing chemical bistability during CO oxidation on a Pd model catalyst (system presented in c)). At sufficiently high surface temperatures, a single well-defined transition point between two (CO- and O-rich) reaction regimes exists; below 440 K a region with two stable reactive states occurs, depending on whether approached from CO-saturated or O-saturated surface (the arrows indicate the direction of the hysteresis). e) Corresponding bistability diagram for the CO oxidation on the above model catalyst. Partially adapted from [3].

A striking deviation from the otherwise well-defined transition point between the two reaction regimes is observed with sufficiently large Pd particles (such as in Figure 21c) and sufficiently low temperatures (in this case below 440 K). As indicated by the lower 2 curves in Figure 21d, the steady state near the transition point differs substantially depending on whether it is approached from an oxygen-precovered or CO-precovered surface. This effect, known as reaction bistability, previously observed [397-399] and simulated [398, 400-402] on well-ordered single crystals, was witnessed for the first time on supported nanoparticles of a well-defined model system, as presented in **Appendix 6** (Ref. [3]).

Time oscillatory phenomena in chemical reactions have already been known since 19th century in electrochemical systems [403] and somewhat later (1920s) observed in the liquid phase chemistry [404]. Oscillatory reactions, however, did not receive much attention until the discovery of Belousov–Zhabotinskii reaction in the 1950s [405-408]. In heterogeneously catalyzed reactions, rate oscillations were first observed in CO oxidation on platinum in the early 1970s [397, 409]. The switching between different steady states of a surface reaction was also found as a consequence of coupling between regions exposing different crystal planes of the same material, such as in the works of Ertl et al. [97, 410], who (in the late 1980s) pioneered the imaging of surface reactions [97, 411] leading to discovery of spatio-temporal pattern formation in heterogeneous catalytic systems [97, 411-413]. It was soon realized that such oscillatory systems belong to a whole class of self-organization phenomena with many instances in chemistry but even far beyond this field (including biology [414, 415] or social sciences [416]). A common denominator of all these systems is that they require conditions far from thermodynamical equilibrium [417] and that the underlying rate equations be nonlinear [397, 412, 415, 417-419].

In this particular case, the origin of the two metastable kinetic states is the following: Under sufficiently high oxygen flux, the Pd NP surface is to a large extent covered by adsorbed O (O_{ad}) and because sticking probability of CO is only moderately influenced by O_{ad}, the reaction rate is high and nearly proportional to CO flux. Above certain critical value of x_{CO} in the gas beam, a kinetic phase transition [398] to predominantly CO-covered surface occurs, yielding much lower reaction rate, because adsorbed CO efficiently inhibits dissociative adsorption of O_2.

Furthermore, size dependence of the reaction bistability was scrutinized, employing Pd NPs prepared by vapor deposition and growth on Al_2O_3, (1.8 nm and 6 nm average diameter, respectively), as well as the aforementioned much larger monodispersed 500 nm Pd NPs prepared by electron beam lithography on SiO_2 – see the micrographs of all three samples in Figure 21a-c. The above well-defined bistability window observed on the 500 nm particles (see the diagram in Figure 21e) was found to be much narrower for 6 nm NPs and seemingly non-existent for the smallest (1.8 nm) and the least ordered NPs, in agreement with theoretical predictions [400].

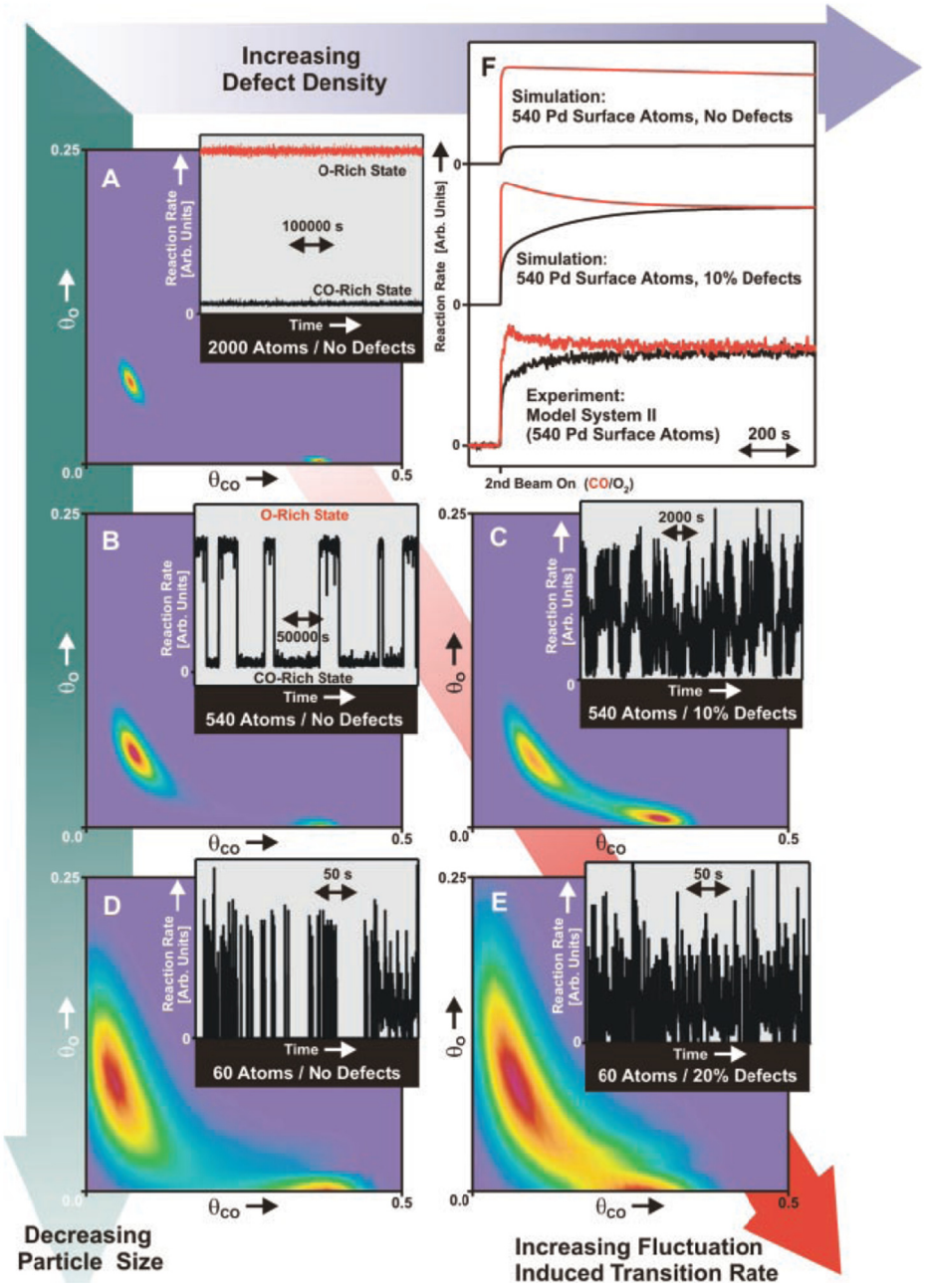

Figure 22: Overview of stochastic mean field simulations, illustrating the combined effect of limited particle size and surface defects on the kinetic bistability of CO oxidation reaction. The heatmaps in a)-e) represent probability distributions in the CO and O coverage space, the insets show the reaction rate on an individual particle for each case. The width of the probability distributions grows with decreasing NP size and increasing density of defects, due to the higher amplitude of fluctuations leading to spontaneous transitions between both reaction regimes. For an ensemble of particles, this results in establishing a dynamic equilibrium between both states. f) The experimental integral reaction rates for 6 nm NPs are compared to the stochastic model, showing that a substantial fraction of defects has to be added to the model in order to reproduce the experimentally observed relaxation times. Adapted from [3].

In fact, a thorough inspection of transient reactivity data [3, 43] revealed that although different reaction rates are initially established by either starting from O- or CO-rich conditions, these differences vanish over a time period strongly varying with the NP size and the concentration of defects on them, see Figure 22. On the largest particles the two states are essentially stable on the timescale of the experiment, while on the smallest ones a common steady state is reached within a few tens of seconds. It has already been known from literature that coupling multistable kinetics to surface diffusion opens up the possibility for the formation of chemical waves and their propagation

over the surface [398, 420, 421], initiating spontaneous transitions from one kinetic regime to the other without an external stimulus. The above mentioned series of experiments supported by theoretical microkinetic modelling lead to a discovery of a relation between the local fluctuations of coverages of adsorbed reaction intermediates and the timescale of these transitions. It was shown that the amplitude of coverage fluctuations increases with both decreasing particle size and increasing surface defect concentration. The impact of adsorbate fluctuations on chemical oscillations far from equilibrium was shortly after supported by microkinetic Monte Carlo simulations of CO oxidation by Zhdanov and Kasemo [422].

3.4 NO_x reduction on Pd/alumina

In contrast to oxidation of hydrocarbons and carbon monoxide which is fairly straightforward, direct reduction of NO_x under lean conditions in modern "lean-burn" diesel engines is a very difficult task [335, 423]. Selective catalytic reduction (SCR) of nitrogen oxides to harmless N_2 and H_2O or O_2 mixture has been the most often realized by injecting a gaseous reductant (usually ammonia or urea [424]) to the exhaust stream; More recently, SCR by hydrocarbons [425, 426], CO (present naturally in the exhaust flux) [427], both leading to additional side-products (mainly CO_2), or the most environmentally friendly reduction by H_2 [423] has been employed. Other reaction routes without the need for an additional reductant have also been explored. Probably the most traditional are Rh-based systems [428] but other noble metals like Pt or Pd [429] have been utilized as well. Often the structural properties of the catalyst surface governing its de-NO_x activity and selectivity (size effects, involvement of different reactive sites and their interplay etc.) are optimized empirically and explanations of microscopic origins of reactivity are in most cases lacking.

A molecular-level characterization of NO interaction (adsorption, dissociation, reduction) with Pd NPs supported on well-ordered alumina (Al_2O_3/NiAl(110)), similar to that referred to earlier in Section 3.2.1 (Figure 14), is part of the work published in [4], included herein as **Appendix 7** (see also related Refs. [5, 6, 29]). RAIR spectroscopy combined with molecular beams (similar setup like in Section 3.2.1) was used to reveal that specific atomic adsorbates, which are often present under reaction conditions, tend to bind to specific sites of the catalyst. Their presence or absence in the vicinity of these sites can, in turn, control the kinetics of the reaction.

A reference experiment on pristine Al_2O_3/NiAl(110) surface [5] showed that NO slowly decomposes at low temperature (100 K) at oxide defect sites (probably along the antiphase domain boundaries), producing a variety of N_xO_y surface adspecies, accompanied by strong structural transformations of the alumina thin film. NO decomposition and reduction to N_2O proceeds via formation of NO dimers, leaving adsorbed oxygen on the surface. By adding platinum this decomposition processes is strongly suppressed due to the preferential coverage of the active sites by the metal deposit. NO adsorption is then observed to occur on the Pd particles only, preferentially populating edge and defect sites, which was also confirmed by isotopic exchange experiments (using ^{14}NO and ^{15}NO) probing the exchange of adsorbed NO with the gas phase. Above 300 K the adsorbed NO dissociates; the dissociation activity on the supported Pd NPs is strongly enhanced as compared to planar Pd surfaces with preferential N-O bond scission at particle edges and steps.

It was further found that the presence of the dissociation products (atomic nitrogen and oxygen) in the vicinity of particle edges and steps controls the NO dissociation activity. Specifically, with the presence of strongly bound atomic nitrogen the probability of NO decomposition is greatly enhanced. The oxygen-precovered surface results in the formation of a mixed adsorbate layer with a

higher population of on-top sites by NO. The NO adsorption at particle defects is strongly inhibited due to the strong interaction of oxygen with these types of sites. NO adsorption on a CO adlayer, on the other hand, gives rise to a compression of the CO layer and a partial shift of the CO adsorbate distribution from the bridge-bonded coordination at particle edges and hollow coordination at (111) facets towards the on-top sites.

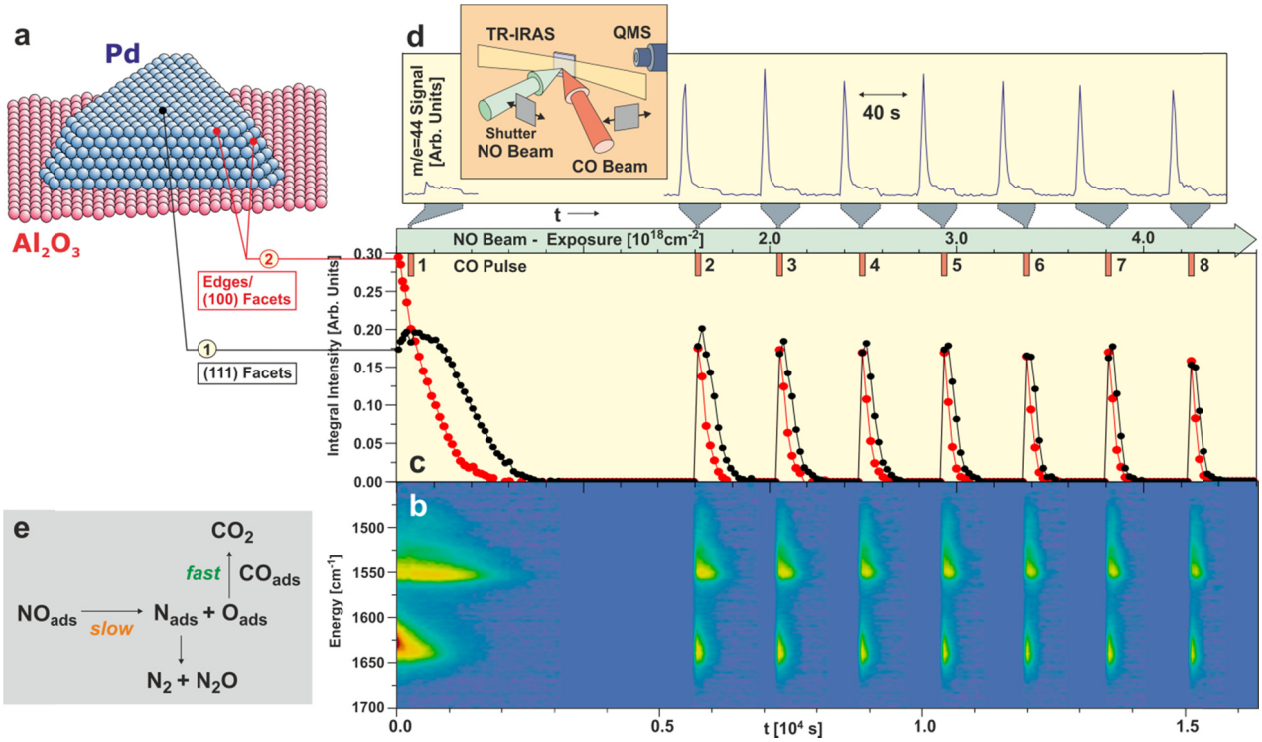

Figure 23: a) Schematic representation of an ordered Pd nanocrystalline particle on a flat Al_2O_3 support, exposing (111) and (100) facets. b) Time resolved RAIRS experiment showing the development of the NO absorption bands (labelled 1 and 2) as a function of NO exposure (x_{NO}) and CO pulsing, c) integral intensity of the two absorption bands in the N–O stretching-frequency region, d) CO_2 mass spectrometer signal recorded during CO pulsing (with scheme of the experimental setup inset). e) Corresponding reaction scheme. Partially adapted from [6].

The above spectroscopic identification of NO adsorption, dissociation, and co-adsorption with O and CO formed a basis for the investigation of the kinetics of thermal NO decomposition process. The IR absorption bands previously assigned to NO binding to threefold hollow sites of (111) facets and to lower-coordinated sites at minority (100) facets, edges and defects, respectively, were monitored by in-situ during NO decomposition by time-resolved RAIRS (TR-RAIRS) at 450 K (here referred to as band 1 and 2, see Figure 23). With continuing exposure an overall loss of NO adsorption capacity is observed, attributed to the accumulation of dissociation products (atomic nitrogen and oxygen) on the NP surface, mainly oxygen, because most of the nitrogen desorbs at 450 K via formation of N_2 or N_2O [430, 431]. This happens preferentially at particle edges (absorption feature 2), leading to faster decay of this IR band as compared to the feature 1, and further confirmed by using CO as a probe molecule [4]. This observation is consistent with an STM study of oxygen adsorption on the same Pd model catalyst, showing preferential adsorption of oxygen at the particle edges [432].

Some strongly adsorbed nitrogen species can, however, remain on the surface [431, 433]. To investigate the potential role of nitrogen adsorbate in the NO adsorption and dissociation kinetics, the initial decomposition was continued with a cycled CO titration experiment as presented in

Figure 23. Short CO pulses were periodically applied to the saturated sample by a second beam source, resulting in efficient removal of the adsorbed oxygen through oxidation to CO_2 [211]. The corresponding CO_2 signal detected by the quadrupole mass spectrometer (Figure 23d) represents the amount of initial oxygen coverage prior to the pulse onset. After the oxygen removal the intensity of the IR band 1 is restored completely unlike the band 2 which is only restored to about 60% of its original intensity. It reveals the presence of strongly bound nitrogen species in the vicinity of NP edge sites partially inhibiting the NO adsorption. The striking observation is that, despite the lower adsorption capacity, the adsorbed nitrogen dramatically increases the rate of NO dissociation (about 5-fold) as can be seen from the much steeper decay of the intensities of both IR bands.

4 Surface chemistry of water

4.1 Motivation and background

As one of the constituents of Earth atmosphere and the most abundant compound in the biosphere, water is essential for all life processes and thus has to be taken into consideration in virtually any environmentally relevant research. Therefore the water–solid interaction has been a topic of interest in a wide variety of scientific disciplines and is one of the most studied adsorption cases since the establishment of modern surface science [434, 435]. The contact layer between water and metals, semiconductors, and oxides [435] is of fundamental importance with respect to issues of corrosion, surface passivation, reoxidation, catalytic activity etc. Regarding the field of heterogeneous catalysis, understanding water-surface interactions is highly relevant in huge number of situations such as water-gas-shift (WGS) reaction, reforming of hydrocarbons, water splitting, automotive exhaust catalysis and many others. Water can be present in catalytic processes in the role of an active agent, intermediate, reaction by-product, chemical medium, or carrier. It is also vital in most electrochemical applications, including the massively expanding field of the fuel cell technology [436]. Last but not least, water molecule also proved an excellent probe for characterization of surface properties like catalytic reactivity, adsorption capacity and competitive coadsorption phenomena, distribution of surface sites, redox processes, role of surace defects, electronic corrugations and charge transfer, etc. [434].

4.2 Water interaction with ceria

Catalysis by ceria represents a very rich matter and thus has been a focus of a number of reviews, see e.g. [340, 370, 371] and references therein. Even on the nominally simple systems of pristine cerium oxides the interaction with water involves quite complex behavior, depending on the oxide structure and stoichiometry. As was already mentioned above, many unique properties of this compound stems from its facile reducibility, making ceria what we call an oxygen buffer. A typical descriptor of the reducibility of an oxide is the cost of oxygen vacancy formation, which measures the tendency of the oxide to lose oxygen or to donate it to an adsorbed species with consequent change in the surface composition. The oxide reducibility can be modified in various ways, for instance, by bulk doping, presence of another metal (see e.g. Section 3.2.2 or Ref. [158]), and/or nanostructuring (as in Section 5.2.3).

Several studies by photoelectron electron spectroscopy [160, 437-440] in accord with first principle calculations [440, 441] suggest that bonding of water to metal surfaces is governed by a complex interplay of a number of factors affecting balance between interaction of water with the surface and via hydrogen bonding with other water molecules. Ambient pressure XPS applied to metals and

oxides [292] confirmed a general trend in water adsorption through an initial formation of hydroxyl group, complemented by molecular water adsorption. With Ru(0001) substrate [442], the surface hydroxyl groups together with adsorbed molecular water were observed only for slightly reduced cerium oxide (CeO_x), whereas on the stoichiometric ceria (CeO_2) only the molecular species were detected. In the former case the OH groups are assumed to be bonded to cerium at the oxygen vacancy site and the released hydrogen atom to nearby surface oxygen of the oxide. A similar conclusion was made for the CeO_x/Au(111) system used in WGS reaction [443]. This process can ultimately lead to full oxidation of the surface.

In **Appendix 8** (published in [32]) this mechanism has been verified thoroughly on ordered cerium oxides using photoelectron spectroscopies (XPS, SRPES, and RPES), scanning tunneling microscopy (STM), and temperature programmed desorption (TPD). The CeO_2 thin film model catalyst was prepared by deposition of ceria in oxygen atmosphere onto a Cu(111) single crystal [148, 444, 445]. By Ar^+ sputtering of this surface with carefully controlled ion doses (followed by mild annealing to heal the surface) oxygen vacancies were generated, yielding a sub-stoichiometric CeO_x thin film. RPES method already described in Section 3.2.2 provided surface-sensitive quantification of the concentration of surface vacancies exposing trivalent cerium cations [439].

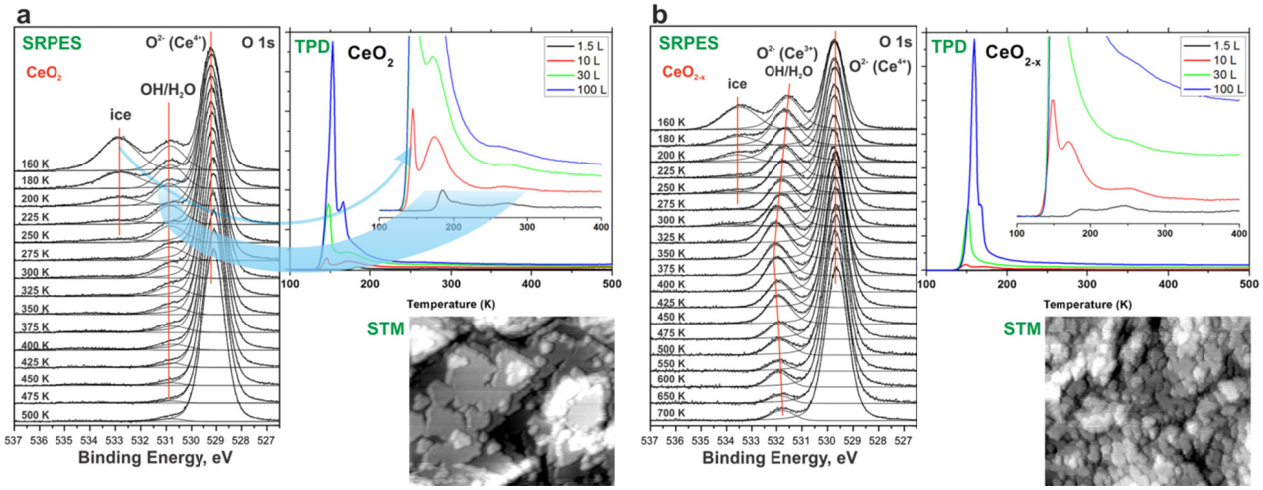

Figure 24: Comparison of water interaction with stoichiometric ceria (CeO_2, panel a) and partially reduced cerium oxide (CeO_{2-x}, panel b) on Cu(111) as observed by SRPES and TPD methods. O 1s core level photoelectron spectra were acquired during stepwise annealing of the respective oxide thin film following exposure to approx. 10 L of H_2O at 160 K, with photon energy of 650 eV. Series of thermal desorption spectra (signal of mass 18 amu) were acquired after various water doses (1.5 L, 10 L, 30 L, and 100 L) at 100 K on both stoichiometric (a) and partially reduced (b) surfaces. The STM images show morphology of as prepared samples before the water exposure; image size 50x40 nm. Adapted from [12] and [32].

The stoichiometric ceria layer exhibits relatively flat morphology with oriented CeO_2(111) terraces, while the ion sputtered CeO_x surface comprises small islands with a characteristic diameter <5 nm, see the STM images in Figure 24. At low temperatures (<120 K) water adsorbs on both cerium oxide surfaces primarily in a molecular form. However, a partial dissociative adsorption accompanied with formation of OH groups is observed. These surface hydroxyls are substantially more stable on the partially reduced CeO_x as evident from the SRPES spectra captured during sample annealing in Figure 24; these species were found to be preferentially bond to oxygen vacancy sites. Upon larger exposures below 120 K the water molecules which cannot accommodate within the first monolayer form a multilayer ice structure. The subsequent annealing leads to molecular desorption of water physisorbed within the multilayer, resulting in a sharp thermodesorption peak

with maximum between 145–155 K, followed by the single layer leaving the surface around 170–185 K. The latter peak is noticeably weaker on CeO_x due to its higher dissociation activity and stronger binding of OH radicals. The broad TPD feature around 275 K is attributed to a recombinative desorption of hydroxyl species with surface bond hydrogen. These observations are in accord with the thermal evolution of the photoelectron spectra seen in Figure 24.

An additional piece of evidence for this behavior has been provided in the related work in [12], where SRPES/RPES and RAIRS characterization of both (fully oxidized and partially reduced) thin films of cerium oxide interacting with water vapor is complemented by density functional (DFT) calculations. Again, mostly molecular H_2O adsorption was identified at 160 K on both cerium oxide surfaces, together with partial formation of hydroxyl (OH) groups. Three typical PES characteristics were used to identify OH groups on ceria: 1) presence of 1π and 3σ states in valence band spectra; 2) increase of the BE separation between the O 1s spectral components of lattice oxygen, O^{2-} (Ce^{4+}), and OH/H_2O; 3) increase of the RER coefficient.

Dissociation of water and formation of hydroxyl adspecies readily takes place on partially reduced CeO_x, with OH groups preferentially occupying the positions of the missing lattice oxygen. However, the interaction of water with this surface does not cause any detectable reoxidation of Ce^{3+} to Ce^{4+} – the dissociation of water is fully reversible, either yielding molecular water (via recombination of OH groups) or releasing hydrogen and oxygen into the gas phase. The oxidation state of the reduced ceria after adsorption and subsequent annealing is fully recovered. The differences in dissociation activity of both oxides is further confirmed by the DFT calculations, showing that the energetically most favorable surface species on stoichiometric CeO_2 terraces is adsorbed water, while its dissociation is disfavored by about 0.2 eV, except at the steps, where the adsorption energy of water is higher but its dissociation was found to dominate over the molecular adsorption on the step edge sites.

The dissociation of water via filling oxygen vacancies with hydroxyls and leaving adsorbed H, along with the above described reverse process of thermal recombination, is a common behavior of all reduced oxides of cerium [160, 438, 439]. However, experiments on a strongly reduced ceria with stoichiometry approaching Ce_2O_3 (i.e., nearly all Ce cations in 3+ oxidation state) [148, 444] found these oxides to be extraordinarily effective in hydrogen production upon exposure to water via an irreversible mechanism. The origin of this peculiar activity has been uncovered in Ref. [40] attached as **Appendix 9**.

Although the probability of water splitting on ceria to yield molecular H_2 and lattice O atoms is hardly detectable on the mildly reduced oxides such as those employed in the studies discussed above, it increases slightly with the growing concentration of O vacancies on the CeO_x surface [160, 438, 439, 442]. The slow kinetics of this irreversible process was predicted to be due to a high barrier to form molecular H_2 from surface OH groups [446]. On cerium oxide at high level of reduction, however, a new reaction channel opens, with dramatically faster water dissociation kinetics, which is observed as a massive recombinative H_2 peak in TPD spectra above approx. 500 K (Figure 25b). It is associated with partial reoxidation of the CeO_x thin film evidenced by an intensity decrease of Ce^{3+} related components of the Ce 3d XPS and by a partial decay of this reaction pathway observed within the following adsorption-desorption cycle. After subjecting a 4 nm thick oxide layer to a total of 4 such cycles the fast dissociation route is effectively suppressed, which quantitatively agrees with a model of gradual incorporation of left-over oxygen within the oxide volume. The structural changes towards ordered cerium oxide phases with higher stoichiometry are observed by both STM and LEED.

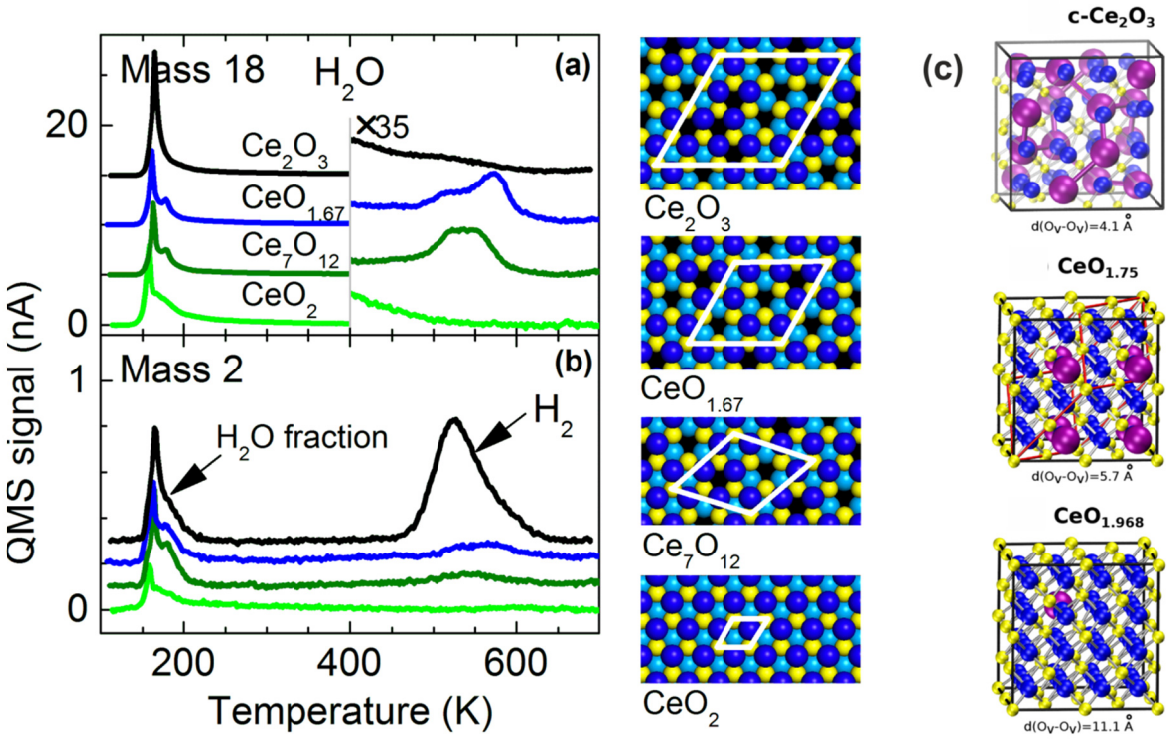

Figure 25: a, b) TPD spectra obtained from ordered thin films of c-Ce_2O_3, $CeO_{1.67}$, t-Ce_7O_{12}, and a reference fully-oxidized CeO_2(111) after adsorption of H_2O – a) mass 18 amu (H_2O), b) mass 2 amu (H_2). H_2O exposure 2.5 L at 100 K. Schematic top views of the above thin film surfaces are shown in the middle panel; black are the oxygen vacancies, white outlines represent the surface unit cells. c) Structural bulk models of cerium oxides at different levels of reduction. O vacancies (O_v) are displayed as purple spheres. Yellow and blue spheres represent Ce and O atoms, respectively. d(O_v-O_v) denotes the minimum distance between vacancies. Adapted from [40].

A careful analysis in tandem with ab initio calculations revealed that the above bulk-related reaction channel is activated during the interaction of H_2O with the bixbyite c-Ce_2O_3 phase. The stabilization of the key intermediate of this reaction – the hydroxyl group – in the bulk of c-Ce_2O_3 is mediated by a particular spatial coordination of O vacancies, which is a network of next-nearest-neighbor (NNN) O vacancies in bixbyite c-Ce_2O_3 structure. In lower amounts these pairs of NNN O vacancies can also be present in less-reduced CeO_x phases, where single vacancies otherwise prevail [159]. The bulk vacancy network of c-Ce_2O_3 is schematically presented in Figure 25c (top), where it is compared to the cases of isolated single vacancy in only mildly non-stoichiometric ceria (bottom) and of regular vacancy pairs in $CeO_{1.75}$ (middle). The formation of vacancy clusters is driven by the electrons left behind by released oxygen which localize on cerium ions and the tendency to exclusively expose the reduced cerium ions, primarily by including subsurface vacancies [159, 447].

Although the involvement of ceria bulk in the overall reactivity has rarely been considered until recently, the above study clearly substantiates its relevance in all chemical processes incorporating water in interaction with cerium oxides. The general validity of the coordination-specific localized character of the enhanced water dissociation activity (associated with the presence of bulk vacancy clusters) provides explanation of not only the early experiments on H_2 generation by thermochemical cycling between Ce_2O_3 and CeO_2 [448], but also in the experiments and applications where CeO_x stoichiometry remains far from Ce_2O_3 [187, 449-451] and where the accumulation of O vacancies may be expected via strain-driven [452] phenomena such as introduction of dislocations, lattice distortions, heterointerfaces, and grain boundaries or cracks [453-455].

5 Surface chemistry of organic molecules

5.1 Motivation and background

Environmental concerns dictate that the energy sources used in our daily lives be clean and not contribute to global climate changes [66, 456-459]. Hydrogen, the simplest and most abundant element in the universe, has been identified as such a source [460, 461] and the transition to a so-called "hydrogen economy" has been occurring since 1970s. Nowadays, hydrogen is commonly considered a versatile fuel of future and it is forecast to become a major source of energy, offering a potentially non-polluting, efficient, inexhaustible, and cost-attractive energy carrier [460-464]. It begins to find its use as a replacement for conventional liquid or gaseous fuels in internal combustion engines. The interest in hydrogen has also been rising due to technical advances in fuel cells [436], being potential successors to batteries in portable electronics, to power plants, and to combustion engines. The continuous global move from solid (typically wood and coal) through liquid (mainly oil) to gas (mainly natural gas) fuels involves an environmentally important transition process of "decarbonization" (see Figure 26a). It can be quantified as the ratio of hydrogen to carbon (H/C) in a fuel or as a quantity of carbonaceous byproducts (most commonly CO_2) per amount of energy generated (as in Figure 26b). The global H/C ratio has been increasing almost exponentially since last 2 centuries [456]. Indeed, it brings increasing demands on an effective and clean production of, ultimately, pure hydrogen. Apart from industrial production of hydrogen and its transport (which is very challenging issue by itself), on-board generation of H_2 appears to be a convenient strategy mainly in terms of safety and distribution infrastructure. So far the major users of H_2, however, are still the large-scale fertilizer and petroleum industries.

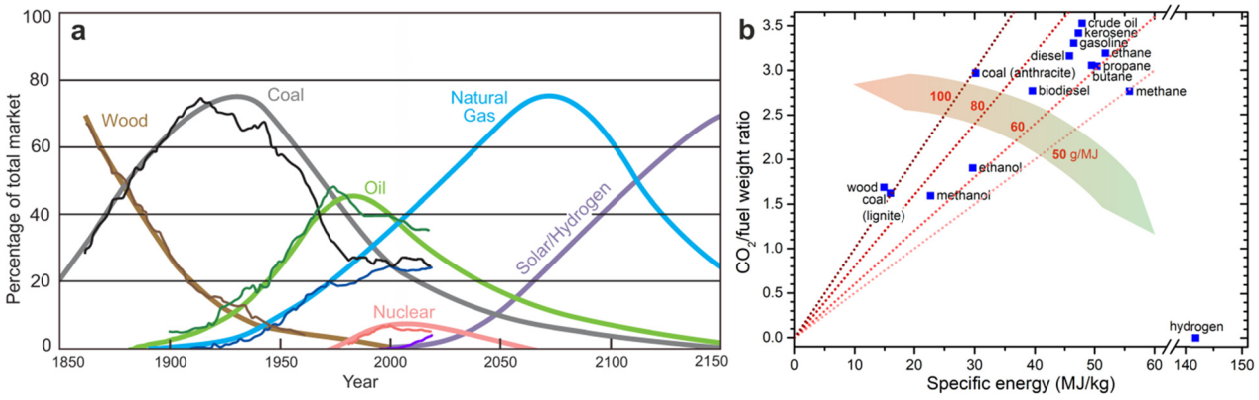

Figure 26: a) The recent history of global energy sources share (% of market) and the projection of an expected transition towards cleaner and less carbon-intensive sources. Adapted from [465] and updated based on BP Statistical Review of World Energy 2018. b) Specific energy (per fuel weight), and CO_2 emissions (expressed as CO_2 to fuel weight ratio) of different fuels; note the break on the specific energy axis. The red lines represent benchmark values of 50, 60, 80, and 100 g of CO_2 released per each MJ of energy produced. Data source: U.S. Department of Energy.

Generally, the technologies for producing H_2 fall into 4 categories: 1) thermochemical (mainly via steam reforming or pyrolysis), 2) electrochemical (electrolysis of water), 3) photobiological (utilization of the natural photosynthetic activity of bacteria and green algae to produce H_2), and 4) photoelectrochemical (direct production of H_2 by light-induced water splitting on a semiconductor surface) [462, 464, 466, 467]. In vast majority of these processes the role of catalysis is irreplaceable [264, 459, 464, 468].

A long sought goal of energy-related research has been the search for an efficient method to produce hydrogen economically by splitting water using sunlight as the primary energy source [469, 470]. As we have demonstrated in the previous chapter (Section 4.2), hydrogen can also be generated from water by thermally activated catalysis by ceria [40]. However, a lot of research remains to be done to make the process of water splitting sufficiently feasible and globally available. Hence fossil fuels (mainly natural gas, which is mostly made up of methane [471]) or, in a better case, renewable hydrocarbons (such as ethanol [457, 472, 473] or methanol [49, 50, 464] - see also Section 5.2) are used as primary sources of hydrogen; a comparative overview has been provided in Ref. [464].

Regarding the elementary steps involved in H_2 production from hydrocarbons, one of the fundamental concerns is the activation of C–H bond and, eventually, its functionalization [158, 264, 474, 475]. It is typically the step that hinders the reaction, due to the large kinetic barrier associated to the cleavage of an isolated (non-acidic) C–H bond and its apolar nature. Therefore, carefully addressing this elementary process – like in our study in **Appendix 16** [36] (see Section 5.4.2 below) – provides a key ingredient for the design of novel efficient catalysts and development of processes for hydrogen production.

In the following, a number of selected contributions in the surface chemistry of simple organic molecules [476] on palladium and platinum based model catalysts, with hydrogen production being of primary concern, will be presented (Sections 5.2 and 5.3). The last section (5.4) will be devoted to related topics of reactive carbon deposition and graphene formation on metal surfaces.

5.2 Methanol catalysis

So far, methanol has been used in chemical industry primarily for petrochemical purposes in synthesis of other organics. However, its global-scale use as an energy carrier and combustion engine fuel has been discussed for decades and, more lately, also as a fuel for alcohol driven fuel cells in vehicles and other mobile devices. Its attractiveness stems mainly from its safety and low production costs [459]. Moreover, methanol can easily be converted to hydrogen by steam reforming or catalytic partial oxidation [477] for further use as an energy carrier or direct on-board utilization as a clean fuel.

5.2.1 Methanol oxidation on Pd/alumina catalyst

In analogy to Chapter 0, we will begin with the chemically more simple case of the traditional oxide-supported metal NP catalyst supported on an inert substrate, namely the $Pd/Al_2O_3/NiAl(110)$ model system already introduced in Section 3.2.1.

The prerequisite in exploring surface chemistry of methanol oxidation is good understanding of its decomposition on the same catalyst, like it has been addressed in [35] and other related works [15, 34]. It proceeds via two competing reaction pathways: dehydrogenation to CO and C–O bond scission leading to formation of adsorbed carbon species. From the perspective of methanol decomposition the previously presented RAIRS identification of CO adsorbed on clean and carbon-covered Pd NPs (see, for instance, Figure 14) is a perfect example of utilizing CO as a probe molecule, like mentioned previously in Section 3.2. In this particular case we have demonstrated selective deposition of carbon on Pd NPs via the C–O scission pathway, which is shown to take part predominantly at defect sites (steps and edges); on contrary, the dehydrogenation pathway exhibits no such preference. Apart from this qualitative conclusion regarding structure dependent reaction selectivity, reaction rates corresponding to individual reaction routes were determined from time-

resolved IR reflection absorption spectra acquired during isotope exchange experiment [321] (by sudden switching between $^{12}CH_3OH$ and $^{13}CH_3OH$ effusive beams) [35]. In accordance with the above, the kinetics of C–O bond breakage drops rapidly with the occupation of reactive sites by carbon, whereas the dehydrogenation kinetics is almost unaffected.

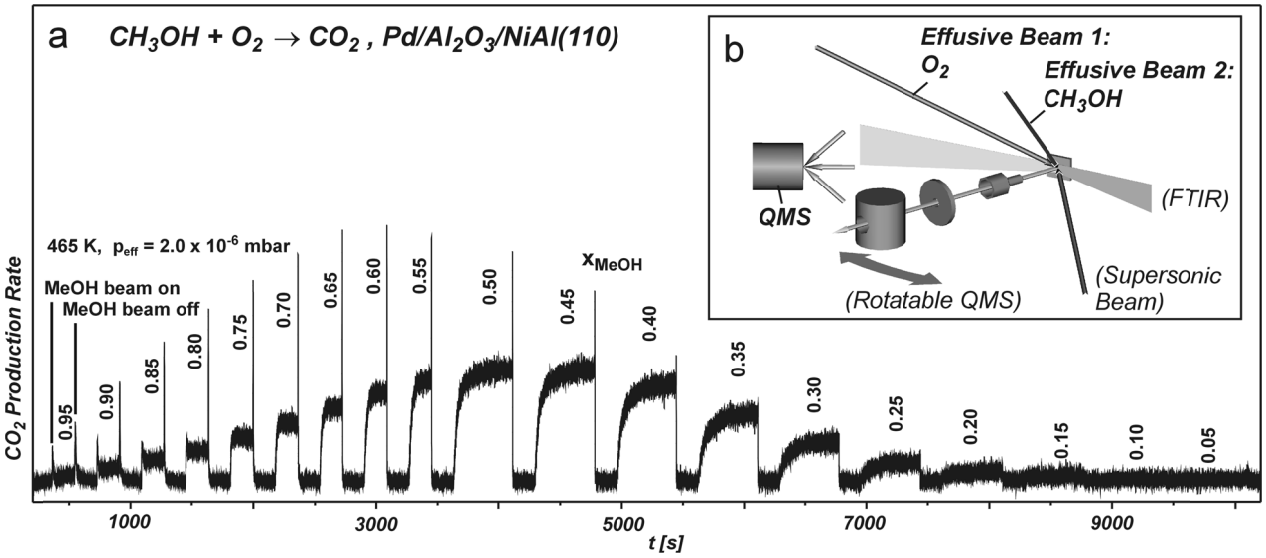

Figure 27: a) Plot of CO_2 signal capturing both transient and steady state production rates of CO_2 during methanol oxidation on $Pd/Al_2O_3/NiAl(110)$ model catalyst as a function of the fraction of methanol x_{MeOH} in the total flux impinging on the sample (surface temperature: 465 K; effective total pressure $2x10^{-6}$ mbar), average size of Pd particle 5.5 nm; b) Schematic description of the experimental setup used. Adapted from [53].

In the follow-up research the structural sensitivity phenomena has been generalized beyond the pure thermal decomposition case. The first direct experimental evidence of distinct reactivity of different types of surface sites coexisting on a single nanoparticle was shown in [15], using methanol oxidation as a probe reaction. This work was elaborated in more detail in [34], included as **Appendix 10**.

In Figure 27 the response of the CO_2 production rate for a continuous O_2 beam and a modulated methanol beam impinging on the surface at 465 K is presented as a function of the fraction of methanol (x_{MeOH}) in the gas flux. Such experiment provides two types of kinetic information: steady state reaction rates and transient reactivity. The steady state reaction rates evaluated for different methanol-oxygen stoichiometries exhibit very different behavior as compared to CO oxidation on the exact same model catalyst, as can be seen in Figure 28, although both processes involve dissociation of C–O bond.

Two reaction regimes can be distinguished: Under methanol rich conditions, the steady state is characterized by large CO coverages (arising from the dominant dehydrogenation reaction channel), inhibiting oxygen adsorption and thus limiting oxidation activity, the more the lower is the surface temperature (Figure 28a). The inhibition effect is, however, not as strong as in the case of direct CO dosing (Figure 28b).

Under oxygen-rich reaction conditions the kinetics of methanol and CO oxidation exhibits even larger differences. In the case of CO, linear dependence is observed (already mentioned in Section 3.3, see also Ref. [396] for details), whilst for methanol oxidation the reaction rates are lower and the dependence on methanol–oxygen ratio non-linear in the oxygen-rich regime, because preadsorbed oxygen has a strongly inhibiting effect on the dehydrogenation process. These observations are

consistent with the transient behavior, analyzed in depth in Ref. [53], including a theoretical modelling of the process.

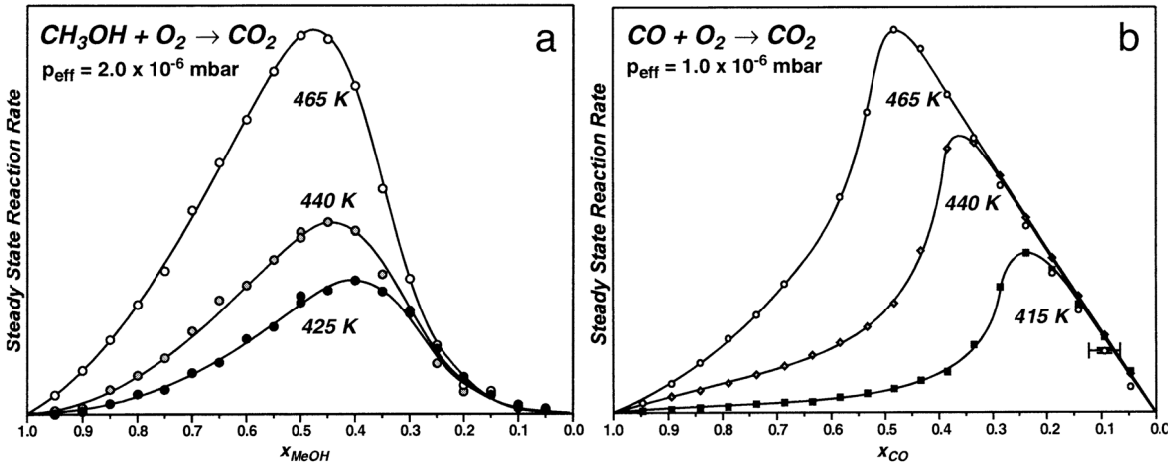

Figure 28: Steady state reaction rates on the $Pd/Al_2O_3/NiAl$ (110) model catalyst as a function of the fraction of the main reactant (methanol or CO) in the impinging gas flux (x_{MeOH} or x_{CO}) and the surface temperature a) for total oxidation of methanol ($p_{total} = 2\times10^{-6}$ mbar) and b) for CO oxidation ($p_{total} = 1\times10^{-6}$ mbar). Average Pd NP size was 5.5 nm. Adapted from [53].

5.2.2 Methanol adsorption and decomposition on Pt/ceria catalyst

As was already emphasized in Section 3.2.2, in contrast to Section 3.2.1, the use of an active support (here a reducible oxide) opens additional routes for surface chemistry due to the strong interaction between the metal particles and the support [374, 377, 478, 479]. Synergistic effect between Pt and CeO_2 has been demonstrated also in electro-oxidation of alcohols when used as anodic material in direct alcohol fuel cells [480-482].

On pristine ceria, methanol adsorbs at low temperatures and partially dissociates to methoxy (CH_3O) upon annealing [483, 484]. The consequent formation of surface bond hydroxyls and adsorbed water results in partial reduction of the cerium oxide surface [485]. When exposed above room temperature, methanol dissociates directly upon adsorption [486].

The publication [31] attached as **Appendix 11** is aimed at understanding methanol adsorption and decomposition on model $Pt/CeO_2(111)$ thin-film catalyst, grown epitaxially on Cu(111) substrate. It is shown that the chemistry of methanol on the ceria supported Pt nanoparticles monitored by XPS, SRPES, and AFM resembles in many aspects the sputtered pure Pt surface with high concentration of atomic steps, corners, and kinks [10], revealing the involvement of the undercoordinated surface sites present on the metal particles. Unlike on densely packed defect-free Pt(111) surface [487, 488], upon annealing the methanol adsorbate, CO is formed through dehydrogenation of methoxy via formyl intermediate. It is followed by partial dissociation of the C–O bond resulting in an accumulation of surface carbon, which is transformed into metal carbide above 500 K on rough Pt(111).

Apart from this structure-determined behavior inherent primarily to the Pt NPs, on Pt/CeO_2 the interaction between the metal and the oxide comes into play via hydrogen spillover from the Pt particles to ceria [42, 489] and simultaneous oxygen spillover in the opposite direction [11]. The latter mechanism facilitates removal of the surface carbon above 500 K, eliminating surface poisoning (i.e., formation of stable carbides) observed on bulk platinum. Dehydrogenation of methanol on Pt NPs followed by hydrogen spillover to ceria, on the other hand, leads to the

formation of surface hydroxyl groups and, consequently, to reduction of adjacent Ce^{4+} centers in ceria to Ce^{3+}. The high efficiency of the Pt/CeO_2 system in methanol decomposition and its resistance to carbon poisoning might explain the high activity and durability of this catalyst observed in methanol oxidation [479] and electrooxidation [480, 481, 490-493].

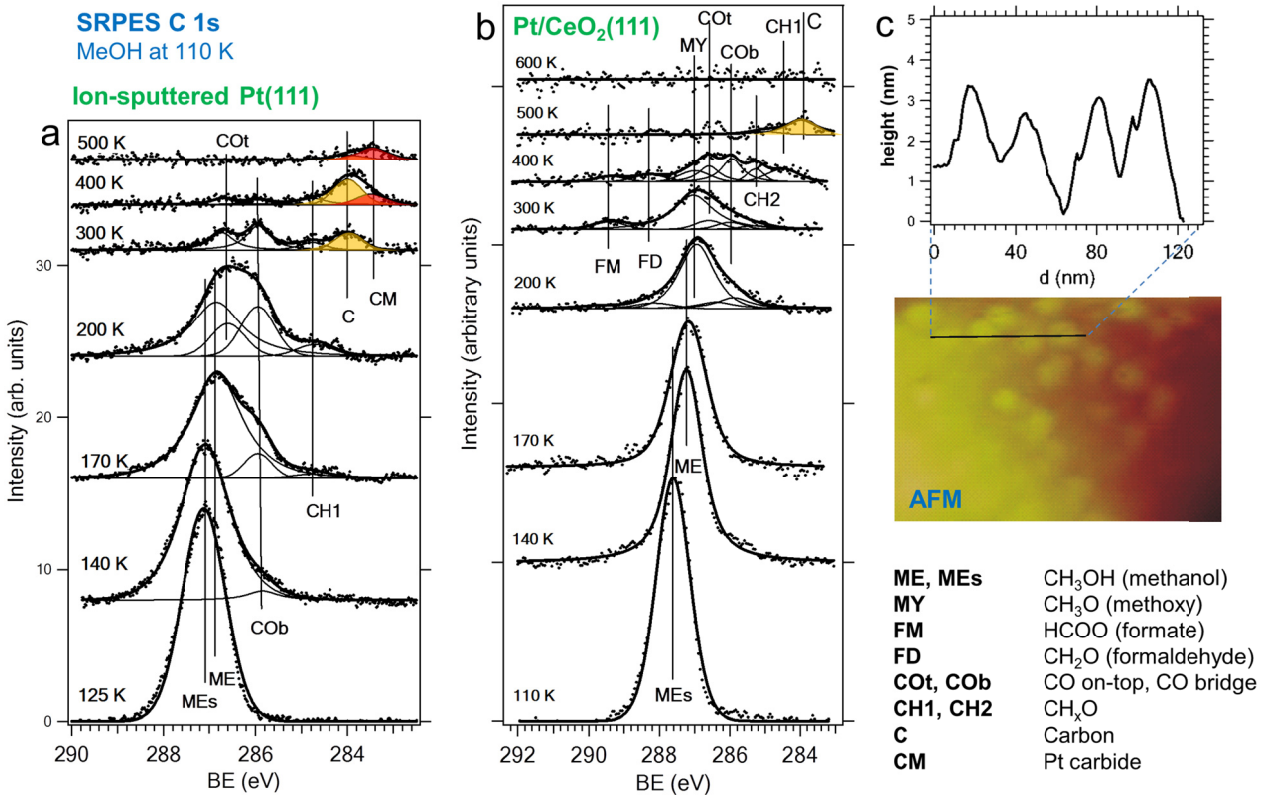

Figure 29: SRPES C 1s spectra following methanol adsorption at 110 K and its consequent step-wise annealing on a) ion-eroded Pt(111) surface and b) $Pt/CeO_2(111)$ model catalyst surface; primary photon energy was hν=380 eV and 410 eV, respectively. The carbon and carbide peaks are highlighted in yellow and red, respectively. c) AFM image of the $Pt/CeO_2(111)$ catalyst with a selected cross-section showing the surface profile. Adapted from [31].

5.2.3 Methanol oxidation on ceria/Pt inverse catalyst

It is often assumed, for the sake of simplicity, that properties of multicomponent heterogeneous catalysts (the components comprising different materials or different crystal planes of the same material) can be regarded as a superposition of the contributions from each individual structural element. This assumption is, however, in certain cases invalid, generally in any system where a communication (or coupling) between adjacent regions takes place. An example of such cooperative system has already been shown in Sections 3.2.2 and 5.2.2, dealing with chemistry of Pt/CeO_2. A combination of both active metal and active oxide compounds is often suitable for a configuration of so-called inverse catalyst, where oxide nanoparticles (NPs), typically transition metal oxides, are supported on a (typically noble) metal substrate [156, 175-177]. Such concept may seem counterintuitive because the design of the traditional catalyst is based on maximizing the effective surface area of the dispersed metal component and, eventually, taking advantage of size-related phenomena. However, this conventional view loses its relevance whenever the oxide actively participates in the surface chemistry and thus, rather than the metal itself, it is the interface between the two phases that gains importance in overall reactivity.

It has been known for long [171] that influence of metal–oxide electronic interactions on the catalyst activity (in terms of activation energies) is much larger for inverse catalysts than for the conventional ones [494, 495]. This is especially the case of noble metals which have high electron negativity and low oxygen affinity, so that transition metal cations of the oxide bind strongly to substrate atoms at the interface, forming oxygen-terminated-bilayer nanostructures, exposing undercoordinated (coordinatively unsaturated) sites which may provide a particular activity or selectivity, primarily in oxidation reactions [156, 174, 264]. At the same time, the strong interactions between the two components prevent further oxidation of the bilayer phase, which would otherwise result in deactivation of the active cations due to their saturation with oxygen.

The smaller are the oxide clusters the higher becomes the fraction of the interfacial reactive sites, effectively enhancing the net reactivity. Moreover, the redox processes are often associated with oxide restructuring [158, 191] which is thermodynamically more facile with smaller oxide structures and can give rise to active nano-oxide phases which would not exist in bulk or would not be sufficiently stable under the given environment [496]. The strain induced by a lattice mismatch between metal and oxide in very thin oxide films, as shown for ceria on some metals in [497, 498], can also contribute to increased redox activity.

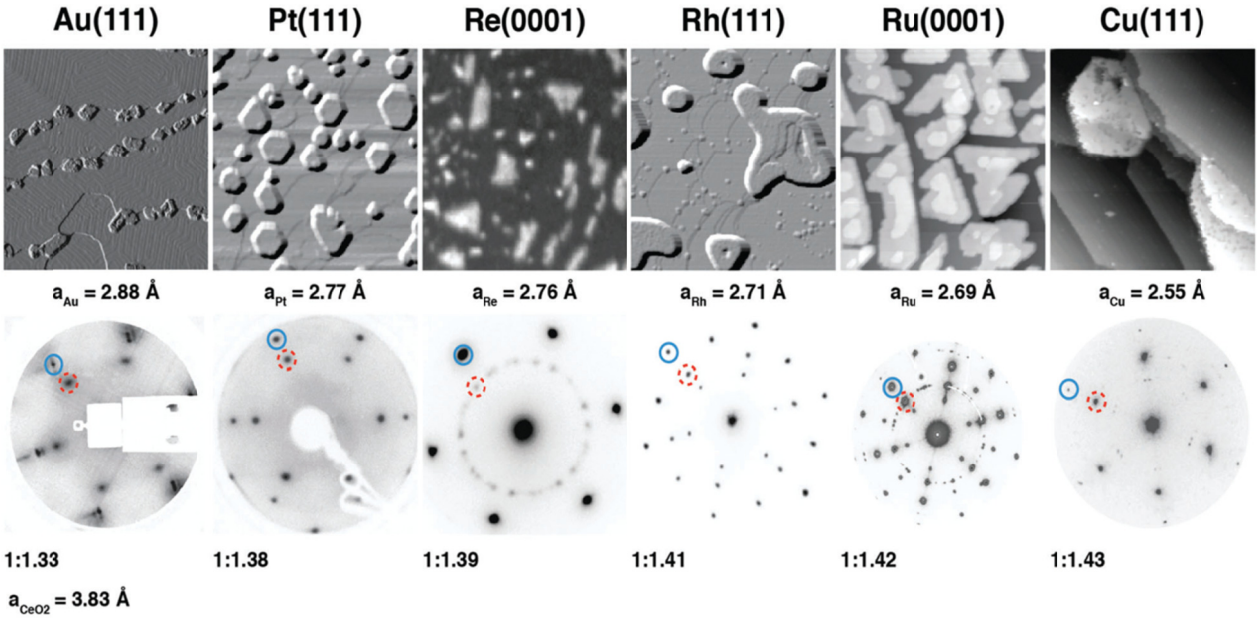

Figure 30: Examples of ceria-based inverse model catalysts: STM/LEEM images and LEED patterns demonstrate the dramatic effect of support on the structure of the ceria islands in inverse catalysts for Au(111), Pt(111), Re(0001), Rh(111), Ru(0001), and Cu(111) substrates. The lattice spacing for the substrates are indicated, along with the ratio relative to the CeO2 (111) surface. The red solid and blue dashed circles highlight the first order diffraction spots from the substrate and ceria, respectively. Size of all STM and LEEM images is 200×200 nm^2; the LEED patterns were acquired at different energies. Adapted from [499].

For ceria, the synergistic interplay between non-continuous oxide and metal substrate has been already demonstrated on Cu [495, 500-506], Au [443, 500, 507-509], Ag [500], Pt [510, 511], Rh [512, 513], Pd [512], Ru [514], and Re [515] surfaces, as well as on other inverse model or powder catalysts [499, 516]. An overview of some of these model systems is given in Figure 30. Recently, our group has also performed a series of detailed characterizations of the inverse model system of ceria on copper [17, 455, 498]. Catalysts consisting of cerium oxide nanoparticles supported on metal

surfaces proved very effective in promoting important industrial reactions such as CO oxidation, WGS, and methanol synthesis from CO_2.

Corresponding model systems turned out to be very instrumental in clarifying the relevant reaction mechanisms. For instance, the complementary chemical properties of coexisting adjacent metal and oxide sites on a copper-ceria inverse catalyst were found responsible for high efficiency for the chemical activation of CO_2 in methanol synthesis [495, 505], which is generally quite challenging task. The extraordinary functionality of the metal–reducible oxide interface was observed in promoting WGS reaction on CeO_2/Au(111). This is remarkable because neither Au(111) nor CeO_2 is able to catalyze the WGS reaction, but together they attain high activity [507, 517].

Generally, it was shown that oxygen atoms can be removed from interface sites at much lower cost than in other regions of the surface, which can completely alter the reactivity of a catalyst. The oxide−metal interaction in CeO_x/M activates the system by generating numerous Ce^{3+} species within the oxide cluster via a charge transfer from the underlying metal [158, 171, 378, 495, 500, 518]. On both CeO_x/Au(111) and CeO_x/Cu(111) the catalytic activity is related to the presence of these active Ce^{3+} centers [495, 517, 518] and the same holds true for other metals mentioned above.

In **Appendix 12** [51], methanol oxidation on ceria/Pt inverse catalyst has been investigated in the temperature range 360−600 K, using thin films prepared by magnetron sputtering deposition technique. Temperature-programmed reaction (TPR) measurements of reactivity at ambient pressure were correlated with complementary chemical and structural information obtained by spectroscopy (XPS) and microscopy (SEM).

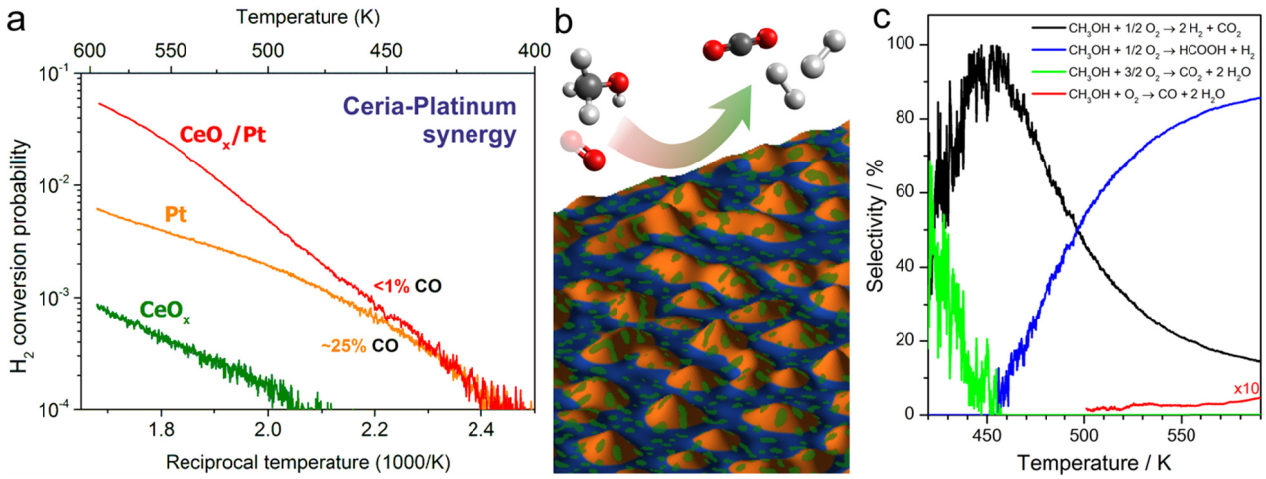

Figure 31: a) Comparison of methanol to hydrogen conversion probability over the non-continuous CeO_2 layer (0.2 nm average thickness) deposited over Pt NPs (1 nm average thickness) supported on silicon wafer (red), compared with the reference pure Pt NPs (1 nm) on the same substrate (orange) and the pristine non-continuous CeO_2 layer (0.2 nm) on silicon (green). All the samples were prepared by magnetron sputtering deposition. The ratio of methanol to oxygen was 2:1, total pressure 1 bar. The reactivity is presented in the form of an Arrhenius plot. b) A composite 3D-surface image of the non-continuous CeO_2/Pt inverse catalyst based on SEM micrographs, showing silicon substrate (blue), Pt NPs (orange) and ceria ad-layer (green). c) Temperature dependence of reaction selectivity in methanol oxidation on the non-continuous CeO_2/Pt inverse catalyst presented in b). The reaction proceeds via 4 different pathways (listed on top of the plot) with varying probability. Adapted from [51].

The high overall reactivity of the ceria−platinum inverse system can be attributed to high reducibility of ceria with low dimensionality. This redox capability is further strongly enhanced on discontinuous ceria, exposing very reactive triple-phase boundaries where ceria islands serve as oxygen donors to facilitate the oxidation of methanolic intermediates on the nearby Pt sites. It is in accord with

previous findings that the ceria/Pt interface is more active with the oxide in the form of NPs rather than extended bulk surface [159]. When the oxidation of methanol (using stoichiometric 2:1 methanol/oxygen mixture) is quantified in terms of total hydrogen yield per surface area such catalyst outperforms pure platinum by over an order of magnitude at 600 K and nearly 100% selectivity toward the dehydrogenation reaction pathway, while generating undetectable amounts of undesired CO byproduct (see Figure 31). The optimal conditions for partial oxidation of methanol (POM) reaction, yielding H_2 and CO_2, are found for 0.2 nm ceria on Pt at around 430 K. At higher temperatures, a gradual switching to a competing pathway leads to the production of formic acid (HCOOH) and hydrogen, yet the amount of carbon monoxide remains very low (below 1%).

5.3 Catalysis of other hydrocarbon oxygenates

One of the sustainable routes towards hydrogen production is based on decomposition or reforming of bio-derived hydrocarbons, particularly oxygenates (such as bio-ethanol or bio-oils) [519]. As in many other processes involving catalysis of organics, surface deactivation due to coke formation is a limiting factor for catalyst durability. The accumulation of surface carbon during bio-oil reforming can be suppressed by using reducible supports such as ceria [520]. However, the microscopic origins of the underlying surface reaction mechanism and their kinetics at microscopic scale remain largely unexplored. Some issues related to mechanisms of activation and deactivation in oxygenate catalysis have been uncovered to some degree for formic acid [33], acetic acid [13, 39], and ethylene glycol [39] using a surface-science-based model approach.

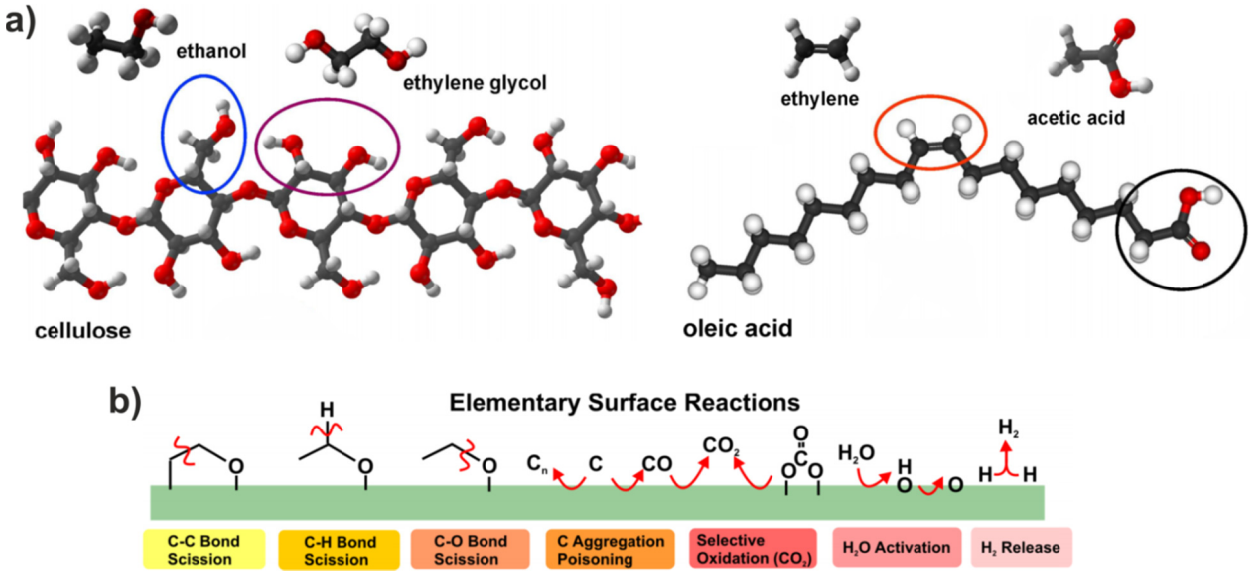

Figure 32: a) Ball-and-stick models of two common types of organic oxygenate molecular structures – a fraction of a cellulose chain (left) and an oleic acid molecule (right). The various dicarbon fragments of these substances comprise bases for ethanol, ethylene glycol, ethylene, and acetic acid molecules; b) Schematic overview of possible elementary surface processes related to chemistry of oxygenates.

In order to understand mechanisms of biomass-based hydrogen production, relevant model compounds with reasonable complexity are explored. As a good starting point, C_2-based bioderived hydrocarbon oxygenates model compounds (acetic acid, ethanol, ethylene glycol) were chosen in our recent studies [39]. These molecules conveniently contain combinations of various functional groups (e.g. CO, OH, COOH, C=C) with very different chemical properties. They represent a relatively simple compounds with the C–C core situated in different molecular environments, which are

present in all oxygenated hydrocarbons – see the molecular illustration in Figure 32a, showing the most abundant organic polymer cellulose and oleic acid, the most common natural fatty acid.

It turns out that the reaction pathways governing the catalyzed decomposition of these basic building blocks of organic molecules (mainly the scission of C–C bond and carbon surface poisoning, see also the overview of surface reactions in Figure 32b) depend substantially on a particular combination of the model compound and the catalyst surface [39], as will be also shown in the rest of this section. A general observation is that ceria actively participates in surface reactions via spillover of surface species between Pt and ceria [11, 13, 33, 42, 332].

5.3.1 Formic acid decomposition on Pt/ceria

On many metallic [521, 522] surfaces, formic acid dissociates to produce formate ($HCOO^-$) and hydrogen (H^+). On oxides, the deprotonation of formic acid occurs via the loss of acidic H^+, yielding formate and hydroxyl radical (OH^-) [523-525]. The formate can further decompose via dehydrogenation or dehydration route, resulting in desorption of CO_2+H_2, or CO+H_2O, respectively. It was found that dehydrogenation is the dominant pathway on metals [521, 522, 526] (which is also the case of Pt(111) [526]) and on basic oxides [527, 528], whereas dehydration pathway prevails on acidic oxides [528, 529]. On the surfaces yielding only a single set of the above products the reaction proceeds via a simple monomolecular decomposition [530, 531], whereas on the surfaces where a mixture of desorbing CO_2, H_2, CO, and H_2O is formed, the reaction may proceed via a bimolecular mechanism [530], involving interaction between two formate species, or between formate and formic acid molecule.

The reaction selectivity can be often tuned via surface temperature [20-21] and, in the case of oxides, by the introduction of vacancies [523, 525]. From the microscopic point of view the preference for a particular decomposition pathway of the surface formate may be promoted by its particular bonding configuration. The article in **Appendix 13** [33] presents a comprehensive characterization of formic acid adsorption and decomposition on cerium oxide thin-film (both fully oxidized and mildly reduced) grown on Cu(111) and Pt/ceria model catalysts by means of SRPES, RPES, RAIRS, and TPD methods.

On these systems, two distinct temperature intervals can be recognized – see Figure 33 where the selected SRPES and TPD data for Pt/CeO_2(111) have been correlated. Below approx. 400 K a bimolecular decomposition mechanism leads to simultaneous desorption of CO_2, H_2, CO, and H_2O, with some methanol by-produced above 210-280 K. At higher temperatures (>400 K), the desorption pattern depends substantially on both the cerium oxide stoichiometry and presence of Pt NPs. On the non-stoichiometric CeO_{2-x} the production of CO_2 is suppressed, whereas its enhancement is observed on Pt/CeO_2(111).

Unlike for the rather intact pristine stoichiometric ceria, the annealing of molecularly adsorbed formic acid on partially reduced CeO_{2-x} results in a significant reoxidation of the surface between 250 and 400 K due to an electron transfer from Ce^{3+} to formate (see the RPES comparison in Figure 33d). With increasing temperature it is followed by an opposite process of reduction due to rapid decomposition of formate via the dehydration route. A completely different scenario is seen on Pt/CeO_2, where hydrogen spillover from Pt to the support (identified by RAIRS) occurs below 260 K, followed by a reverse hydrogen spillover from ceria to Pt NPs at higher temperatures, resulting in desorption of molecular hydrogen starting above 350 K (see Figure 33a-c). Some hydrogen is, in parallel, removed in the form of methane. Moreover, traces of formaldehyde have also been found on all samples.

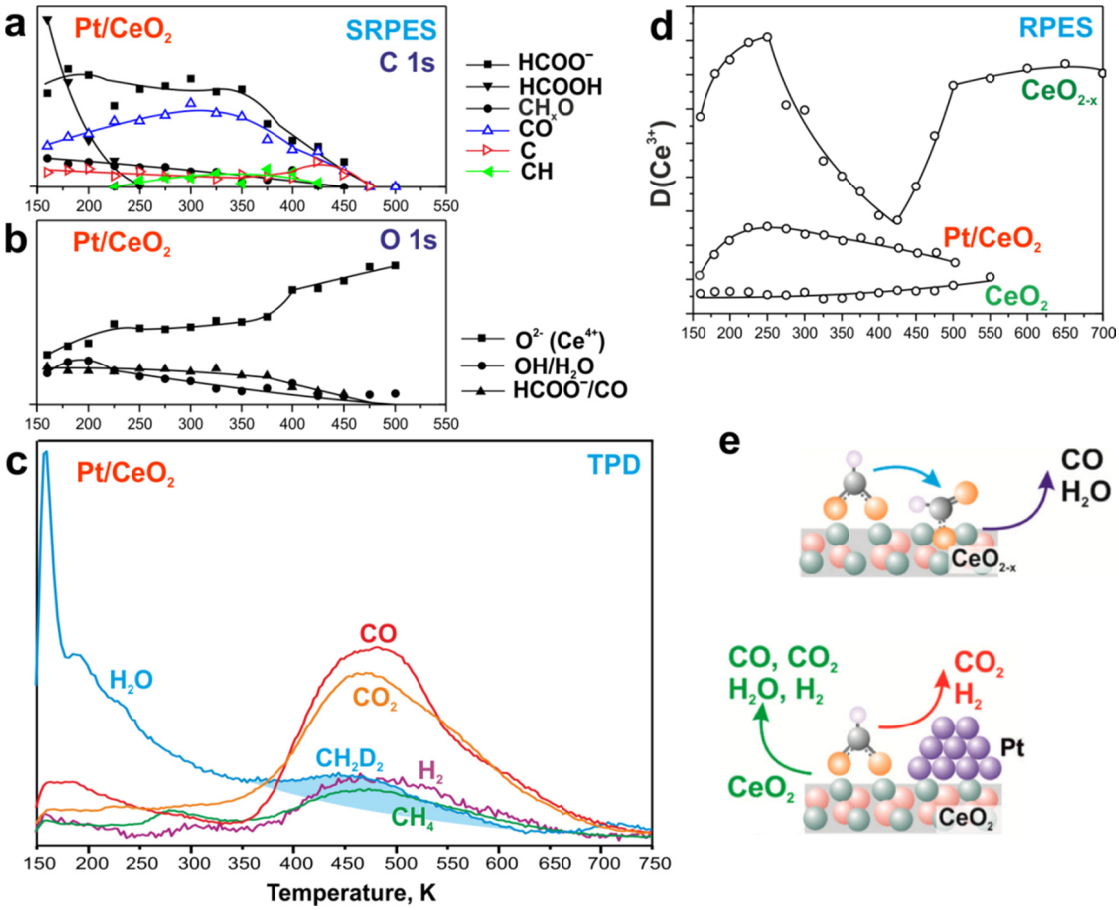

Figure 33: Thermal decomposition of formic acid on $CeO_2(111)$, CeO_{2-x}, and Pt/$CeO_2(111)$ following exposure to 10 L of DCOOH at 150 K.. a), b) Evolution of SRPES integral intensities of individual components of C 1s (a) and O 1s (b) spectra with temperature, and c) The corresponding TPD spectrum with a simplified assignment of features (some mass signals consist of multiple contributions from different molecules but only the major component is shown, except for mass 18 where the low temperature part originates primarily from water, while the peak superposed on the high temperature tail originates from partially deuteriated methane). d) Comparison of the Ce^{3+} RPES resonance enhancements [$D(Ce^{3+})$] during annealing of formic acid adsorbate on all three surfaces. e) A basic depiction of the main processes taking part on the CeO_{2-x}, and Pt/CeO_2 model systems during annealing. Partially adapted from [33].

The above study renders a connection between the reaction selectivity during thermal decomposition of formic acid adsorbed on cerium oxide and the simultaneous change of its oxidation state. Furthermore, it demonstrates the essential role of the spillover phenomena in the presence of active metal nanoparticles on the oxide substrate.

5.3.2 Acetic acid decomposition on Pt/ceria

In several aspects similar topic involving chemistry of acetic acid on ceria and Pt/ceria model catalysts has been covered in **Appendix 14** (ref. [13]). In addition to the formic acid case, acetic acid combines the carboxyl functionality with both C-C and C-H bonds, thus representing an ideal model component for fundamental studies of reforming mechanisms [532].

In analogy to the formic acid the initial step following adsorption of acetic acid at low temperature (150 K) on all surfaces ($CeO_2(111)$, CeO_{2-x}, and Pt/$CeO_2(111)$) is partial loss of acidic hydrogen yielding surface bond acetate (CH_3COO^-) species. Several products are formed upon annealing, including ketene (H_2C_2O), acetaldehyde (CH_3CHO), H_2, water, CO, CO_2, methanol, and methane. In Figure 34a TPD spectra of the most important reaction products are shown for all three systems,

along with the corresponding SRPES C 1s signals corresponding to acetate and methoxy radicals and to carbonaceous surface species. As evidenced by SRPES, acetates are relatively stable up to about 425-475 K.

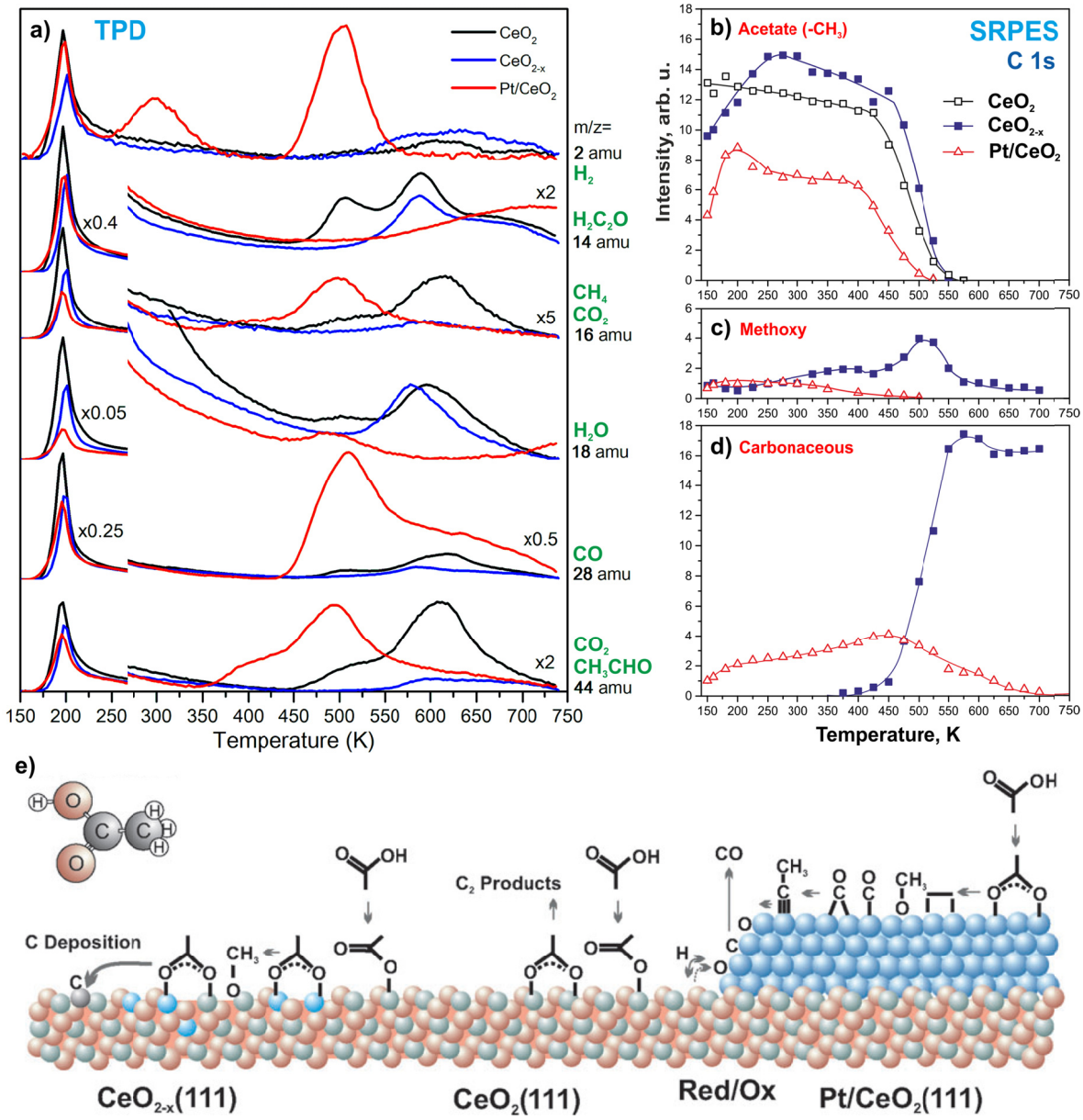

Figure 34: Thermal decomposition of acetic acid on $CeO_2(111)$, CeO_{2-x}, and $Pt/CeO_2(111)$ following exposure to 15 L of CH_3COOH at 150 K.. a) TPD spectra for selected molecular masses; the spectra are scaled with respected to the topmost one (for m/z=2amu), the assigned molecules for each spectrum are indicated in green. b)-d) Evolution of SRPES integral intensities of selected individual components of C 1s spectra with temperature. e) A schematic depiction of the processes taking part on the cerium oxide and Pt/ceria surfaces during annealing of acetic acid adsorbate, showing reaction intermediates and products. Partially adapted from [13] and [39].

On CeO_2, strong water desorption occurs around 300 K, with a second peak near 600 K. Most other products exhibit desorption peaks centered around the latter temperature mark (~580-620 K), with an exception of ketene featuring an additional peak at 506 K. No change in oxidation state of cerium (reduction) is observed during the annealing procedure. On partially reduced CeO_{2-x}, no water peak is seen below 500 K. The steady increase of acetate concentration detected by SRPES up to about 250 K reveals continuing conversion of acetic acid to acetate during annealing, presumably activated

at oxygen defect sites not present on CeO_2. In the higher temperature region the main difference from stoichiometric ceria is that the decomposition route leading to ketene desorption near 500 K is suppressed, as well as the production of CO_2 and CO which is nearly eliminated in the whole range above 450 K. It is suggested to be due to the rupture of C−O bond within acetate near Ce^{3+} centers, giving rise to observed reoxidation of CeO_{2-x} accompanied with a formation of strongly adsorbed carbonaceous (C_2H_x) species, not present on pristine CeO_2 at all (see Figure 34d).

The situation is somewhat more complex on Pt/ceria. A mixed adsorbate comprising molecular acetic acid and acetate is formed at low temperatures on both ceria and platinum. Such identification is allowed owing to the high energy resolution of SRPES in which distinct groups in C 1s spectra (methyl and carboxyl/carboxylate) binding to either ceria or platinum can be resolved by fitting routine. The increase of acetate signal on ceria between 150–200 K results from deprotonation of molecularly adsorbed acetic acid to acetate on Pt particles followed by its spillover to the support. The denser acetate layer on ceria tends to promote binding at different (monodentate) adsorption geometry above 250 K. Decomposition of these monodentate acetate species yields large amounts of hydrogen and CO at the expense of the formation of ketene and acetone, as observed by TPD (Figure 34a). The decomposition process leads to carbon accumulation on both Pt NPs and on ceria, but it is reacted off above 450 K by thermally activated self-cleaning process, related to reverse oxygen spillover from the ceria support to the Pt particles. The carbon deposits are oxidatively removed even from the ceria support above 600 K on Pt/CeO_2, effectively preventing carbon deactivation of this catalyst in potential reactions involving acetic acid.

An illustrative overview of different processes which take part on all types of surfaces discussed above is provided in Figure 34e. Again, the interaction of Pt/ceria with acetic acid clearly demonstrates the synergy between metal and oxide components mutually "communicating" via bi-directional spillover, as well as the important role of the facile reducibility of the support in the process.

5.4 Hydrocarbons and graphene

Graphene is a two-dimensional honeycomb lattice of sp^2-bonded carbon atoms with very distinct physico-chemical properties [533-537]. Although already known since over 4 decades by surface science and catalysis communities [538-542], it has attracted an enormous interest since it has been first isolated in a free-standing form via exfoliation of highly oriented pyrolytic graphite (HOPG) [543, 544], followed by a Nobel prize award relatively shortly after in 2010. Apart from the originally used method of micromechanical cleavage, other means of graphene preparation were developed since then, with the most common being thermal decomposition of SiC [533, 536, 545, 546], reduction of graphene oxide [533, 547, 548], or growth on metal surfaces [538, 549]. The growth on metals is usually realized by either segregation of bulk-dissolved carbon [550], or by chemical vapor deposition (CVD) technique [536, 538, 549, 551, 552], typically using a hydrocarbon as a reactant molecule.

From the surface physics and chemistry standpoint there are two central motivations in studying graphene on metals: 1) understanding passivation mechanisms of catalysts, where deposition of carbon in different forms (of which graphene is often the most resilient) is one of the main deactivation routes [119, 287, 473, 553], and 2) understanding structural nuances and microscopic details of growth of high quality graphene, potentially usable in applications.

5.4.1 Ethene decomposition on platinum

Even before the term "graphene" was coined, flat or two-dimensional graphitic structures were identified on some metal and metal carbide surfaces by diffraction [539, 540, 554-557], spectroscopy [542, 557-559], or scanning probe microscopy [541, 559-561] methods. In our follow-up research extending the previous pioneering study of Comsa et al. [541] we investigated thermal decomposition of ethene (ethylene) on Pt(111) single crystal surface by scanning tunneling microscopy, as can be seen in **Appendix 15** [19].

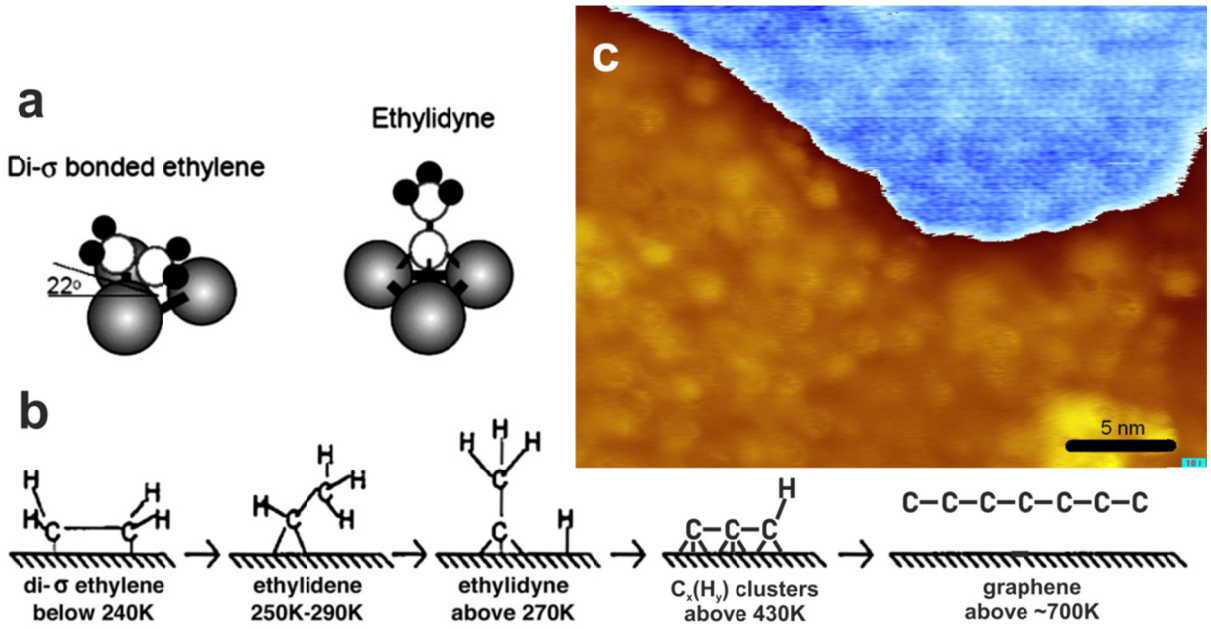

Figure 35: Thermal decomposition of ethene (ethylene) on Pt(111) single-crystal surface. a) Models of adsorption geometries of di-σ-bonded ethylene and the intermediate ethylidyne on Pt(111). b) Schematic overview of subsequent stages of ethene decomposition, showing conversion from di-σ-bonded ethylene to ethylidene, ethylidyne, carbonaceous clusters and, finally, to graphene layer. c) STM image of the Pt(111) surface after sixth ethene adsorption/annealing cycle (comprising saturation by CO at 300 K followed by annealing up to 700 K), densely covered by carbon nanoparticles (lower part, colored in brown/yellow). In the upper part (colored in blue) the contrast has been enhanced to reveal the regular atomic structure of the single-layer graphitic layer with its honeycomb moiré superstructure resulting from higher-order commensurability of graphene and Pt(111) [19]. Partially adapted from [562].

The main goal of this experiment was to provide a clue in determining mechanism of carbon growth via dehydrogenation of ethene, the simplest alkene. Dosing ethene onto Pt(111) at room temperature leads to the formation of partially dehydrogenated intermediate ethylidyne. Further annealing induces progressive dehydrogenation, resulting in homogeneously distributed disordered carbon clusters consisting of about 30-35 carbon atoms, forming above approx. 450 K. The question was whether exposing the surface to additional ethene after the initial decomposition of C_2H_4 adsorbate and its consequent annealing leads preferably to an increase of carbon particle density or of their size; it was found that latter was the case. The sample turned nearly inactive already when approx. 70% of its surface became covered by carbon (after 4-5 dosing/annealing cycles), indicating a possible ensemble effect in the ethene dehydrogenation over Pt(111).

The second most important finding was that 2D graphitic layers had formed near platinum step edges at temperatures significantly lower than observed previously by other groups. It was suggested that the formation of graphene patches can be facilitated via decrease of the activation barrier for

carbon phase transition from non-graphitic to graphitic type due to stronger lateral interactions of the increasingly dense carbon deposits.

5.4.2 C−H bond activation on platinum

To understand the interaction of hydrocarbons with catalytically active surfaces, an insight into the mechanisms of C−H bond activation is crucial. For instance, the initial cleavage of C−H bond occurring in alkane dissociative chemisorption to yield chemisorbed alkyl and hydrogen is often the rate-limiting step in industrial catalytic processes involving alkanes [264, 474, 475, 563]. Moreover, dissociative chemisorption of alkanes is a model system for activated polyatomic gas-surface reactions for which molecular complexity can be varied and multidimensional experimental measurements can be used to challenge emerging theoretical models of gas-surface reactivity.

In **Appendix 16** (published in [36] with an erratum in [37]) we combined precise sticking probability measurements of alkanes on Pt(111) single crystal using effusive molecular beams with theoretical model based on microcanonical unimolecular rate theory (MURT) of dissociative chemisorption [564-566]. Two cases were addressed in the study: 1) quasi-thermal dissociative sticking (i.e., gas beam temperature equal to surface temperature, $T_g=T_s=T$), representing conditions comparable to those found in industrial catalysis and 2) non-equilibrium dissociative sticking ($T_g \neq T_s$) for which the reactivity is intimately coupled to gas-surface energy transfer.

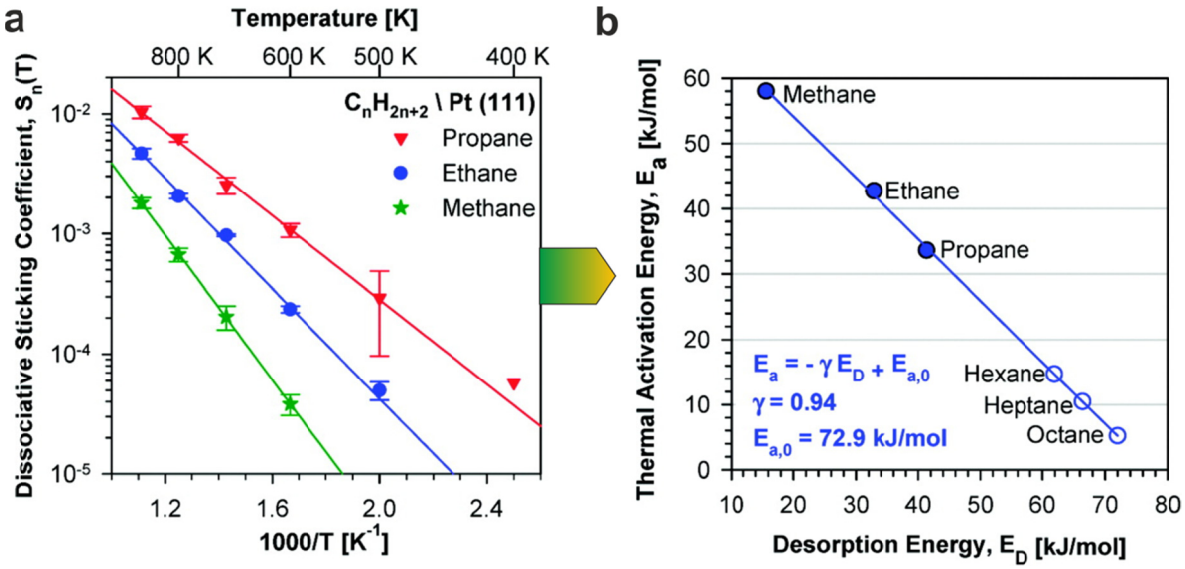

Figure 36: a) Arrhenius plot of quasi-thermal dissociative sticking coefficients, $S_n(T)$, for several alkanes on Pt(111), measured with an effusive molecular beam incident along the surface normal thermalized to the surface temperature (i.e., $T_g=T_s=T$); b) Evans−Polanyi plot of the activation energy for dissociative chemisorption [derived from measured temperature dependence of dissociative sticking coefficient as presented in a)] versus desorption energy for several alkanes on Pt(111) (solid points measured; open points extrapolated). Adapted from [36].

Both thermal effusive beam (determining temperature dependence of dissociative sticking coefficient) and TPD experiments (determining activation energy for desorption) indicate that the activation energy for dissociative chemisorption of n-alkanes falls as the alkane size and desorption energy increases [36, 37, 567], as can be seen in Figure 36b. The experimental activation energy for alkane quasi-thermal dissociative sticking (E_a) exhibits linear correlation with the alkane desorption energy from the physisorption well (E_D), which can be interpreted as an Evans-Polanyi relation [76, 563, 568] because the E_D should approximate the van der Waals stabilization energy [569, 570] of the chemisorbed alkyl radical product of alkane dissociative chemisorption. For the non-equilibrium

experiments, explicit accounting of the gas-surface energy transfer [564] becomes increasingly important as the alkane size is increased.

An extension of this work by measurement of angle-resolved thermal dissociative sticking coefficients [571] showed that the obtained values are dynamically biased for the smallest alkanes (methane and ethane) with respect to purely statistical behavior, which brings significant complications in quantitative modeling of catalytic processes. A plausible explanation of these deviations is that the molecular vibrational energy contributes to surmounting the activation barrier to thermal dissociative chemisorption, hence with increasing alkane size (with which the number of vibrational modes increases as well) the energy balance will be dominated by vibrations; as an experimental consequence the angular variation of dissociative sticking coefficient will become vanishingly small.

5.4.3 CVD of graphene on platinum

With development of new techniques of surface analysis a visualization of the graphene growth process in real time has been made possible. In the study presented in **Appendix 17** (published in [20]), low-energy electron microscopy (LEEM) [572, 573] has been employed, providing 500 ms temporal and 5-10 nm lateral resolution with the given experimental setup and conditions. The LEEM observations were complemented by a set of alkene decomposition experiments using both high-temperature CVD [253] and ambient-temperature postdosing Auger electron spectroscopy (AES), in order to quantify the carbon deposition process in a spatially averaged manner.

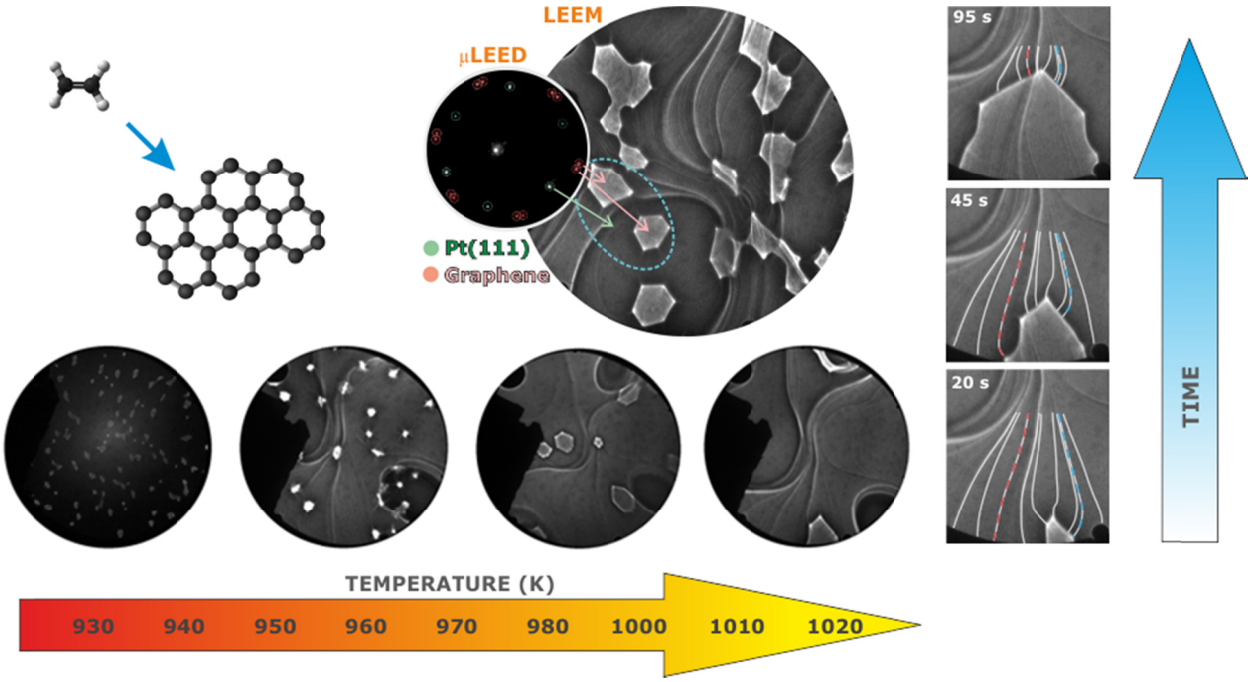

Figure 37: Graphene growth via CVD on Pt(111) visualized by LEEM. Top: Three regions in the LEED image has been indicated using selected area microdiffraction (μLEED) as Pt(111) and two graphene islands with different orientations [(√19×√19)R23.4° and (√7×√7)R19.1°]. Bottom: The four images illustrate size and density dependence of graphene islands as a function of surface temperature during growth; Right: A sequence of three time snapshots of graphene growth at 1014 K, revealing graphene-induced structural changes of Pt surface. Adapted from [20].

Ethene CVD on single-crystal oriented (111) platinum surface at temperatures near 1000 K results in 2-dimensional graphene islands, in vast majority with (√19×√19)R23.4° and (√7×√7)R19.1°

orientations relative to the Pt(111) lattice. Although the initial nucleation takes place at platinum steps, graphene patches grow readily over the steps and step bunches. The growth proceeds in both directions – away from the lower and upper Pt step edges, in contrast to the uni-directional growth exclusively at the lower step edges, previously observed by temperature-programmed growth (TPG) [19, 560, 574]. The average island size increases significantly with temperature, yielding single-orientation high-quality structures with smooth edges and diameters exceeding 10 μm at temperatures only slightly above 1000 K. Quite surprisingly considering the rather decoupled character of the platinum–graphene system, growing graphene is able to induce noticeable morphological changes in the hot platinum surface (step bunching and reshaping), such as in Figure 37 (right).

The graphene coverage captured in LEEM images was further quantified for temperatures between 927 and 1014 K; the values were consistently lower than those determined by an integral method (AES following exposure of Pt(111) to ethylene), especially at lower temperatures, because the size of the smallest graphene islands and, eventually, carbonaceous clusters was under the resolution of the microscope. The sticking coefficients determined by AES up to 850 K were consistent with a precursor-mediated thermalized trapping model for ethylene dissociative chemisorption [575]. However, this model had to be extended with a parallel reaction to account for the reversed tendency of the reaction rate, effectively increasing apparent sticking probability at higher surface temperatures [20]. It may happen due to surface structural changes such as roughening transitions, or the onset of additional reactive channels that ultimately lead to surface carbon.

Despite the recent boom in graphene literature there has been an ongoing debate on the exact mechanisms of graphene nucleation and growth. The unique two-dimensional polymeric structure of sp^2-bonded carbon causes graphene to grow on metal substrates through mechanisms that are different from those known from a conventional heteroepitaxy. Several works has indicated that it happens via attachment from 2D gas of carbonaceous precursors (carbon clusters or C_xH_y fragments) rather than via a direct grow from the already established graphene island edges. The recent work presented in **Appendix 18** (reference [18]) provided an experimental support to the previously rendered idea of graphene growth via attachment of C_n clusters, with a predicted optimal size of n=5 [576]; this was later complemented by a theoretical study leading to the same conclusion [577]. It has also been reported that coalescence of much larger pre-organized structures is possible as well [578], yet the C_5 chain appears to be the most elementary preferred building block of graphene growth, sometimes called a principal graphene „feeding species".

The spectroscopic characterization of the CVD growth of graphene on Pt(111) using high-resolution synchrotron radiation excited photoelectron spectroscopy (SRPES) confirmed that although the initial dehydrogenation of 1-alkenes to adsorbed alkylidynes starts to occur at essentially the same temperature (200-240 K) regardless the alkene chain length, the further loss of hydrogen commences at lower temperatures the longer the hydrocarbon chain. At higher temperature when graphitization takes place, the kinetics of the graphene formation also exhibits a noticeable dependence on the alkene molecule size. The lowest apparent activation energy and the highest turnover rate were obtained for pentene (C_5 alkene) as predicted.

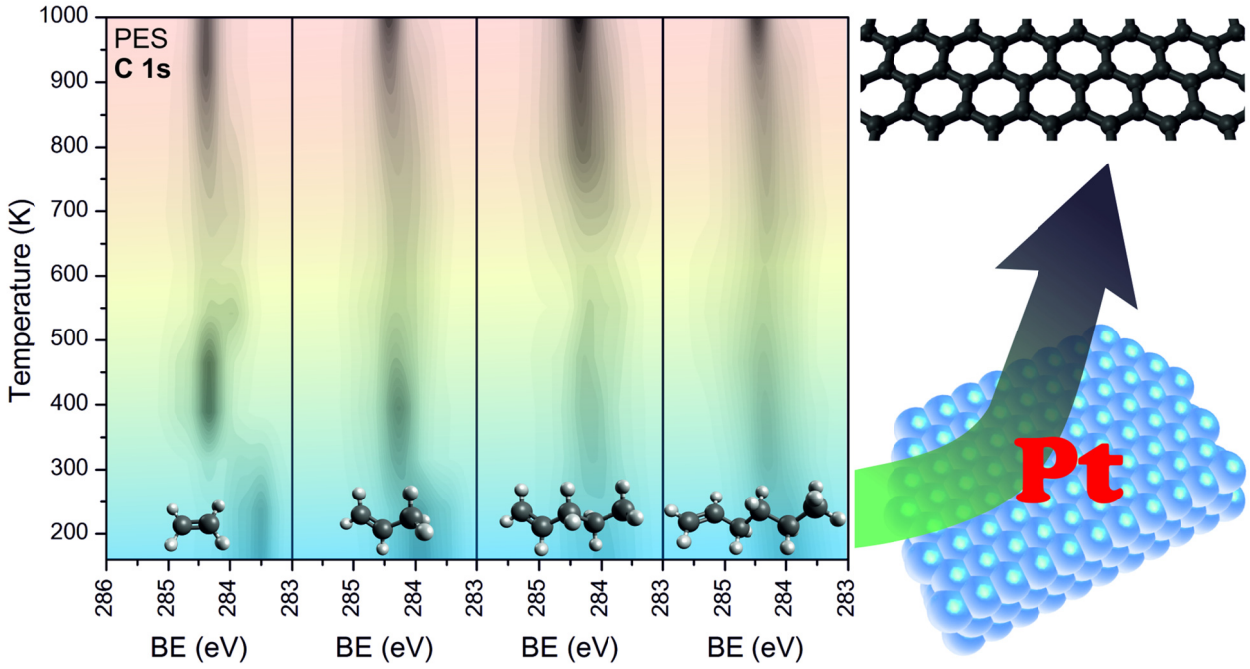

Figure 38: Evolution of the photoelectron spectroscopy C 1s signal from Pt(111) pre-exposed to 2 L of (left to right) ethene, propene, 1-pentene, and 1-hexene during annealing from 160 K to 1000 K. The graphene-related signal at 284.4 eV at high temperatures is the strongest when 1-pentene is used, providing one of the indicators of the preference for C_5 aggregates in graphene growth. The spectra are presented in the form of surface plot - the darker, the higher the SRPES intensity. Adapted from [18].

6 Concluding remarks

One of the main goals of this thesis has been to demonstrate that, from an experimental point of view, coupling kinetic reactitivity experiments with detailed microscopic information provided by *in-situ* spectroscopies and microscopies is an extremely powerful tool in elucidating the relationships between the structural and reactivity properties of heterogeneous catalysts. In most cases, model systems with strictly controlled complexity were utilized in order to allow such degree of characterization. But even by employing merely integral methods within a well-designed experiment, local phenomena can, in some cases, be addressed at microscopic level, like in the works included as Appendices 1, 11, and 18. The synergistic power of using multiple experimental methods can be further enhanced by complementing with theoretical calculations or numerical simulations of the investigated systems, see, e.g., Appendices 2, 4, 6, 9, and 16 using this approach.

It has been shown on several examples that the size and structure of metal nanoparticles or stoichiometry and structure of oxides can govern the reaction selectivity in a very distinct manner. For instance, in Appendix 7 the role of different adsorption and reaction sites on supported nanoparticles during NO decomposition is elucidated; a locally-resolved structural dependence of methanol decomposition and oxidation is presented in Appendix 10. An experimental evidence of strong relation between specific arrangement of oxide vacancies and reaction selectivity in water dissociation on cerium oxide, bolstered by theoretical calculations, is given in Appendix 9. The dissociation and recombination of water on ceria can, in turn, substantially alter its electronics structure, as can be seen in Appendix 8. Reducibility of ceria can be further enhanced in the inverse configuration (Appendix 12) where the oxide is present in the form of small islands on platinum, with potentially positive consequences for reactivity. A purely geometrical particle size effects turned

out to be responsible for formation of spatial non-homogeneities on Pd/alumina nanocatalyst during methanol oxidation due to surface diffusion limitations (such as in Appendix 2).

Another key phenomena in reactivity of multicomponent heterogeneous catalysts is a mutual communication (electronic and/or chemical) between the individual components. The results presented in Appendix 1 indicate that particle-size dependent electronic metal-substrate interaction plays an important role in CO binding and dissociation on alumina supported Pd nanoparticles, especially on the aluminum-rich oxide substrates. A successful attempt to experimentally quantify electron transfer between a strongly interacting reducible oxide support (ceria) and metal nanoparticles of various sizes can be seen in Appendix 4. A whole class of communication phenomena is represented by spillover effects, well documented experimentally, e.g., in Appendices 3, 13, and 14. Oxygen spillover from ceria to Pt also plays a decisive role in activity of the inverse catalyst in Appendix 12. These surface diffusion processes are closely related to surface dynamics effects [315, 316] which can eventually lead to macroscopically detectable phenomena such as reaction bistability (or, more generally, multistability); we have demonstrated in Appendix 6 that in some cases atomistic origins of such multistable behavior can be uncovered.

An attempt to at least partially overcome the infamous pressure and complexity gap was made in Appendix 5 (and related works in [48, 50]) dealing with platinum oxide, considered one of the active phases present during oxidative processes on catalysts containing platinum under realistic conditions.

Finally, a contribution to the currently hot topic of graphene science has been provided in Appendices 15, 17, and 18 by combining microscopic and spectroscopic methods to shed some light on the formation of this unique 2D material via decomposition of hydrocarbons, supported by the combined experimental and theoretical insight into the activation of C–H bond on platinum (Appendix 16).

7 Outlook

With environmental concerns getting into the front of public interest, several implications arise for the ever-growing field of catalysis. Currently in the forefront of interest are the sustainability and energetic issues [458] stirring up topics such as catalytic breakdown of biomass, functionalization of abundant naturally occurring hydrocarbons, and facile electrolysis of water. The need for protection of limited natural resources motivates continued search for cheaper, earth-abundant, replacements of noble metals or reduction of their use via improved material utilization and/or enhanced catalytic effectivity, e.g., through development of novel tailored structures. Increasing emphasis has also been given to catalyst recovery issues (their regeneration or recycling [22, 61]). Last but not least, a related issue of potential health impacts of exposures to increasingly abundant nanomaterials [579, 580], which has emerged only relatively recently, should definitely not be overseen as well.

All the above points impose numerous challenges for both industrial and academic research [581]. From the academic point of view, even getting to "merely" understand atomistic details of reaction mechanisms of already known catalytic systems can lead to much more rational optimization, as well as to development of brand new catalysts. Many degrees of freedom are available in the fabrication of novel catalytic materials, including structural aspects (dispersion, porosity, periodicity, vacations, low-coordinated surface sites such as steps, edges, or controlled defects [110, 111, 184], surface strain, limited dimensionality, etc.) or combinations of different materials (such as bimetals, mixed

oxides, core-shell structures, etc.). One of the recent frontiers in heterogeneous catalysis is known as single-atom catalysis, representing a limiting case of metal dispersion and thus maximized material utilization [207-209, 283, 582, 583]. Single-atom catalysis shares the advantages of both homogeneous catalysts (isolated active sites) and heterogeneous catalysts (stability and facile separation), and are therefore expected to be able to bridge the fields of homo- and heterogeneous catalysis.

With continuing innovations of surface science tools and methods [66, 68, 218], including all areas from sample design through characterization to theoretical models, the vital question of relevance of model systems to their real-life analogues in catalysis has been becoming an increasingly significant issue [584]. It has stimulated the progress in the development of so-called *(in) operando* methods [24, 106, 217, 260, 290, 585], capable of monitoring catalytic surfaces directly under realistic reaction conditions. Some of these techniques also represent an outreach of surface science to liquid-phase chemistry or to electrocatalysis, which had been an almost exclusive domain of chemists until recently.

Amongst modern implementations of enhanced instrumental equipment aimed at bridging pressure and materials gap are the near-ambient pressure XPS (NAP-XPS) [24, 217, 258, 291-293, 296, 297] (see Figure 39, left panel), operando FTIR [196, 258, 322, 323, 363] and *in-situ* UV/vis [586], IR/vis sum frequency generation (SFG) [196, 587], Raman [588], or electrochemical IR spectroscopy [324, 562], operando or high-pressure STM (HP-STM, also called Reactor STM) [109, 217, 258, 589-591], electrochemical AFM (EC-AFM) [592, 593], operando SXRD [217, 594], operando or environmental transmission electron microscopy (ETEM) [24, 109, 217, 258, 294, 303, 595], environmental (or atmospheric) scanning electron microscopy (ESEM, ASEM) [295, 299, 300, 304], X-ray spectromicroscopy (SPEM) [305], and scanning transmission X-ray microscopy (STXM) [301, 596], just to name some of them. Special microreactors providing integration of multiple analytical methods has been designed as well [597], see the example in Figure 39 (right). Apart from advances on the analysis side, nanomaterial engineering has been taking its part by employing, e.g. nanoscale ion beam lithography (IBL) [201, 598, 599], nanoimprint lithography (NIL) [201, 600], ion projection lithography (IPL) [599, 601], pulsed laser deposition (PLD) [233, 234], self-assembled nanostructures or monolayers (SAMs) [206, 602, 603] or their patterning [604], graphene supports [603, 605] and templates based on carbon [606] or other materials [607], controlled surface faceting [108], and several other techniques.

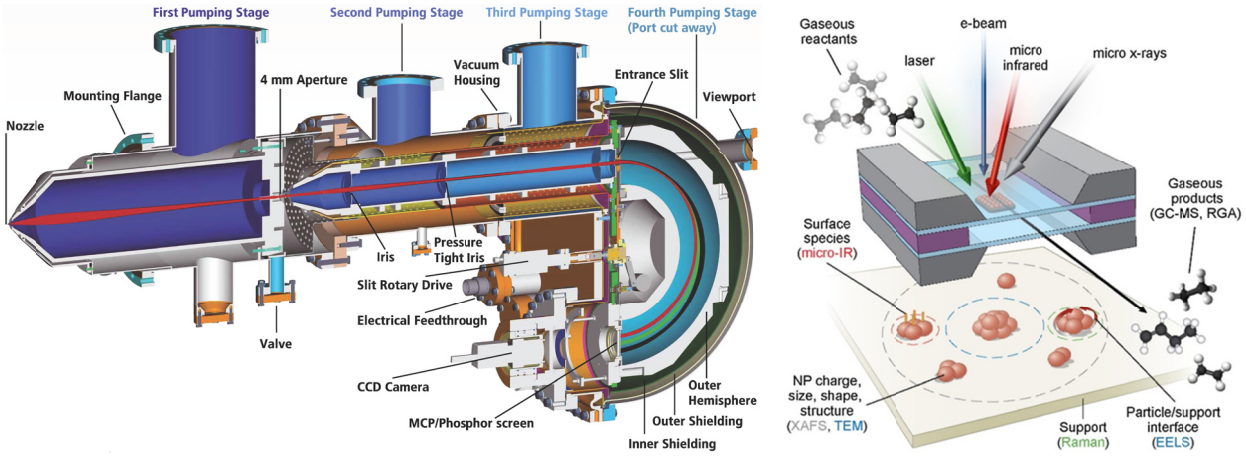

Figure 39: Two different approaches to operando research in heterogeneous catalysis. Left: Differential pumping – Cross section of Specs Phoibos 150 NAP-XPS recently installed at the Department of surface and plasma science at Charles University. The schematic shows simulated electron trajectories with an angle

span of ±22 ° and three different energies. The four differential pumping zones are colored in different shades of blue. Courtesy of SPECS Surface Nano Analysis GmbH. Right: Separation – Schematic of a microcell allowing ambient pressure reaction observations by standard surface science tools. The catalyst is confined between two silicon nitride windows, and the reaction gases flow through the system to interact with the confined catalyst at atmospheric pressure. In this case, four different beams (electron, X-ray, IR, and laser) probe different parts of the catalytic system simultaneously. Adapted from [597].

However, even the established, currently considered "standard" instrumentation may allow to achieve a higher degree of understanding by employing new strategies (experimental or theoretical), implementing a greater control over the investigated systems, and by finding links between catalysis and other nanomaterial-oriented fields (e.g., colloid chemistry or nanoelectronics [608]). For instance, a sophisticated nanofabrication recipe was recently utilized to prepare controlled and precisely tunable model system in order to quantify hydrogen spillover phenomena in Ref. [609]. Preparation of materials with accurately size-selected clusters [199, 358], synthesis of tailored alloy nanoparticles [195], and fabrication of self-assembled solid structures [610] (just to give a few examples) have made a significant progress in the last years as well.

Hand in hand with the rise in computing power, more emphasis is being put on engaging multiple characterization methods mentioned above in tandem with theoretical calculations. Theory has been making rapid progress in the area of catalysis, providing insights into the mechanistic details and energetics of chemical reactions or even giving directions in the design of new catalytic materials [122, 611-615]. The complexity of the systems which the theory is able to handle keeps increasing; the current capabilities of theoretical modelling cover, e.g., relatively large supported clusters, crystal slabs with dopants or structural defects, thin films, extended adsorbate assemblies, and material growth processes. Intensive recruitment of computational and modelling approaches [616, 617] utilizing microkinetic simulations [217, 618-622] and quantum mechanics methods such as ab initio [217, 621, 623, 624], density functional theory (DFT) [611, 620, 621, 625-627], quantum molecular dynamics [620, 621, 628], and their variants became almost routine in modern trends of surface science and catalysis.

Industrial catalysis is a multidisciplinary activity with fundamental research being one of the key components [581]. In contrast to the extensive and sometimes rather intuitive approaches natural to chemical engineering, the surface science approach relies heavily on the reductionist view that if all the key factors affecting individual discrete steps involved (such as adsorption, desorption, poisoning, surface diffusion, reorganization and restructuring, etc.) are sufficiently evaluated, one ought to be better placed to rationally design superior catalysts. Although it is fair to admit that the chemist's way has been typically more successful in finding altogether new catalysts so far, it is largely a merit of the model system studies that the face of heterogeneous catalysis has changed substantially over the course of past few decades, through providing an unprecedented level of insight into the – sometimes seemingly mysterious – realm of catalysis.

8 References

1. Thomas, J.M., Summarizing comments on the discussion and a prospectus for urgent future action. Philos T R Soc A **374**(2061), 2016.
2. Seh, Z.W., Kibsgaard, J., Dickens, C.F., Chorkendorff, I.B., et al., Combining theory and experiment in electrocatalysis: Insights into materials design. Science **355**(6321), 2017.
3. Johanek, V., Laurin, M., Grant, A.W., Kasemo, B., et al., Fluctuations and bistabilities on catalyst nanoparticles. Science **304**(5677), 2004, 1639-1644.
4. Johanek, V., Schauermann, S., Laurin, M., Gopinath, C.S., et al., On the role of different adsorption and reaction sites on supported nanoparticles during a catalytic reaction: NO decomposition on a Pd/alumina model catalyst. J. Phys. Chem. B **108**(38), 2004, 14244-14254.
5. Schauermann, S., Johanek, V., Laurin, M., Libuda, J., and Freund, H.J., Low temperature decomposition of NO on ordered alumina films. Chem. Phys. Lett. **381**(3-4), 2003, 298-305.
6. Johanek, V., Schauermann, S., Laurin, M., Libuda, J., and Freund, H.J., Site occupation and activity of catalyst nanoparticles monitored by in situ vibrational spectroscopy. Angew Chem Int Edit **42**(26), 2003, 3035-3038.
7. Johanek, V., Tsud, N., Matolin, V., and Stara, I., TPD and XPS study of the CO adsorption on transition-SP metal systems: Pd and Al. Vacuum **63**(1-2), 2001, 15-22.
8. Johanek, V., Stara, I., and Matolin, V., Role of Pd-Al bimetallic interaction in CO adsorption and catalytic properties of bulk PdAl alloy: XPS, ISS, TDS, and SIMS study. Surf. Sci. **507**, 2002, 92-98.
9. Matolin, V., Johanek, V., Stara, I., Tsud, N., and Veltruska, K., XPS, ISS and TDS study of bimetallic interaction between Pd and Al: CO interaction with supported Pd/alumina catalysts. Surf. Sci. **507**, 2002, 803-807.
10. Matolinova, I., Johanek, V., Myslivecek, J., Prince, K.C., et al., CO and methanol adsorption on (2 x 1)Pt(110) and ion-eroded Pt(111) model catalysts. Surf. Interface Anal. **43**(10), 2011, 1325-1331.
11. Happel, M., Myslivecek, J., Johanek, V., Dvorak, F., et al., Adsorption sites, metal-support interactions, and oxygen spillover identified by vibrational spectroscopy of adsorbed CO: A model study on Pt/ceria catalysts. J. Catal. **289**, 2012, 118-126.
12. Lykhach, Y., Johánek, V., Aleksandrov, H.A., Kozlov, S.M., et al., Water Chemistry on Model Ceria and Pt/Ceria Catalysts. J. Phys. Chem. C **116**(22), 2012, 12103-12113.
13. Neitzel, A., Lykhach, Y., Johanek, V., Tsud, N., et al., Decomposition of Acetic Acid on Model Pt/CeO2 Catalysts: The Effect of Surface Crowding. J. Phys. Chem. C **119**(24), 2015, 13721-13734.
14. Neitzel, A., Lykhach, Y., Johanek, V., Tsud, N., et al., Role of Oxygen in Acetic Acid Decomposition on Pt(111). J. Phys. Chem. C **118**(26), 2014, 14316-14325.
15. Schauermann, S., Hoffmann, J., Johanek, V., Hartmann, J., et al., Catalytic activity and poisoning of specific sites on supported metal nanoparticles. Angew Chem Int Edit **41**(14), 2002, 2532-2535.
16. Matolinova, I., Johanek, V., Skala, T., Veltruska, K., and Matolin, V., XPS, TDS and static SIMS studies of binary Pd/Al system properties: correlation between Pd-Al bimetallic interaction and CO adsorption. Appl. Surf. Sci. **245**(1-4), 2005, 87-93.
17. Tovt, A., Stetsovych, V., Dvořák, F., Johánek, V., and Mysliveček, J., Ordered phases of reduced ceria as inverse model catalysts. Appl. Surf. Sci. **465**, 2019, 557-563.
18. Johánek, V., Nehasil, V., Skála, T., and Tsud, N., Carbon Chain Length Dependence of Graphene Formation via Thermal Decomposition of Alkenes on Pt(111). J. Phys. Chem. C, 2018, in press (published online).
19. Johanek, V., De la Ree, A.B., and Hemminger, J.C., Scanning Tunneling Microscopy Investigation of the Conversion of Ethylene to Carbon Clusters and Graphite on Pt(111). J. Phys. Chem. C **113**(11), 2009, 4441-4444.

20. Cushing, G.W., Johánek, V., Navin, J.K., and Harrison, I., Graphene Growth on Pt(111) by Ethylene Chemical Vapor Deposition at Surface Temperatures near 1000 K. J. Phys. Chem. C **119**(9), 2015, 4759-4768.
21. Johánek, V., Cushing, G.W., Navin, J.K., and Harrison, I., Real-time Observation of Graphene Oxidation on Pt(111) by Low-energy Electron Microscopy. Surf. Sci. **644**, 2016, 165-169.
22. Ertl, G., Knözinger, H., Schüth, F., and Weitkamp, J., eds. Handbook of Heterogeneous Catalysis. 2008, Wiley-VCH Verlag GmbH & Co. KGaA: Weinheim, Germany.
23. Haw, J.F., ed. In-Situ Spectroscopy in Heterogeneous Catalysis. 2004, Wiley-VCH.
24. Zhang, S.R., Nguyen, L., Zhu, Y., Zhan, S.H., et al., In-Situ Studies of Nanocatalysis. Acc. Chem. Res. **46**(8), 2013, 1731-1739.
25. Johanek, V., Stara, I., Tsud, N., Veltruska, K., and Matolin, V., CO adsorption on Al2O3-supported Pd clusters: XPS study. Appl. Surf. Sci. **162**, 2000, 679-684.
26. Tsud, N., Johanek, V., Stara, I., Veltruska, K., and Matolin, V., CO adsorption on palladium model catalysts: XPS Pd-Al2O3 interaction study. Surf. Sci. **467**(1-3), 2000, 169-176.
27. Matolin, V., Johanek, V., Stara, I., Tsud, N., and Veltruska, K., XPS and TPD study of CO interaction with Pd-Al and Pd-Al2O3 systems. J. Electron Spectrosc. Relat. Phenom. **114**, 2001, 327-332.
28. Matolin, V., Stara, I., Tsud, N., and Johanek, V., XPS and TDS study of CO interaction with Pd-AlOx systems. Prog. Surf. Sci. **67**(1-8), 2001, 167-181.
29. Schauermann, S., Johanek, V., Laurin, M., Libuda, J., and Freund, H.J., Interaction of NO with alumina supported palladium model catalysts. Phys. Chem. Chem. Phys. **5**(22), 2003, 5139-5148.
30. Yudanov, I.V., Sahnoun, R., Neyman, K.M., Rosch, N., et al., CO adsorption on Pd nanoparticles: Density functional and vibrational spectroscopy studies. J. Phys. Chem. B **107**(1), 2003, 255-264.
31. Matolin, V., Johanek, V., Skoda, M., Tsud, N., et al., Methanol Adsorption and Decomposition on Pt/CeO2(111)/Cu(111) Thin Film Model Catalyst. Langmuir **26**(16), 2010, 13333-13341.
32. Matolin, V., Matolinova, I., Dvorak, F., Johanek, V., et al., Water interaction with CeO2(111)/Cu(111) model catalyst surface. Catal. Today **181**(1), 2012, 124-132.
33. Lykhach, Y., Happel, M., Johanek, V., Skala, T., et al., Adsorption and Decomposition of Formic Acid on Model Ceria and Pt/Ceria Catalysts. J. Phys. Chem. C **117**(24), 2013, 12483-12494.
34. Schauermann, S., Hoffmann, J., Johanek, V., Hartmann, J., and Libuda, J., Adsorption, decomposition and oxidation of methanol on alumina supported palladium particles. Phys. Chem. Chem. Phys. **4**(15), 2002, 3909-3918.
35. Schauermann, S., Hoffmann, J., Johanek, V., Hartmann, J., et al., The molecular origins of selectivity in methanol decomposition on Pd nanoparticles. Catal. Lett. **84**(3-4), 2002, 209-217.
36. Cushing, G.W., Navin, J.K., Donald, S.B., Valadez, L., et al., C-H Bond Activation of Light Alkanes on Pt(111): Dissociative Sticking Coefficients, Evans-Polanyi Relation, and Gas-Surface Energy Transfer. J. Phys. Chem. C **114**(40), 2010, 17222-17232.
37. Cushing, G.W., Navin, J.K., Donald, S.B., Valadez, L., et al., C-H Bond Activation of Light Alkanes on Pt(111): Dissociative Sticking Coefficients, Evans-Polanyi Relation, and Gas-Surface Energy Transfer (vol 114, pg 17222, 2010). J. Phys. Chem. C **114**(51), 2010, 22790-22790.
38. Happel, M., Lykhach, Y., Tsud, N., Skala, T., et al., SO2 Decomposition on Pt/CeO2(111) Model Catalysts: On the Reaction Mechanism and the Influence of H-2 and CO. J. Phys. Chem. C **116**(20), 2012, 10959-10967.
39. Lykhach, Y., Neitzel, A., Sevcikova, K., Johanek, V., et al., The Mechanism of Hydrocarbon Oxygenate Reforming: C-C Bond Scission, Carbon Formation, and Noble-Metal-Free Oxide Catalysts. Chemsuschem **7**(1), 2014, 77-81.
40. Dvorak, F., Szabova, L., Johanek, V., Camellone, M.F., et al., Bulk Hydroxylation and Effective Water Splitting by Highly Reduced Cerium Oxide: The Role of O Vacancy Coordination. Acs Catal **8**(5), 2018, 4354-4363.

41. Johanek, V., Laurin, M., Hoffmann, J., Schauermann, S., et al., Adsorbate mobilities on catalyst nanoparticles studied via the angular distribution of desorbing products. Surf. Sci. **561**(2-3), 2004, L218-L224.
42. Lykhach, Y., Staudt, T., Vorokhta, M., Skala, T., et al., Hydrogen spillover monitored by resonant photoemission spectroscopy. J. Catal. **285**(1), 2012, 6-9.
43. Laurin, M., Johanek, V., Grant, A.W., Kasemo, B., et al., Local reaction rates and surface diffusion on nanolithographically prepared model catalysts: Experiments and simulations. J. Chem. Phys. **122**(8), 2005, Art. # 084713.
44. Tsud, N., Johanek, V., Stara, I., Veltruska, K., and Matolin, V., XPS, ISS and TPD study of Pd-Sn interactions on Pd-SnOx systems. Thin Solid Films **391**(2), 2001, 204-208.
45. Lykhach, Y., Kozlov, S.M., Skala, T., Tovt, A., et al., Counting electrons on supported nanoparticles. Nat. Mater. **15**(3), 2016, 284-289.
46. Tovt, A., Bagolini, L., Dvořák, F., Tran, N.-D., et al., Controlling Pt dispersion on ceria by surface oxygen content. Acs Catal, 2018, submitted.
47. Neitzel, A., Lykhach, Y., Skala, T., Tsud, N., et al., Hydrogen activation on Pt-Sn nanoalloys supported on mixed Sn-Ce oxide films. Phys. Chem. Chem. Phys. **16**(26), 2014, 13209-13219.
48. Johánek, V., Václavů, M., Matolínová, I., Khalakhan, I., et al., High low-temperature CO oxidation activity of platinum oxide prepared by magnetron sputtering. Appl. Surf. Sci. **345**, 2015, 319-328.
49. Rednyk, A., Johánek, V., Khalakhan, I., Dubau, M., et al., Methanol oxidation on sputter-coated platinum oxide catalysts. Int. J. Hydrogen Energy **41**(1), 2016, 265-275.
50. Rednyk, A., Ostroverkh, A., and Johánek, V., Hydrogen production via methanol oxidation on platinum oxide thin film catalyst: Influence of methanol-to-oxygen ratio. Int. J. Hydrogen Energy **42**(49), 2017, 29254-29261.
51. Ostroverkh, A., Johanek, V., Kus, P., Sediva, R., and Matolin, V., Efficient Ceria-Platinum Inverse Catalyst for Partial Oxidation of Methanol. Langmuir **32**(25), 2016, 6297-6309.
52. Polášek, J., Johánek, V., Ostroverkh, A., and Mašek, K., Methanol oxidation on pure and platinum-doped tungsten oxide supported by activated carbon. Mater. Chem. Phys., 2018, submitted.
53. Hoffmann, J., Schauermann, S., Johanek, V., Hartmann, J., and Libuda, J., The kinetics of methanol oxidation on a supported Pd model catalyst: molecular beam and TR-IRAS experiments. J. Catal. **213**(2), 2003, 176-190.
54. Bertarione, S., Scarano, D., Zecchina, A., Johanek, V., et al., Surface reactivity of Pd nanoparticles supported on polycrystalline substrates as compared to thin film model catalysts: Infrared study of CO adsorption. J. Phys. Chem. B **108**(11), 2004, 3603-3613.
55. Bertarione, S., Scarano, D., Zecchina, A., Johanek, V., et al., Surface reactivity of Pd nanoparticles supported on polycrystalline substrates as compared to thin film model catalysts: infrared study of CH3OH adsorption. J. Catal. **223**(1), 2004, 64-73.
56. Laurin, M., Johanek, V., Grant, A.W., Kasemo, B., et al., Transient and steady state CO oxidation kinetics on nanolithographically prepared supported Pd model catalysts: Experiments and simulations. J. Chem. Phys. **123**(5), 2005, Art. # 054701.
57. Chasvin, N., Diez, A., Pronsato, E., Sediva, R., et al., Theoretical and experimental study of ethanol adsorption and dissociation on beta-Mo2C surfaces. Mol Catal **439**, 2017, 163-170.
58. Thomas, J.M. and Thomas, W.J., Principle and Practice of Heterogeneous Catalysis, 2nd Edition. 2015, Weinheim: Wiley-VCH.
59. Rideal, E.K., Concepts in Catalysis. 1968, London: Academic Press.
60. Nilsson, A., Pettersson, L.G.M., and Nørskov, J.K., eds. Chemical Bonding at Surfaces and Interfaces. 2008, Elsevier Science. 532.
61. Astruc, D., Lu, F., and Aranzaes, J.R., Nanoparticles as recyclable catalysts: The frontier between homogeneous and heterogeneous catalysis. Angew Chem Int Edit **44**(48), 2005, 7852-7872.
62. Gates, B.C., Supported Metal-Clusters - Synthesis, Structure, and Catalysis. Chem. Rev. (Washington, DC, U. S.) **95**(3), 1995, 511-522.

63. Rosei, F., Nanostructured surfaces: challenges and frontiers in nanotechnology. J Phys-Condens Mat **16**(17), 2004, S1373-S1436.
64. Yang, F., Deng, D.H., Pan, X.L., Fu, Q., and Bao, X.H., Understanding nano effects in catalysis. Natl Sci Rev **2**(2), 2015, 183-201.
65. Freund, H.J., Clusters and islands on oxides: from catalysis via electronics and magnetism to optics. Surf. Sci. **500**(1-3), 2002, 271-299.
66. Somorjai, G.A., Frei, H., and Park, J.Y., Advancing the Frontiers in Nanocatalysis, Biointerfaces, and Renewable Energy Conversion by Innovations of Surface Techniques. J. Am. Chem. Soc. **131**(46), 2009, 16589-16605.
67. Thomas, J.M., Heterogeneous catalysis: Enigmas, illusions, challenges, realities, and emergent strategies of design. J. Chem. Phys. **128**(18), 2008, Art. # 182502.
68. Sinfelt, J.H., Role of surface science in catalysis. Surf. Sci. **500**(1-3), 2002, 923-946.
69. Boudart, M., Turnover Rates in Heterogeneous Catalysis. Chem. Rev. (Washington, DC, U. S.) **95**(3), 1995, 661-666.
70. Gennari, F., Seneci, P., and Miertus, S., Application of combinatorial technologies for catalyst design and development. Catal Rev **42**(3), 2000, 385-402.
71. Dagani, R., A faster route to new materials. Chem. Eng. News **77**(10), 1999, 51-+.
72. Norskov, J.K., Bligaard, T., Logadottir, A., Bahn, S., et al., Universality in heterogeneous catalysis. J. Catal. **209**(2), 2002, 275-278.
73. Abild-Pedersen, F., Greeley, J., Studt, F., Rossmeisl, J., et al., Scaling properties of adsorption energies for hydrogen-containing molecules on transition-metal surfaces. Phys. Rev. Lett. **99**(1), 2007.
74. Dahl, S., Logadottir, A., Jacobsen, C.J.H., and Norskov, J.K., Electronic factors in catalysis: the volcano curve and the effect of promotion in catalytic ammonia synthesis. Appl Catal a-Gen **222**(1-2), 2001, 19-29.
75. Brønsted, J.N. and Pedersen, K.J., The catalytic disintegration of nitramide and its physical-chemical relevance. Z. Phys. Chem. (Muenchen, Ger.) **108**, 1924.
76. van Santen, R.A., Neurock, M., and Shetty, S.G., Reactivity Theory of Transition-Metal Surfaces: A Bronsted-Evans-Polanyi Linear Activation Energy-Free-Energy Analysis. Chem. Rev. (Washington, DC, U. S.) **110**(4), 2010, 2005-2048.
77. Hinshelwood, C.N., The Kinetics of Chemical Change. 1940, Oxford: Oxford University Press.
78. Hougen, O.A. and Watson, K.M., Chemical Process Principles. Part three. Kinetics and Catalysis. 1947, New York: J. Wiley and Sons.
79. Evans, M.G. and Polanyi, M., Further considerations on the thermodynamics of chemical equilibria and reaction rates. Transactions of the Faraday Society **32**(0), 1936, 1333-1360.
80. Bell, R.P., The theory of reactions involving proton transfers. Proceedings of the Royal Society of London. Series A - Mathematical and Physical Sciences **154**(882), 1936, 414-429.
81. Hammett, L.P. and Paul, M.A., The Relation between the Rates of Some Acid Catalyzed Reactions and the Acidity Function, H0. J. Am. Chem. Soc. **56**(4), 1934, 830-832.
82. Medford, A.J., Vojvodic, A., Hummelshoj, J.S., Voss, J., et al., From the Sabatier principle to a predictive theory of transition-metal heterogeneous catalysis. J. Catal. **328**, 2015, 36-42.
83. Sabatier, P., La catalyse en chimie organique. 1920, Paris et Liège: Librairie Polytechnique.
84. Zeigarnik, A.V., Valdes-Perez, R.E., and Pesenti, J., Comparative properties of transition metal catalysts inferred from activation energies of elementary steps of catalytic reactions. J. Phys. Chem. B **104**(5), 2000, 997-1008.
85. Abild-Pedersen, F., Computational catalyst screening: Scaling, bond-order and catalysis. Catal. Today **272**, 2016, 6-13.
86. Greeley, J., Jaramillo, T.F., Bonde, J., Chorkendorff, I.B., and Norskov, J.K., Computational high-throughput screening of electrocatalytic materials for hydrogen evolution. Nat. Mater. **5**(11), 2006, 909-913.
87. Fino, D., Bensaid, S., Piumetti, M., and Russo, N., A review on the catalytic combustion of soot in Diesel particulate filters for automotive applications: From powder catalysts to structured reactors. Appl Catal a-Gen **509**, 2016, 75-96.

88. Boudart, M., Model catalysts: reductionism for understanding. Top. Catal. **13**(1-2), 2000, 147-149.
89. Datye, A.K., Modeling of heterogeneous catalysts using simple geometry supports. Top. Catal. **13**(1-2), 2000, 131-138.
90. Libuda, J., Schalow, T., Brandt, B., Laurin, M., and Schauermann, S., Model studies in heterogeneous catalysis at the microscopic level: from the structure and composition of surfaces to reaction kinetics. Microchim. Acta **156**(1-2), 2006, 9-20.
91. Goodman, D.W., Model Studies in Catalysis Using Surface Science Probes. Chem. Rev. (Washington, DC, U. S.) **95**(3), 1995, 523-536.
92. Baumer, M. and Freund, H.J., Metal deposits on well-ordered oxide films. Prog. Surf. Sci. **61**(7-8), 1999, 127-198.
93. Campbell, C.T., Ultrathin metal films and particles on oxide surfaces: Structural, electronic and chemisorptive properties. Surf. Sci. Rep. **27**(1-3), 1997, 1-111.
94. Henry, C.R., Surface studies of supported model catalysts. Surf. Sci. Rep. **31**(7-8), 1998, 235-325.
95. Kuhlenbeck, H., Shaikhutdinov, S., and Freund, H.J., Well-Ordered Transition Metal Oxide Layers in Model Catalysis - A Series of Case Studies. Chem. Rev. (Washington, DC, U. S.) **113**(6), 2013, 3986-4034.
96. Libuda, J. and Freund, H.J., Molecular beam experiments on model catalysts. Surf. Sci. Rep. **57**(7-8), 2005, 157-298.
97. Ertl, G., Reactions at surfaces: From atoms to complexity (Nobel lecture). Angew Chem Int Edit **47**(19), 2008, 3524-3535.
98. Goodman, D.W., Catalysis - from Single-Crystals to the Real-World. Surf. Sci. **299**(1-3), 1994, 837-848.
99. Liu, L.C. and Corma, A., Metal Catalysts for Heterogeneous Catalysis: From Single Atoms to Nanoclusters and Nanoparticles. Chem. Rev. (Washington, DC, U. S.) **118**(10), 2018, 4981-5079.
100. Prieto, G. and Schuth, F., Bridging the gap between insightful simplicity and successful complexity: From fundamental studies on model systems to technical catalysts. J. Catal. **328**, 2015, 59-71.
101. Goodman, D.W., Model Catalytic Studies over Metal Single-Crystals. Acc. Chem. Res. **17**(5), 1984, 194-200.
102. Rodriguez, J.A. and Goodman, D.W., High-Pressure Catalytic Reactions over Single-Crystal Metal-Surfaces. Surf. Sci. Rep. **14**(1-2), 1991, 1-107.
103. Ponec, V. and Bond, G.C., Catalysis by Metals and Alloys. 1995: Elsevier. 744.
104. Bent, B.E., Mimicking aspects of heterogeneous catalysis: Generating, isolating, and reacting proposed surface intermediates on single crystals in vacuum. Chem. Rev. (Washington, DC, U. S.) **96**(4), 1996, 1361-1390.
105. Pandey, K.C., Reconstruction of Semiconductor Surfaces - Buckling, Ionicity, and Pi-Bonded Chains. Phys. Rev. Lett. **49**(3), 1982, 223-226.
106. Dou, J., Sun, Z.C., Opalade, A.A., Wang, N., et al., Operando chemistry of catalyst surfaces during catalysis. Chem. Soc. Rev. **46**(7), 2017, 2001-2027.
107. Guo, X.C. and Madix, R.J., Imaging surface reactions at atomic resolution: A wealth of behavior on the nanoscale. J. Phys. Chem. B **107**(14), 2003, 3105-3116.
108. Chen, Q. and Richardson, N.V., Surface facetting induced by adsorbates. Prog. Surf. Sci. **73**(4-8), 2003, 59-77.
109. Tao, F. and Crozier, P.A., Atomic-Scale Observations of Catalyst Structures under Reaction Conditions and during Catalysis. Chem. Rev. (Washington, DC, U. S.) **116**(6), 2016, 3487-3539.
110. Freund, H.J., Libuda, J., Baumer, M., Risse, T., and Carlsson, A., Cluster, facets, and edges: Site-dependent selective chemistry on model catalysts. Chem. Rec. **3**(3), 2003, 181-200.
111. Ni, B. and Wang, X., Face the Edges: Catalytic Active Sites of Nanomaterials. Adv Sci **2**(7), 2015.

112. Zambelli, T., Wintterlin, J., Trost, J., and Ertl, G., Identification of the "active sites" of a surface-catalyzed reaction. Science **273**(5282), 1996, 1688-1690.
113. Norskov, J.K., Bligaard, T., Hvolbaek, B., Abild-Pedersen, F., et al., The nature of the active site in heterogeneous metal catalysis. Chem. Soc. Rev. **37**(10), 2008, 2163-2171.
114. Hammer, B., Special sites at noble and late transition metal catalysts. Top. Catal. **37**(1), 2006, 3-16.
115. Montemore, M.M., van Spronsen, M.A., Madix, R.J., and Friend, C.M., O-2 Activation by Metal Surfaces: Implications for Bonding and Reactivity on Heterogeneous Catalysts. Chem. Rev. (Washington, DC, U. S.) **118**(5), 2018, 2816-2862.
116. Yates, J.T., Surface-Chemistry at Metallic Step Defect Sites. J Vac Sci Technol A **13**(3), 1995, 1359-1367.
117. Streber, R., Papp, C., Lorenz, M.P.A., Bayer, A., et al., Sulfur Oxidation on Pt(355): It Is the Steps! Angew Chem Int Edit **48**(51), 2009, 9743-9746.
118. Vang, R.T., Honkala, K., Dahl, S., Vestergaard, E.K., et al., Controlling the catalytic bond-breaking selectivity of Ni surfaces by step blocking. Nat. Mater. **4**(2), 2005, 160-162.
119. Bengaard, H.S., Norskov, J.K., Sehested, J., Clausen, B.S., et al., Steam reforming and graphite formation on Ni catalysts. J. Catal. **209**(2), 2002, 365-384.
120. Jones, G., Jakobsen, J.G., Shim, S.S., Kleis, J., et al., First principles calculations and experimental insight into methane steam reforming over transition metal catalysts. J. Catal. **259**(1), 2008, 147-160.
121. Honkala, K., Hellman, A., Remediakis, I.N., Logadottir, A., et al., Ammonia synthesis from first-principles calculations. Science **307**(5709), 2005, 555-558.
122. Greeley, J. and Mavrikakis, M., Alloy catalysts designed from first principles. Nat. Mater. **3**(11), 2004, 810-815.
123. Chen, J.G., Menning, C.A., and Zellner, M.B., Monolayer bimetallic surfaces: Experimental and theoretical studies of trends in electronic and chemical properties. Surf. Sci. Rep. **63**(5), 2008, 201-254.
124. Rodriguez, J.A., Physical and chemical properties of bimetallic surfaces. Surf. Sci. Rep. **24**(7-8), 1996, 223-287.
125. Campbell, C.T., Bimetallic Surface-Chemistry. Annu. Rev. Phys. Chem. **41**, 1990, 775-837.
126. Abbet, S., Judai, K., Klinger, L., and Heiz, U., Synthesis of monodispersed model catalysts using softlanding cluster deposition. Pure Appl. Chem. **74**(9), 2002, 1527-1535.
127. Diebold, U., Li, S.C., and Schmid, M., Oxide Surface Science. Annual Review of Physical Chemistry, Vol 61 **61**, 2010, 129-148.
128. Campbell, C.T. and Sauer, J., Introduction: Surface Chemistry of Oxides. Chem. Rev. (Washington, DC, U. S.) **113**(6), 2013, 3859-3862.
129. Henrich, V.E. and Cox, P.A., The Surface Science of Metal Oxides. 1996: Cambridge University Press. 464.
130. Cox, P.A., Transition Metal Oxides: An Introduction to Their Electronic Structure and Properties. 2010: Oxford University Press. 304.
131. Cappus, D., Hassel, M., Neuhaus, E., Heber, M., et al., Polar Surfaces of Oxides - Reactivity and Reconstruction. Surf. Sci. **337**(3), 1995, 268-277.
132. Noguera, C., Polar oxide surfaces. J Phys-Condens Mat **12**(31), 2000, R367-R410.
133. Goniakowski, J., Finocchi, F., and Noguera, C., Polarity of oxide surfaces and nanostructures. Reports on Progress in Physics **71**(1), 2008.
134. Tasker, P.W., The stability of ionic crystal surfaces. J. Phys. C: Solid State Phys. **12**, 1979.
135. Ventrice, C.A., Bertrams, T., Hannemann, H., Brodde, A., and Neddermeyer, H., Stable Reconstruction of the Polar (111) Surface of NiO on Au(111). Phys. Rev. B **49**(8), 1994, 5773-5776.
136. Freund, H.J., Dillmann, B., Seiferth, O., Klivenyi, G., et al., Molecules on oxide surfaces. Catal. Today **32**(1-4), 1996, 1-10.
137. Dulub, O., Diebold, U., and Kresse, G., Novel stabilization mechanism on polar surfaces: ZnO(0001)-Zn. Phys. Rev. Lett. **90**(1), 2003.

138. Lauritsen, J.V., Porsgaard, S., Rasmussen, M.K., Jensen, M.C.R., et al., Stabilization Principles for Polar Surfaces of ZnO. ACS Nano **5**(7), 2011, 5987-5994.
139. Henderson, M.A., Structural sensitivity in the dissociation of water on TiO2 single-crystal surfaces. Langmuir **12**(21), 1996, 5093-5098.
140. Diebold, U., The surface science of titanium dioxide. Surf. Sci. Rep. **48**(5-8), 2003, 53-229.
141. Gong, X.Q., Selloni, A., Batzill, M., and Diebold, U., Steps on anatase TiO2(101). Nat. Mater. **5**(8), 2006, 665-670.
142. Setvin, M., Hao, X.F., Daniel, B., Pavelec, J., et al., Charge Trapping at the Step Edges of TiO2 Anatase (101). Angew Chem Int Edit **53**(18), 2014, 4714-4716.
143. Gong, X.Q., Selloni, A., Dulub, O., Jacobson, P., and Diebold, U., Small au and pt clusters at the anatase TiO2(101) surface: Behavior at terraces, steps, and surface oxygen vacancies. J. Am. Chem. Soc. **130**(1), 2008, 370-381.
144. Torbrugge, S., Cranney, M., and Reichling, M., Morphology of step structures on CeO2(111). Appl. Phys. Lett. **93**(7), 2008.
145. Nilius, N., Kozlov, S.M., Jerratsch, J.F., Baron, M., et al., Formation of One-Dimensional Electronic States along the Step Edges of CeO2(111). ACS Nano **6**(2), 2012, 1126-1133.
146. Kozlov, S.M., Vines, F., Nilius, N., Shaikhutdinov, S., and Neyman, K.M., Absolute Surface Step Energies: Accurate Theoretical Methods Applied to Ceria Nanoislands. J Phys Chem Lett **3**(15), 2012, 1956-1961.
147. Kozlov, S.M. and Neyman, K.M., O vacancies on steps on the CeO2(111) surface. Phys. Chem. Chem. Phys. **16**(17), 2014, 7823-7829.
148. Dvorak, F., Stetsovych, O., Steger, M., Cherradi, E., et al., Adjusting Morphology and Surface Reduction of CeO2(111) Thin Films on Cu(111). J. Phys. Chem. C **115**(15), 2011, 7496-7503.
149. Batzill, M. and Diebold, U., The surface and materials science of tin oxide. Prog. Surf. Sci. **79**(2-4), 2005, 47-154.
150. Heinke, L., Lichtenstein, L., Simon, G.H., Konig, T., et al., Structure and electronic properties of step edges in the aluminum oxide film on NiAl(110). Phys. Rev. B **82**(7), 2010.
151. Heffelfinger, J.R., Bench, M.W., and Carter, C.B., Steps and the structure of the (0001)alpha-alumina surface. Surf. Sci. **370**(1), 1997, L168-L172.
152. Zhou, G.W., Luo, L.L., Li, L., Ciston, J., et al., Step-Edge-Induced Oxide Growth During the Oxidation of Cu Surfaces. Phys. Rev. Lett. **109**(23), 2012.
153. Chizallet, C., Costentin, G., Che, M., Delbecq, F., and Sautet, P., Revisiting acido-basicity of the MgO surface by periodic density functional theory calculations: Role of surface topology and ion coordination on water dissociation. J. Phys. Chem. B **110**(32), 2006, 15878-15886.
154. Di Cosimo, J.I., Díez, V.K., Ferretti, C., and Apesteguía, C.R., Basic catalysis on MgO: generation, characterization and catalytic properties of active sites, in Catalysis. 2014, The Royal Society of Chemistry. p. 1-28.
155. Woll, C., The chemistry and physics of zinc oxide surfaces. Prog. Surf. Sci. **82**(2-3), 2007, 55-120.
156. Fu, Q., Yang, F., and Bao, X.H., Interface-Confined Oxide Nanostructures for Catalytic Oxidation Reactions. Acc. Chem. Res. **46**(8), 2013, 1692-1701.
157. Jupille, J. and Thornton, G., eds. Defects at Oxide Surfaces. 2015, Springer International Publishing: Switzerland. 462.
158. Puigdollers, A.R., Schlexer, P., Tosoni, S., and Pacchioni, G., Increasing Oxide Reducibility: The Role of Metal/Oxide Interfaces in the Formation of Oxygen Vacancies. Acs Catal **7**(10), 2017, 6493-6513.
159. Esch, F., Fabris, S., Zhou, L., Montini, T., et al., Electron localization determines defect formation on ceria substrates. Science **309**(5735), 2005, 752-755.
160. Chen, B.H., Ma, Y.S., Ding, L.B., Xu, L.S., et al., Reactivity of Hydroxyls and Water on a CeO2(111) Thin Film Surface: The Role of Oxygen Vacancy. J. Phys. Chem. C **117**(11), 2013, 5800-5810.
161. Campbell, C.T., Waltzing with O-2. Science **299**(5605), 2003, 357-357.

162. Schaub, R., Wahlstrom, E., Ronnau, A., Laegsgaard, E., et al., Oxygen-mediated diffusion of oxygen vacancies on the TiO2(110) surface. Science **299**(5605), 2003, 377-379.
163. Wahlstrom, E., Vestergaard, E.K., Schaub, R., Ronnau, A., et al., Electron transfer-induced dynamics of oxygen molecules on the TiO2(110) surface. Science **303**(5657), 2004, 511-513.
164. Rasmussen, M.D., Molina, L.M., and Hammer, B., Adsorption, diffusion, and dissociation of molecular oxygen at defected TiO2(110): A density functional theory study. J. Chem. Phys. **120**(2), 2004, 988-997.
165. Zecchina, A., Lamberti, C., and Bordiga, S., Surface acidity and basicity: General concepts. Catal. Today **41**(1-3), 1998, 169-177.
166. Somorjai, A.G. and Li, Y., Introduction to Surface Chemistry and Catalysis, 2nd Edition. 2010: Wiley. 800.
167. Metiu, H., Chretien, S., Hu, Z.P., Li, B., and Sun, X.Y., Chemistry of Lewis Acid-Base Pairs on Oxide Surfaces. J. Phys. Chem. C **116**(19), 2012, 10439-10450.
168. Freund, H.J. and Pacchioni, G., Oxide ultra-thin films on metals: new materials for the design of supported metal catalysts. Chem. Soc. Rev. **37**(10), 2008, 2224-2242.
169. Kuhlenbeck, H. and Freund, H.J., Growth and Properties of Ultrathin Epitaxial Layers, in The Chemical Physics of Solid Surfaces, D.A. King and D.P. Woodruff, Editors. 1997, Elsevier: Amsterdam. p. 340.
170. Netzer, F.P. and Fortunelli, A., eds. Oxide Materials at the Two-Dimensional Limit. 2016, Springer: Cham.
171. Schwab, G.-M., Electronics of Supported Catalysts, in Advances in Catalysis, D.D. Eley, H. Pines, and P.B. Weisz, Editors. 1979, Academic Press. p. 1-22.
172. Freund, H.J., The Surface Science of Catalysis and More, Using Ultrathin Oxide Films as Templates: A Perspective. J. Am. Chem. Soc. **138**(29), 2016, 8985-8996.
173. Freysoldt, C., Rinke, P., and Scheffler, M., Ultrathin oxides: Bulk-oxide-like model surfaces or unique films? Phys. Rev. Lett. **99**(8), 2007.
174. Fu, Q., Li, W.X., Yao, Y.X., Liu, H.Y., et al., Interface-Confined Ferrous Centers for Catalytic Oxidation. Science **328**(5982), 2010, 1141-1144.
175. Boffa, A., Lin, C., Bell, A.T., and Somorjai, G.A., Promotion of Co and Co2 Hydrogenation over Rh by Metal-Oxides - the Influence of Oxide Lewis Acidity and Reducibility. J. Catal. **149**(1), 1994, 149-158.
176. Hrbek, J., Inverse oxide/metal catalysts: Surface science models for fundamental studies in catalysis. Abstr. Pap. Am. Chem. Soc. **240**, 2010.
177. Rodriguez, J.A. and Hrbek, J., Inverse oxide/metal catalysts: A versatile approach for activity tests and mechanistic studies. Surf. Sci. **604**(3-4), 2010, 241-244.
178. Lee, K.R. and Kwon, Y.U., Hard Templates for Fabrication of Nanostructured Films. NANO **5**(2), 2010, 75-87.
179. Nilius, N., Ganduglia-Pirovano, M.V., Brazdova, V., Kulawik, M., et al., Electronic properties and charge state of gold monomers and chains adsorbed on alumina thin films on NiAl(110). Phys. Rev. B **81**(4), 2010.
180. Eberhardt, W., Clusters as new materials. Surf. Sci. **500**(1-3), 2002, 242-270.
181. St Clair, T.P. and Goodman, D.W., Metal nanoclusters supported on metal oxide thin films: bridging the materials gap. Top. Catal. **13**(1-2), 2000, 5-19.
182. Rainer, D.R. and Goodman, D.W., Metal clusters on ultrathin oxide films: model catalysts for surface science studies. Journal of Molecular Catalysis A-Chemical **131**(1-3), 1998, 259-283.
183. Frank, M. and Baumer, M., From atoms to crystallites: adsorption on oxide-supported metal particles. Phys. Chem. Chem. Phys. **2**(17), 2000, 3723-3737.
184. Henry, C.R., Morphology of supported nanoparticles. Prog. Surf. Sci. **80**(3-4), 2005, 92-116.
185. Muller, S.A., Degler, D., Feldmann, C., Turk, M., et al., Exploiting Synergies in Catalysis and Gas Sensing using Noble Metal-Loaded Oxide Composites. Chemcatchem **10**(5), 2018, 864-880.
186. Schalow, T., Laurin, M., Brandt, B., Schauermann, S., et al., Oxygen storage at the metal/oxide interface of catalyst nanoparticles. Angew Chem Int Edit **44**(46), 2005, 7601-7605.

187. Hornes, A., Hungria, A.B., Bera, P., Camara, A.L., et al., Inverse CeO2/CuO Catalyst As an Alternative to Classical Direct Configurations for Preferential Oxidation of CO in Hydrogen-Rich Stream. J. Am. Chem. Soc. **132**(1), 2010, 34-+.
188. Freund, H.J., Ernst, N., Risse, T., Hamann, H., and Rupprechter, G., Models in heterogeneous catalysis: Surface science quo vadis? Physica Status Solidi A-Applied Research **187**(1), 2001, 257-274.
189. Cao, S.W., Tao, F., Tang, Y., Li, Y.T., and Yu, J.G., Size- and shape-dependent catalytic performances of oxidation and reduction reactions on nanocatalysts. Chem. Soc. Rev. **45**(17), 2016, 4747-4765.
190. Burda, C., Chen, X.B., Narayanan, R., and El-Sayed, M.A., Chemistry and properties of nanocrystals of different shapes. Chem. Rev. (Washington, DC, U. S.) **105**(4), 2005, 1025-1102.
191. Luches, P. and Valeri, S., Structure, Morphology and Reducibility of Epitaxial Cerium Oxide Ultrathin Films and Nanostructures. Materials **8**(9), 2015, 5818-5833.
192. Fernández-García, M. and Rodriguez, J.A., Metal Oxide Nanoparticles, in Encyclopedia of Inorganic Chemistry, R.B. King, R.H. Crabtree, C.M. Lukehart, et al., Editors. 2009.
193. Hakim, S.H., Sener, C., Alba-Rubio, A.C., Gostanian, T.M., et al., Synthesis of supported bimetallic nanoparticles with controlled size and composition distributions for active site elucidation. J. Catal. **328**, 2015, 75-90.
194. Wong, A., Lin, Q., Griffin, S., Nicholls, A., and Regalbuto, J.R., Synthesis of ultrasmall, homogeneously alloyed, bimetallic nanoparticles on silica supports. Science **358**(6369), 2017, 1427-1430.
195. Chen, P.C., Liu, G.L., Zhou, Y., Brown, K.A., et al., Tip-Directed Synthesis of Multimetallic Nanoparticles. J. Am. Chem. Soc. **137**(28), 2015, 9167-9173.
196. Rupprechter, G. and Weilach, C., Spectroscopic studies of surface-gas interactions and catalyst restructuring at ambient pressure: mind the gap! J Phys-Condens Mat **20**(18), 2008.
197. Kusada, K., Kobayashi, H., Ikeda, R., Kubota, Y., et al., Solid Solution Alloy Nanoparticles of Immiscible Pd and Ru Elements Neighboring on Rh: Changeover of the Thermodynamic Behavior for Hydrogen Storage and Enhanced CO-Oxidizing Ability. J. Am. Chem. Soc. **136**(5), 2014, 1864-1871.
198. Wang, F.L., Kusada, K., Wu, D.S., Yamamoto, T., et al., Solid-Solution Alloy Nanoparticles of the Immiscible Iridium-Copper System with a Wide Composition Range for Enhanced Electrocatalytic Applications. Angew Chem Int Edit **57**(17), 2018, 4505-4509.
199. Tyo, E.C. and Vajda, S., Catalysis by clusters with precise numbers of atoms. Nat. Nanotechnol. **10**(7), 2015, 577-588.
200. Heiz, U., Sanchez, A., Abbet, S., and Schneider, W.D., Catalytic oxidation of carbon monoxide on monodispersed platinum clusters: Each atom counts. J. Am. Chem. Soc. **121**(13), 1999, 3214-3217.
201. Contreras, A.M., Grunes, J., Yan, X.M., Liddle, A., and Somorjai, G.A., Fabrication of platinum nanoparticles and nanowires by electron beam lithography (EBL) and nanoimprint lithography (NIL): comparison of ethylene hydrogenation kinetics. Catal. Lett. **100**(3-4), 2005, 115-124.
202. Plummer, E.W., Ismail, Matzdorf, R., Melechko, A.V., et al., Surfaces: a playground for physics with broken symmetry in reduced dimensionality. Surf. Sci. **500**(1-3), 2002, 1-27.
203. Henry, C.R., 2D-Arrays of Nanoparticles as Model Catalysts. Catal. Lett. **145**(3), 2015, 731-749.
204. Lin, H.X., Chen, L., Liu, D.Y., Lei, Z.C., et al., Constructing Two-Dimensional Nanoparticle Arrays on Layered Materials Inspired by Atomic Epitaxial Growth. J. Am. Chem. Soc. **137**(8), 2015, 2828-2831.
205. Tang, Z.Y. and Kotov, N.A., One-dimensional assemblies of nanoparticles: Preparation, properties, and promise. Adv. Mater. (Weinheim, Ger.) **17**(8), 2005, 951-962.
206. Wiame, F., Strategies for the growth of large-scale self-organized structures. Thin Solid Films **642**, 2017, 258-275.
207. Yang, X.F., Wang, A.Q., Qiao, B.T., Li, J., et al., Single-Atom Catalysts: A New Frontier in Heterogeneous Catalysis. Acc. Chem. Res. **46**(8), 2013, 1740-1748.

208. Bruix, A., Lykhach, Y., Matolinova, I., Neitzel, A., et al., Maximum Noble-Metal Efficiency in Catalytic Materials: Atomically Dispersed Surface Platinum. Angew Chem Int Edit **53**(39), 2014, 10525-10530.
209. Wang, A.Q., Li, J., and Zhang, T., Heterogeneous single-atom catalysis. Nat Rev Chem **2**(6), 2018, 65-81.
210. Goodman, D.W., Correlations between surface science models and "real-world" catalysts. J. Phys. Chem. **100**(31), 1996, 13090-13102.
211. Libuda, J. and Freund, H.J., Reaction kinetics on complex model catalysts under single scattering conditions. J. Phys. Chem. B **106**(19), 2002, 4901-4915.
212. Freund, H.J., Kuhlenbeck, H., Libuda, J., Rupprechter, G., et al., Bridging the pressure and materials gaps between catalysis and surface science: clean and modified oxide surfaces. Top. Catal. **15**(2-4), 2001, 201-209.
213. Freund, H.J., Baumer, M., and Kuhlenbeck, H., Catalysis and surface science: What do we learn from studies of oxide-supported cluster model systems? Adv. Catal. **45**, 2000, 333-384.
214. Over, H. and Muhler, M., Catalytic CO oxidation over ruthenium - bridging the pressure gap. Prog. Surf. Sci. **72**(1-4), 2003, 3-17.
215. Hendriksen, B.L.M., Bobaru, S.C., and Frenken, J.W.M., Looking at heterogeneous catalysis at atmospheric pressure using tunnel vision. Top. Catal. **36**(1-4), 2005, 43-54.
216. Mars, P. and van Krevelen, D.W., Oxidations carried out by means of vanadium oxide catalysts. Chem. Eng. Sci. **3**(Supplement 1), 1954, 41-59.
217. Frenken, J. and Groot, I., eds. Operando Research in Heterogeneous Catalysis. 2017, Springer. 222.
218. Woodruff, D.P., Bridging the pressure gap: Can we get local quantitative structural information at 'near-ambient' pressures? Surf. Sci. **652**, 2016, 4-6.
219. Whatmore, R.W., Nanotechnology - what is it? Should we be worried? Occup Med-Oxford **56**(5), 2006, 295-299.
220. Schwarz, J.A., Contescu, C., and Contescu, A., Methods for Preparation of Catalytic Materials. Chem. Rev. (Washington, DC, U. S.) **95**(3), 1995, 477-510.
221. Freund, H.J., Baumer, M., Libuda, J., Risse, T., et al., Preparation and characterization of model catalysts: from ultrahigh vacuum to in situ conditions at the atomic dimension. J. Catal. **216**(1-2), 2003, 223-235.
222. Roldan Cuenya, B., Synthesis and catalytic properties of metal nanoparticles: Size, shape, support, composition, and oxidation state effects. Thin Solid Films **518**(12), 2010, 3127-3150.
223. Arthur, J.R., Molecular beam epitaxy. Surf. Sci. **500**(1-3), 2002, 189-217.
224. Tu, C.W. and Harris Jr., J.S., eds. Molecular Beam Epitaxy. 1990, North Holland: Amsterdam.
225. Newman, N., Fu, T.C., Liu, X., Lilientalweber, Z., et al., Fundamental Materials-Issues Involved in the Growth of Gan by Molecular Beam Epitaxy. Diamond, Sic and Nitride Wide Bandgap Semiconductors **339**, 1994, 483-489.
226. Sitter, M.A. and Sitter, H., Molecular beam epitaxy, Fundamentals and Current Status. 2 ed. 1996, Berlin: Springer,.
227. Chambers, S.A., Epitaxial growth and properties of thin film oxides. Surf. Sci. Rep. **39**(5-6), 2000, 105-180.
228. Vedrine, J.C., Metal Oxides in Heterogeneous Catalysis. 1 ed. 2018: Elsevier. 618.
229. Iijima, K., Terashima, T., Bando, Y., Kamigaki, K., and Terauchi, H., Atomic Layer Growth of Oxide Thin-Films with Perovskite-Type Structure by Reactive Evaporation. J. Appl. Phys. **72**(7), 1992, 2840-2845.
230. Matolin, V., Cabala, M., Chab, V., Matolinova, I., et al., A resonant photoelectron spectroscopy study of Sn(O-x) doped CeO2 catalysts. Surf. Interface Anal. **40**(3-4), 2008, 225-230.
231. Xu, X., Oh, W.S., and Goodman, D.W., Interfacial reactions between oxide films and refractory metal substrates. Langmuir **12**(20), 1996, 4877-4881.
232. Jaeger, R.M., Kuhlenbeck, H., Freund, H.J., Wuttig, M., et al., Formation of a Well-Ordered Aluminum-Oxide Overlayer by Oxidation of NiAl(110). Surf. Sci. **259**(3), 1991, 235-252.

233. Singh, R.K. and Narayan, J., Pulsed-Laser Evaporation Technique for Deposition of Thin-Films - Physics and Theoretical-Model. Phys. Rev. B **41**(13), 1990, 8843-8859.
234. Willmott, P.R. and Huber, J.R., Pulsed laser vaporization and deposition. Rev. Mod. Phys. **72**(1), 2000, 315-328.
235. Brauer, G., Szyszka, B., Vergohl, M., and Bandorf, R., Magnetron sputtering - Milestones of 30 years. Vacuum **84**(12), 2010, 1354-1359.
236. Thornton, J.A., Magnetron Sputtering - Basic Physics and Application to Cylindrical Magnetrons. J Vac Sci Technol **15**(2), 1978, 171-177.
237. Kelly, P.J. and Arnell, R.D., Magnetron sputtering: a review of recent developments and applications. Vacuum **56**(3), 2000, 159-172.
238. Sarakinos, K., Alami, J., and Konstantinidis, S., High power pulsed magnetron sputtering: A review on scientific and engineering state of the art. Surf. Coat. Technol. **204**(11), 2010, 1661-1684.
239. Safi, I., Recent aspects concerning DC reactive magnetron sputtering of thin films: A review. Surf. Coat. Technol. **127**(2-3), 2000, 203-219.
240. Bunshah, R.F. and Deshpandey, C., Plasma-Assisted Deposition Techniques for Hard Coatings. Vacuum **41**(7-9), 1990, 2190-2195.
241. Musil, J., Baroch, P., Vlcek, J., Nam, K.H., and Han, J.G., Reactive magnetron sputtering of thin films: present status and trends. Thin Solid Films **475**(1-2), 2005, 208-218.
242. Choy, K.L., Chemical vapour deposition of coatings. Prog Mater Sci **48**(2), 2003, 57-170.
243. Meyerson, B.S., Low-Temperature Silicon Epitaxy by Ultrahigh-Vacuum Chemical Vapor-Deposition. Appl. Phys. Lett. **48**(12), 1986, 797-799.
244. Hoffman, D.M., Chemical-Vapor-Deposition of Nitride Thin-Films. Polyhedron **13**(8), 1994, 1169-1179.
245. Rand, M.J., Chemical Vapor-Deposition of Thin-Film Platinum. J. Electrochem. Soc. **119**(8), 1972, C238-&.
246. Okumura, M., Nakamura, S., Tsubota, S., Nakamura, T., et al., Chemical vapor deposition of gold on Al2O3, SiO2, and TiO2 for the oxidation of CO and of H-2. Catal. Lett. **51**(1-2), 1998, 53-58.
247. Barreca, D., Massignan, C., Daolio, S., Fabrizio, M., et al., Composition and microstructure of cobalt oxide thin films obtained from a novel cobalt(II) precursor by chemical vapor deposition. Chem. Mater. **13**(2), 2001, 588-593.
248. Wu, J.J. and Liu, S.C., Low-temperature growth of well-aligned ZnO nanorods by chemical vapor deposition. Adv. Mater. (Weinheim, Ger.) **14**(3), 2002, 215-+.
249. Kumar, M. and Ando, Y., Chemical Vapor Deposition of Carbon Nanotubes: A Review on Growth Mechanism and Mass Production. J. Nanosci. Nanotechnol. **10**(6), 2010, 3739-3758.
250. Li, Y.L., Kinloch, I.A., and Windle, A.H., Direct spinning of carbon nanotube fibers from chemical vapor deposition synthesis. Science **304**(5668), 2004, 276-278.
251. Reina, A., Jia, X.T., Ho, J., Nezich, D., et al., Large Area, Few-Layer Graphene Films on Arbitrary Substrates by Chemical Vapor Deposition. Nano Lett. **9**(1), 2009, 30-35.
252. Shi, Y.M., Hamsen, C., Jia, X.T., Kim, K.K., et al., Synthesis of Few-Layer Hexagonal Boron Nitride Thin Film by Chemical Vapor Deposition. Nano Lett. **10**(10), 2010, 4134-4139.
253. Zhang, Y., Zhang, L.Y., and Zhou, C.W., Review of Chemical Vapor Deposition of Graphene and Related Applications. Acc. Chem. Res. **46**(10), 2013, 2329-2339.
254. Kim, K.K., Hsu, A., Jia, X.T., Kim, S.M., et al., Synthesis of Monolayer Hexagonal Boron Nitride on Cu Foil Using Chemical Vapor Deposition. Nano Lett. **12**(1), 2012, 161-166.
255. Anderson, J.R., Structure of Metallic Catalysts. 1975, New York: Academic Press.
256. Gunter, P.L.J., Niemantsverdriet, J.W., Ribeiro, F.H., and Somorjai, G.A., Surface science approach to modeling supported catalysts. Catal Rev **39**(1-2), 1997, 77-168.
257. Heiz, U., Vanolli, F., Trento, L., and Schneider, W.D., Chemical reactivity of size-selected supported clusters: An experimental setup. Rev. Sci. Instrum. **68**(5), 1997, 1986-1994.
258. Che, M. and Védrine , J.C., eds. Characterization of Solid Materials and Heterogeneous Catalysts: From Structure to Surface Reactivity. 2012, Wiley-VCH: Weinheim.

259. Mozetic, M., Vesel, A., Primc, G., Eisenmenger-Sittner, C., et al., Recent developments in surface science and engineering, thin films, nanoscience, biomaterials, plasma science, and vacuum technology. Thin Solid Films **660**, 2018, 120-160.
260. Grunwaldt, J.D., Wagner, J.B., and Dunin-Borkowski, R.E., Imaging Catalysts at Work: A Hierarchical Approach from the Macro- to the Meso- and Nano-scale. ChemCatChem **5**(1), 2013, 62-80.
261. Zaera, F., Outstanding mechanistic questions in heterogeneous catalysis. J. Phys. Chem. B **106**(16), 2002, 4043-4052.
262. Hansen, P.L., Wagner, J.B., Helveg, S., Rostrup-Nielsen, J.R., et al., Atom-resolved imaging of dynamic shape changes in supported copper nanocrystals. Science **295**(5562), 2002, 2053-2055.
263. Over, H., Crystallographic study of interaction between adspecies on metal surfaces. Prog. Surf. Sci. **58**(4), 1998, 249-376.
264. Somorjai, G.A., Contreras, A.M., Montano, M., and Rioux, R.M., Clusters, surfaces, and catalysis. Proc. Natl. Acad. Sci. U. S. A. **103**(28), 2006, 10577-10583.
265. Heinz, K., Geometrical and Chemical Restructuring of Clean Metal-Surfaces as Retrieved by Leed. Surf. Sci. **299**(1-3), 1994, 433-446.
266. Freund, H.J., Models for oxidation catalyst: Characterization and reaction at the atomic level. Catal. Today **117**(1-3), 2006, 6-14.
267. Gruyters, M. and King, D.A., Effects of restructuring in adsorption and reaction dynamics at metal surfaces. J Chem Soc Faraday T **93**(17), 1997, 2947-2956.
268. Graoui, H., Giorgio, S., and Henry, C.R., Shape variations of Pd particles under oxygen adsorption. Surf. Sci. **417**(2-3), 1998, 350-360.
269. Vendelbo, S.B., Elkjaer, C.F., Falsig, H., Puspitasari, I., et al., Visualization of oscillatory behaviour of Pt nanoparticles catalysing CO oxidation. Nat. Mater. **13**(9), 2014, 884-890.
270. Zhou, Y., Jin, C.C., Li, Y., and Shen, W.J., Dynamic behavior of metal nanoparticles for catalysis. Nano Today **20**, 2018, 101-120.
271. Resasco, J., Dai, S., Graham, G., Pan, X., and Christopher, P., Combining In-Situ Transmission Electron Microscopy and Infrared Spectroscopy for Understanding Dynamic and Atomic-Scale Features of Supported Metal Catalysts. The Journal of Physical Chemistry C **122**(44), 2018, 25143-25157.
272. Berko, A. and Solymosi, F., Adsorption-induced structural changes of Rh supported by TiO2(110)-(1x2): An STM study. J. Catal. **183**(1), 1999, 91-101.
273. Neitzel, A., Johanek, V., Lykhach, Y., Skala, T., et al., Reduction of Pt2+ species in model Pt-CeO2 fuel cell catalysts upon reaction with methanol. Appl. Surf. Sci. **387**, 2016, 674-681.
274. Wu, T.X., Pan, X.Q., Zhang, Y.B., Miao, Z.Z., et al., Investigation of the Redispersion of Pt Nanoparticles on Polyhedral Ceria Nanoparticles. J Phys Chem Lett **5**(14), 2014, 2479-2483.
275. Tsuji, H. and Hattori, H., Oxide surfaces that catalyse an acid-base reaction with surface lattice oxygen exchange: Evidence of nucleophilicity of oxide surfaces. ChemPhysChem **5**(5), 2004, 733-736.
276. Feng, Z.X., Lu, J.L., Feng, H., Stair, P.C., et al., Catalysts Transform While Molecules React: An Atomic-Scale View. J Phys Chem Lett **4**(2), 2013, 285-291.
277. Kung, H.H., Transition Metal Oxides: Surface Chemistry and Catalysis. 1989: Elsevier.
278. Liu, J.J., Fung, V., Wang, Y., Du, K.M., et al., Promotion of catalytic selectivity on transition metal oxide through restructuring surface lattice. Appl Catal B-Environ **237**, 2018, 957-969.
279. Ostendorf, F., Torbrugge, S., and Reichling, M., Atomic scale evidence for faceting stabilization of a polar oxide surface. Phys. Rev. B **77**(4), 2008.
280. Bao, H.Z., Zhang, W.H., Hua, Q., Jiang, Z.Q., et al., Crystal-Plane-Controlled Surface Restructuring and Catalytic Performance of Oxide Nanocrystals. Angew Chem Int Edit **50**(51), 2011, 12294-12298.
281. Zugic, B., Wang, L.C., Heine, C., Zakharov, D.N., et al., Dynamic restructuring drives catalytic activity on nanoporous gold-silver alloy catalysts. Nat. Mater. **16**(5), 2017, 558-+.
282. Tao, F., Grass, M.E., Zhang, Y.W., Butcher, D.R., et al., Reaction-Driven Restructuring of Rh-Pd and Pt-Pd Core-Shell Nanoparticles. Science **322**(5903), 2008, 932-934.

283. Neitzel, A., Figueroba, A., Lykhach, Y., Skala, T., et al., Atomically Dispersed Pd, Ni, and Pt Species in Ceria-Based Catalysts: Principal Differences in Stability and Reactivity. J. Phys. Chem. C **120**(18), 2016, 9852-9862.
284. Sushumna, I. and Ruckenstein, E., Redispersion of Pt/Alumina Via Film Formation. J. Catal. **108**(1), 1987, 77-96.
285. Campbell, C.T., Parker, S.C., and Starr, D.E., The effect of size-dependent nanoparticle energetics on catalyst sintering. Science **298**(5594), 2002, 811-814.
286. Yang, F., Chen, M.S., and Goodman, D.W., Sintering of Au Particles Supported on TiO2(110) during CO Oxidation. J. Phys. Chem. C **113**(1), 2009, 254-260.
287. Bartholomew, C.H., Mechanisms of catalyst deactivation. Appl Catal a-Gen **212**(1-2), 2001, 17-60.
288. Hansen, T.W., Delariva, A.T., Challa, S.R., and Datye, A.K., Sintering of Catalytic Nanoparticles: Particle Migration or Ostwald Ripening? Acc. Chem. Res. **46**(8), 2013, 1720-1730.
289. Somorjai, G.A., The evolution of surface chemistry. A personal view of building the future on past and present accomplishments. J. Phys. Chem. B **106**(36), 2002, 9201-9213.
290. Topsoe, H., Developments in operando studies and in situ characterization of heterogeneous catalysts. J. Catal. **216**(1-2), 2003, 155-164.
291. Salmeron, M. and Schlogl, R., Ambient pressure photoelectron spectroscopy: A new tool for surface science and nanotechnology. Surf. Sci. Rep. **63**(4), 2008, 169-199.
292. Yamamoto, S., Bluhm, H., Andersson, K., Ketteler, G., et al., In situ x-ray photoelectron spectroscopy studies of water on metals and oxides at ambient conditions. J Phys-Condens Mat **20**(18), 2008, Art. # 184025.
293. Knop-Gericke, A., Kleimenov, E., Havecker, M., Blume, R., et al., X-Ray Photoelectron Spectroscopy for Investigation of Heterogeneous Catalytic Processes. Adv. Catal. **52**, 2009, 213-272.
294. Wagner, J.B., Cavalca, F., Damsgaard, C.D., Duchstein, L.D.L., and Hansen, T.W., Exploring the environmental transmission electron microscope. Micron **43**(11), 2012, 1169-1175.
295. Danilatos, G.D., An Atmospheric Scanning Electron-Microscope (ASEM). Scanning **3**(3), 1980, 215-217.
296. Kolmakov, A., Dikin, D.A., Cote, L.J., Huang, J.X., et al., Graphene oxide windows for in situ environmental cell photoelectron spectroscopy. Nat. Nanotechnol. **6**(10), 2011, 651-657.
297. Kraus, J., Reichelt, R., Gunther, S., Gregoratti, L., et al., Photoelectron spectroscopy of wet and gaseous samples through graphene membranes. Nanoscale **6**(23), 2014, 14394-14403.
298. Weatherup, R.S., Eren, B., Hao, Y.B., Bluhm, H., and Salmeron, M.B., Graphene Membranes for Atmospheric Pressure Photoelectron Spectroscopy. J Phys Chem Lett **7**(9), 2016, 1622-1627.
299. Parsons, D.F., Structure of Wet Specimens in Electron-Microscopy. Science **186**(4162), 1974, 407-414.
300. Thiberge, S., Zik, O., and Moses, E., An apparatus for imaging liquids, cells, and other wet samples in the scanning electron microscopy. Rev. Sci. Instrum. **75**(7), 2004, 2280-2289.
301. Yoon, T.H., Applications of Soft X-ray Spectromicroscopy in Material and Environmental Sciences. Appl. Spectrosc. Rev. **44**(2), 2009, 91-122.
302. Sharma, R. and Weiss, K., Development of a TEM to study in situ structural and chemical changes at an atomic level during gas-solid interactions at elevated temperatures. Microsc Res Techniq **42**(4), 1998, 270-280.
303. de Jonge, N., Bigelow, W.C., and Veith, G.M., Atmospheric Pressure Scanning Transmission Electron Microscopy. Nano Lett. **10**(3), 2010, 1028-1031.
304. Swift, J.A. and Brown, A.C., Environmental Cell for Examination of Wet Biological Specimens at Atmospheric Pressure by Transmission Scanning Electron Microscopy. J Phys E Sci Instrum **3**(11), 1970, 924-&.

305. Sezen, H., Aleman, B., Amati, M., Dalmiglio, M., and Gregoratti, L., Spatially Resolved Chemical Characterization with Scanning Photoemission Spectromicroscopy: Towards Near-Ambient-Pressure Experiments. ChemCatChem **7**(22), 2015, 3665-3673.
306. Foxon, C.T., Boudry, M.R., and Joyce, B.A., Evaluation of surface kinetic data by the transform analysis of modulated molecular beam measurements. Surf. Sci. **44**(1), 1974, 69-92.
307. D'Evelyn, M.P. and Madix, R.J., Reactive scattering from solid surfaces. Surf. Sci. Rep. **3**(8), 1983, 413-495.
308. Scoles, G., ed. Atomic and Molecular Beam Methods. Vol. 1. 1988, Oxford University Press: New York.
309. Lee, Y.T., Molecular-Beam Studies of Elementary Chemical Processes - (Nobel Lecture). Angewandte Chemie-International Edition in English **26**(10), 1987, 939-951.
310. Barker, J.A. and Auerbach, D.J., Gas—surface interactions and dynamics; Thermal energy atomic and molecular beam studies. Surf. Sci. Rep. **4**(1), 1984, 1-99.
311. Libuda, J., Meusel, I., Hartmann, J., and Freund, H.J., A molecular beam/surface spectroscopy apparatus for the study of reactions on complex model catalysts. Rev. Sci. Instrum. **71**(12), 2000, 4395-4408.
312. King, D.A. and Wells, M.G., Molecular-Beam Investigation of Adsorption Kinetics on Bulk Metal Targets - Nitrogen on Tungsten. Surf. Sci. **29**(2), 1972, 454-+.
313. Guo, X.C. and King, D.A., Measuring the Absolute Sticking Probability at Desorption Temperatures. Surf. Sci. **302**(1-2), 1994, L251-L255.
314. Matsushima, T., Surface structural information carried by desorbing reaction products. Prog. Surf. Sci. **82**(7-8), 2007, 435-477.
315. Polanyi, J.C., Some Concepts in Reaction Dynamics. Acc. Chem. Res. **5**(5), 1972, 161-168.
316. Polanyi, J.C. and Zewail, A.H., Direct Observation of the Transition-State. Acc. Chem. Res. **28**(3), 1995, 119-132.
317. Rettner, C.T., Auerbach, D.J., Tully, J.C., and Kleyn, A.W., Chemical dynamics at the gas-surface interface. J. Phys. Chem. **100**(31), 1996, 13021-13033.
318. Bonn, M., Kleyn, A.W., and Kroes, G.J., Real time chemical dynamics at surfaces. Surf. Sci. **500**(1-3), 2002, 475-499.
319. Jacobs, D.C., The Role of Internal Energy and Approach Geometry in Molecule/Surface Reactive Scattering. J Phys-Condens Mat **7**(6), 1995, 1023-1045.
320. Comsa, G. and David, R., Dynamical parameters of desorbing molecules. Surf. Sci. Rep. **5**(4), 1985, 145-198.
321. Shannon, S.L. and Goodwin, J.G., Characterization of Catalytic Surfaces by Isotopic-Transient Kinetics during Steady-State Reaction. Chem. Rev. (Washington, DC, U. S.) **95**(3), 1995, 677-695.
322. Ryczkowski, J., IR spectroscopy in catalysis. Catal. Today **68**(4), 2001, 263-381.
323. Vimont, A., Thibault-Starzyk, F., and Daturi, M., Analysing and understanding the active site by IR spectroscopy. Chem. Soc. Rev. **39**(12), 2010, 4928-4950.
324. Weaver, M.J., Raman and infrared spectroscopies as in situ probes of catalytic adsorbate chemistry at electrochemical and related metal-gas interfaces: some perspectives and prospects. Top. Catal. **8**(1-2), 1999, 65-73.
325. Chesters, M.A., Infrared-Spectroscopy of Molecules on Metal Single-Crystal Surfaces. J. Electron Spectrosc. Relat. Phenom. **38**(1-4), 1986, 123-140.
326. Evans, J., Hayden, B., Mosselmans, F., and Murray, A., The Chemistry of Rhodium on TiO2(110) Deposited by MOCVD of [Rh(Co)(2)Cl](2) and MVD. Surf. Sci. **301**(1-3), 1994, 61-82.
327. Camplin, J.P., Cook, J.C., and Mccash, E.M., Reflection-Absorption IR Spectroscopy at Cryogenic Temperatures. J Chem Soc Faraday T **91**(20), 1995, 3563-3567.
328. Becker, A., Taran, C., Uhmann, W., and Siebert, F., Time-Resolved FTIR Spectroscopy Using a Step-Scan Interferometer. 7th International Conference on Fourier Transform Spectroscopy **1145**, 1989, 512-513.

329. Schulz, R.R. and Rossel, C., Beetle-Like Scanning Tunneling Microscope for Ultrahigh-Vacuum and Low-Temperature Applications. Rev. Sci. Instrum. **65**(6), 1994, 1918-1922.
330. Meyer, G., A simple low-temperature ultrahigh-vacuum scanning tunneling microscope capable of atomic manipulation. Rev. Sci. Instrum. **67**(8), 1996, 2960-2965.
331. Vasina, R., Kolarik, V., Dolezel, P., Mynar, M., et al., Mechanical design aspects of a soft X-ray plane grating monochromator. Nucl Instrum Meth A **467**, 2001, 561-564.
332. Vayssilov, G.N., Lykhach, Y., Migani, A., Staudt, T., et al., Support nanostructure boosts oxygen transfer to catalytically active platinum nanoparticles. Nat. Mater. **10**(4), 2011, 310-315.
333. Matolin, V., Matolinova, I., Sedlacek, L., Prince, K.C., and Skala, T., A resonant photoemission applied to cerium oxide based nanocrystals. Nanotechnology **20**(21), 2009.
334. Chen, J.G., NEXAFS investigations of transition metal oxides, nitrides, carbides, sulfides and other interstitial compounds. Surf. Sci. Rep. **30**(1-3), 1997, 1-152.
335. Twigg, M.V., Progress and future challenges in controlling automotive exhaust gas emissions. Appl Catal B-Environ **70**(1-4), 2007, 2-15.
336. Twigg, M.V., Catalytic control of emissions from cars. Catal. Today **163**(1), 2011, 33-41.
337. Arakawa, H., Aresta, M., Armor, J.N., Barteau, M.A., et al., Catalysis research of relevance to carbon management: Progress, challenges, and opportunities. Chem. Rev. (Washington, DC, U. S.) **101**(4), 2001, 953-996.
338. Parvulescu, V.I., Grange, P., and Delmon, B., Catalytic removal of NO. Catal. Today **46**(4), 1998, 233-316.
339. Bueno-Lopez, A., Diesel soot combustion ceria catalysts. Appl Catal B-Environ **146**, 2014, 1-11.
340. Trovarelli, A., ed. Catalysis by ceria and related materials. 2002, Imperial College Press: London.
341. Freund, H.J., Meijer, G., Scheffler, M., Schlogl, R., and Wolf, M., CO Oxidation as a Prototypical Reaction for Heterogeneous Processes. Angew Chem Int Edit **50**(43), 2011, 10064-10094.
342. Dörre, E. and Hübner, H., Alumina-Processing Properties and Applications. 1984, Berlin: Springer-Verlag.
343. Pines, H. and Haag, W.O., Alumina - Catalyst and Support 1. Alumina, Its Intrinsic Acidity and Catalytic Activity. J. Am. Chem. Soc. **82**(10), 1960, 2471-2483.
344. Levin, I. and Brandon, D., Metastable alumina polymorphs: Crystal structures and transition sequences. J. Am. Ceram. Soc. **81**(8), 1998, 1995-2012.
345. Chang, H.J., Choi, Y.M., Kong, K.J., and Ryu, B.H., Atomic and electronic structures of amorphous Al2O3. Chem. Phys. Lett. **391**(4-6), 2004, 293-296.
346. Kim, Y. and Hsu, T., A Reflection Electron-Microscopic (REM) Study of Alpha-Al2O3(0001) Surfaces. Surf. Sci. **258**(1-3), 1991, 131-146.
347. Batra, I.P., Electronic-Structure of Alpha-Al2O3. J Phys C Solid State **15**(26), 1982, 5399-5410.
348. Batyrev, I., Alavi, A., and Finnis, M.W., Ab initio calculations on the Al2O3(0001) surface. Faraday Discuss. **114**, 1999, 33-43.
349. Trueba, M. and Trasatti, S.P., gamma-Alumina as a support for catalysts: A review of fundamental aspects. Eur. J. Inorg. Chem. (17), 2005, 3393-3403.
350. McHale, J.M., Auroux, A., Perrotta, A.J., and Navrotsky, A., Surface energies and thermodynamic phase stability in nanocrystalline aluminas. Science **277**(5327), 1997, 788-791.
351. Guczi, L., Peto, G., Beck, A., and Paszti, Z., Electronic structure and catalytic properties of transition metal nanoparticles: the effect of size reduction. Top. Catal. **29**(3-4), 2004, 129-138.
352. Kleis, J., Greeley, J., Romero, N.A., Morozov, V.A., et al., Finite Size Effects in Chemical Bonding: From Small Clusters to Solids. Catal. Lett. **141**(8), 2011, 1067-1071.
353. Behafarid, F., Ono, L.K., Mostafa, S., Croy, J.R., et al., Electronic properties and charge transfer phenomena in Pt nanoparticles on gamma-Al2O3: size, shape, support, and adsorbate effects. Phys. Chem. Chem. Phys. **14**(33), 2012, 11766-11779.
354. Stara, I. and Matolin, V., The Influence of Particle-Size on CO Adsorption on Pd Alumina Model Catalysts. Surf. Sci. **313**(1-2), 1994, 99-106.
355. Hammer, B., Morikawa, Y., and Norskov, J.K., CO chemisorption at metal surfaces and overlayers. Phys. Rev. Lett. **76**(12), 1996, 2141-2144.

356. Khonde, K., Darville, J., and Gilles, J.M., The Interaction of CO with Al(100) - A Multi-Technique Study. Vacuum **31**(10-1), 1981, 499-501.
357. Toofan, J. and Watson, P.R., The termination of the alpha-Al2O3 (0001) surface: a LEED crystallography determination. Surf. Sci. **401**(2), 1998, 162-172.
358. Heiz, U., Sherwood, R., Cox, D.M., Kaldor, A., and Yates, J.T., Dynamics of the desorption of carbon monoxide from size-selected supported platinum clusters. Nato Adv Sci Inst Se **465**, 1995, 37-47.
359. Cox, D.M., Kaldor, A., Fayet, P., Eberhardt, W., et al., Effect of Cluster Size on Chemical and Electronic-Properties. ACS Symp. Ser. **437**, 1990, 172-187.
360. Allian, A.D., Takanabe, K., Fujdala, K.L., Hao, X., et al., Chemisorption of CO and Mechanism of CO Oxidation on Supported Platinum Nanoclusters. J. Am. Chem. Soc. **133**(12), 2011, 4498-4517.
361. Rodriguez, J.A. and Goodman, D.W., The Nature of the Metal Metal Bond in Bimetallic Surfaces. Science **257**(5072), 1992, 897-903.
362. Haller, G.L. and Resasco, D.E., Metal Support Interaction - Group-VIII Metals and Reducible Oxides. Adv. Catal. **36**, 1989, 173-235.
363. Hirschmugl, C.J., Frontiers in infrared spectroscopy at surfaces and interfaces. Surf. Sci. **500**(1-3), 2002, 577-604.
364. Libuda, J., Winkelmann, F., Baumer, M., Freund, H.J., et al., Structure and Defects of an Ordered Alumina Film on NiAl(110). Surf. Sci. **318**(1-2), 1994, 61-73.
365. Kulawik, M., Nilius, N., Rust, H.P., and Freund, H.J., Atomic structure of antiphase domain boundaries of a thin Al2O3 film on NiAl(110). Phys. Rev. Lett. **91**(25), 2003.
366. Meusel, I., Hoffmann, J., Hartmann, J., Heemeier, M., et al., The interaction of oxygen with alumina-supported palladium particles. Catal. Lett. **71**(1-2), 2001, 5-13.
367. Binggeli, N. and Altarelli, M., Surface reactivity and quantum-size effects on the electronic density decay length of ultrathin metal films. Phys. Rev. Lett. **96**(3), 2006.
368. Santen, R.A., Tranca, I., and Hensen, E.J.M., Theory of surface chemistry and reactivity of reducible oxides. Catal. Today **244**, 2015, 63-84.
369. Pacchioni, G. and Freund, H., Electron Transfer at Oxide Surfaces. The MgO Paradigm: from Defects to Ultrathin Films. Chem. Rev. (Washington, DC, U. S.) **113**(6), 2013, 4035-4072.
370. Montini, T., Melchionna, M., Monai, M., and Fornasiero, P., Fundamentals and Catalytic Applications of CeO2-Based Materials. Chem. Rev. (Washington, DC, U. S.) **116**(10), 2016, 5987-6041.
371. Mullins, D.R., The surface chemistry of cerium oxide. Surf. Sci. Rep. **70**(1), 2015, 42-85.
372. Conner, W.C. and Falconer, J.L., Spillover in Heterogeneous Catalysis. Chem. Rev. (Washington, DC, U. S.) **95**(3), 1995, 759-788.
373. Campbell, C.T., Catalyst-Support Interactions Electronic Perturbations. Nature Chem. **4**(8), 2012, 597-598.
374. Bruix, A., Rodriguez, J.A., Ramirez, P.J., Senanayake, S.D., et al., A New Type of Strong Metal-Support Interaction and the Production of H-2 through the Transformation of Water on Pt/CeO2(111) and Pt/CeOx/TiO2(110) Catalysts. J. Am. Chem. Soc. **134**(21), 2012, 8968-8974.
375. Farmer, J.A. and Campbell, C.T., Ceria Maintains Smaller Metal Catalyst Particles by Strong Metal-Support Bonding. Science **329**(5994), 2010, 933-936.
376. Nagai, Y., Hirabayashi, T., Dohmae, K., Takagi, N., et al., Sintering inhibition mechanism of platinum supported on ceria-based oxide and Pt-oxide-support interaction. J. Catal. **242**(1), 2006, 103-109.
377. Tauster, S.J., Fung, S.C., and Garten, R.L., Strong Metal-Support Interactions - Group-8 Noble-Metals Supported on TiO2. J. Am. Chem. Soc. **100**(1), 1978, 170-175.
378. Tauster, S.J., Fung, S.C., Baker, R.T.K., and Horsley, J.A., Strong-Interactions in Supported-Metal Catalysts. Science **211**(4487), 1981, 1121-1125.

379. Shinjoh, H., Hatanaka, M., Nagai, Y., Tanabe, T., et al., Suppression of Noble Metal Sintering Based on the Support Anchoring Effect and its Application in Automotive Three-Way Catalysis. Top. Catal. **52**(13-20), 2009, 1967-1971.
380. Jones, J., Xiong, H.F., Delariva, A.T., Peterson, E.J., et al., Thermally stable single-atom platinum-on-ceria catalysts via atom trapping. Science **353**(6295), 2016, 150-154.
381. Meher, S.K. and Rao, G.R., Polymer-Assisted Hydrothermal Synthesis of Highly Reducible Shuttle-Shaped CeO2: Microstructural Effect on Promoting Pt/C for Methanol Electrooxidation. Acs Catal **2**(12), 2012, 2795-2809.
382. Ou, D.R., Mori, T., Fugane, K., Togasaki, H., et al., Stability of Ceria Supports in Pt-CeOx/C Catalysts. J. Phys. Chem. C **115**(39), 2011, 19239-19245.
383. Brandt, B., Schalow, T., Laurin, M., Schauermann, S., et al., Oxidation, reduction, and reactivity of supported Pd nanoparticles: Mechanism and microkinetics. J. Phys. Chem. C **111**(2), 2007, 938-949.
384. Baumer, M., Libuda, J., Neyman, K.M., Rosch, N., et al., Adsorption and reaction of methanol on supported palladium catalysts: microscopic-level studies from ultrahigh vacuum to ambient pressure conditions. Phys. Chem. Chem. Phys. **9**(27), 2007, 3541-3558.
385. Schalow, T., Brandt, B., Starr, D.E., Laurin, M., et al., Size-dependent oxidation mechanism of supported Pd nanoparticles. Angew Chem Int Edit **45**(22), 2006, 3693-3697.
386. He, Y., Liu, J.C., Luo, L.L., Wang, Y.G., et al., Size-dependent dynamic structures of supported gold nanoparticles in CO oxidation reaction condition. Proc. Natl. Acad. Sci. U. S. A. **115**(30), 2018, 7700-7705.
387. Mullins, D.R., Overbury, S.H., and Huntley, D.R., Electron spectroscopy of single crystal and polycrystalline cerium oxide surfaces. Surf. Sci. **409**(2), 1998, 307-319.
388. Fabris, S., de Gironcoli, S., Baroni, S., Vicario, G., and Balducci, G., Taming multiple valency with density functionals: A case study of defective ceria. Phys. Rev. B **71**(4), 2005.
389. Boubnov, A., Dahl, S., Johnson, E., Molina, A.P., et al., Structure-activity relationships of Pt/Al2O3 catalysts for CO and NO oxidation at diesel exhaust conditions. Appl Catal B-Environ **126**, 2012, 315-325.
390. Bethune, D.S., Kiang, C.H., Devries, M.S., Gorman, G., et al., Cobalt-Catalyzed Growth of Carbon Nanotubes with Single-Atomic-Layerwalls. Nature **363**(6430), 1993, 605-607.
391. Wildoer, J.W.G., Venema, L.C., Rinzler, A.G., Smalley, R.E., and Dekker, C., Electronic structure of atomically resolved carbon nanotubes. Nature **391**(6662), 1998, 59-62.
392. Odom, T.W., Huang, J.L., Kim, P., and Lieber, C.M., Atomic structure and electronic properties of single-walled carbon nanotubes. Nature **391**(6662), 1998, 62-64.
393. Mcbride, J.R., Graham, G.W., Peters, C.R., and Weber, W.H., Growth and Characterization of Reactively Sputtered Thin-Film Platinum Oxides. J. Appl. Phys. **69**(3), 1991, 1596-1604.
394. Bonzel, H.P. and Ku, R., Mechanisms of the catalytic carbon monoxide oxidation on Pt(110). Surf. Sci. **33**(1), 1972, 91-106.
395. Ertl, G., Oscillatory Catalytic Reactions at Single-Crystal Surfaces, in Advances in Catalysis, H.P. D.D. Eley and B.W. Paul, Editors. 1990, Academic Press. p. 213-277.
396. Meusel, I., Hoffmann, J., Hartmann, J., Libuda, J., and Freund, H.J., Size dependent reaction kinetics on supported model catalysts: A molecular beam/IRAS study of the CO oxidation on alumina-supported Pd particles. J. Phys. Chem. B **105**(17), 2001, 3567-3576.
397. Imbihl, R. and Ertl, G., Oscillatory Kinetics in Heterogeneous Catalysis. Chem. Rev. (Washington, DC, U. S.) **95**(3), 1995, 697-733.
398. Zhdanov, V.P. and Kasemo, B., Kinetic Phase-Transitions in Simple Reactions on Solid-Surfaces. Surf. Sci. Rep. **20**(3), 1994, 111-189.
399. Wehner, S., Baumann, F., and Kuppers, J., Kinetic hysteresis in the CO oxidation reaction on Ir(111) surfaces. Chem. Phys. Lett. **370**(1-2), 2003, 126-131.
400. Zhdanov, V.P. and Kasemo, B., Bistability in catalytic reactions on the nm scale. Surf. Sci. **496**(3), 2002, 251-263.
401. Imbihl, R., Cox, M.P., and Ertl, G., Kinetic Oscillations in the Catalytic Co Oxidation on Pt(100) - Theory. J. Chem. Phys. **83**(4), 1985, 1578-1587.

402. Dagonnier, R. and Nuyts, J., Oscillating CO Oxidation on a Pt Surface. J. Chem. Phys. **65**(6), 1976, 2061-2065.
403. Fechner, G.T., Time series in the electrochemical oscillatory regime. Schweigg. J. **53**, 1828, 61-76.
404. Bray, W.C., A periodic reaction in homogeneous solution and its relation to catalysis. J. Am. Chem. Soc. **43**(6), 1921, 1262-1267.
405. Belousov, B.P., in Autowave Processes in Diffusion–Reaction Systems. 1951, Gorkii State University: Gorkii.
406. Zhabotinskii, A.M., Periodic Oxidizing Reactions in Liquid Phase. Dokl Akad Nauk Sssr+ **157**(2), 1964, 392-&.
407. Zaikin, A.N. and Zhabotinsky, A.M., Concentration Wave Propagation in 2-Dimensional Liquid-Phase Self-Oscillating System. Nature **225**(5232), 1970, 535-+.
408. Zhabotinsky, A.M. and Zaikin, A.N., Autowave Processes in a Distributed Chemical System. J. Theor. Biol. **40**(1), 1973, 45-+.
409. Beusch, H., Wicke, E., and Fieguth, P., Thermally and kinetically produced instabilities in reaction behavior of individual catalyst grains. Chem. Ing. Tech. **44**(7), 1972, 445-&.
410. Gorodetskii, V., Lauterbach, J., Rotermund, H.H., Block, J.H., and Ertl, G., Coupling between Adjacent Crystal Planes in Heterogeneous Catalysis by Propagating Reaction-Diffusion Waves. Nature **370**(6487), 1994, 276-279.
411. Rotermund, H.H., Real time imaging of catalytic reactions on surfaces: Past, present and future. Surf. Sci. **603**(10-12), 2009, 1662-1670.
412. Imbihl, R., Nonlinear dynamics on catalytic surfaces: The contribution of surface science. Surf. Sci. **603**(10-12), 2009, 1671-1679.
413. Luss, D. and Sheintuch, M., Spatiotemporal patterns in catalytic systems. Catal. Today **105**(2), 2005, 254-274.
414. Prigogin, I., Lefever, R., Goldbete, A., and Herschko, M., Symmetry Breaking Instabilities in Biological Systems. Nature **223**(5209), 1969, 913-&.
415. Murray, J.D., Mathematical Biology. 1990, Berlin: Springer.
416. Sulis, W. and Trofimova, I., eds. Nonlinear Dynamics in the Life and Social Sciences. NATO Science Series: Life Sciences. Vol. 320. 2001, IOS Press.
417. Nicolis, G. and Prigogine, I., Self-Organization in Nonequilibrium Systems. 1977, New York: Wiley.
418. Imbihl, R., Nonlinear dynamics on catalytic surfaces. Catal. Today **105**(2), 2005, 206-222.
419. Winfree, A., When Time Breaks Down. 1987, Princeton: Princeton University Press.
420. Jakubith, S., Rotermund, H.H., Engel, W., Vonoertzen, A., and Ertl, G., Spatiotemporal Concentration Patterns in a Surface-Reaction - Propagating and Standing Waves, Rotating Spirals, and Turbulence. Phys. Rev. Lett. **65**(24), 1990, 3013-3016.
421. Rotermund, H.H., Engel, W., Kordesch, M., and Ertl, G., Imaging of Spatiotemporal Pattern Evolution during Carbon-Monoxide Oxidation on Platinum. Nature **343**(6256), 1990, 355-357.
422. Zhdanov, V.P. and Kasemo, B., Fluctuations in kinetic oscillations on nm-sized catalyst particles. Surf. Sci. **588**(1-3), 2005, L220-L226.
423. Savva, P.G. and Costa, C.N., Hydrogen Lean-DeNO(x) as an Alternative to the Ammonia and Hydrocarbon Selective Catalytic Reduction (SCR). Catal Rev **53**(2), 2011, 91-151.
424. Bosch, H. and Janssen, F., Formation and control of nitrogen oxides. Catal. Today **2**(4), 1988, 369-379.
425. Burch, R. and Millington, P.J., Selective Reduction of Nitrogen-Oxides by Hydrocarbons under Lean-Burn Conditions Using Supported Platinum-Group Metal-Catalysts. Catal. Today **26**(2), 1995, 185-206.
426. Mrad, R., Aissat, A., Cousin, R., Courcot, D., and Siffert, S., Catalysts for NOx selective catalytic reduction by hydrocarbons (HC-SCR). Applied Catalysis A: General **504**, 2015, 542-548.
427. Hamada, H. and Haneda, M., A review of selective catalytic reduction of nitrogen oxides with hydrogen and carbon monoxide. Appl Catal a-Gen **421**, 2012, 1-13.

428. Zhdanov, V.P. and Kasemo, B., Mechanism and kinetics of the NO-CO reaction on Rh. Surf. Sci. Rep. **29**(2), 1997, 35-90.
429. Salasc, S., Skoglundh, M., and Fridell, E., A comparison between Pt and Pd in NOx storage catalysts. Appl Catal B-Environ **36**(2), 2002, 145-160.
430. Sharpe, R.G. and Bowker, M., The adsorption and decomposition of NO on Pd(110). Surf. Sci. **360**(1-3), 1996, 21-30.
431. Hirsimaki, M. and Valden, M., Adsorption and thermal behavior of CO and NO on Pd{110} and Pd{320}. J. Chem. Phys. **114**(5), 2001, 2345-2354.
432. Hansen, K.H., Sljivancanin, Z., Laegsgaard, E., Besenbacher, F., and Stensgaard, I., Adsorption of O-2 and NO on Pd nanocrystals supported on Al2O3/NiAl(110): overlayer and edge structures. Surf. Sci. **505**(1-3), 2002, 25-38.
433. Rainer, D.R., Vesecky, S.M., Koranne, M., Oh, W.S., and Goodman, D.W., The CO+NO reaction over Pd: A combined study using single-crystal, planar-model-supported, and high-surface-area Pd/Al2O3 catalysts. J. Catal. **167**(1), 1997, 234-241.
434. Henderson, M.A., The interaction of water with solid surfaces: fundamental aspects revisited. Surf. Sci. Rep. **46**(1-8), 2002, 5-308.
435. Thiel, P.A. and Madey, T.E., The Interaction of Water with Solid-Surfaces - Fundamental-Aspects. Surf. Sci. Rep. **7**(6-8), 1987, 211-385.
436. Larminie, J. and Dicks, A., Fuel Cell Systems Explained. 2003: J. Wiley.
437. Andersson, K., Gomez, A., Glover, C., Nordlund, D., et al., Molecularly intact and dissociative adsorption of water on clean Cu(110): A comparison with the water/Ru(001) system. Surf. Sci. **585**(3), 2005, L183-L189.
438. Gao, Y.X., Li, R.T., Chen, S.L., Luo, L.F., et al., Morphology-dependent interplay of reduction behaviors, oxygen vacancies and hydroxyl reactivity of CeO2 nanocrystals. Phys. Chem. Chem. Phys. **17**(47), 2015, 31862-31871.
439. Mullins, D.R., Albrecht, P.M., Chen, T.L., Calaza, F.C., et al., Water Dissociation on CeO2(100) and CeO2(111) Thin Films. J. Phys. Chem. C **116**(36), 2012, 19419-19428.
440. Schiros, T., Andersson, K.J., Pettersson, L.G.M., Nilsson, A., and Ogasawara, H., Chemical bonding of water to metal surfaces studied with core-level spectroscopies. J. Electron Spectrosc. Relat. Phenom. **177**(2-3), 2010, 85-98.
441. Schiros, T., Ogasawara, H., Naslund, L.A., Andersson, K.J., et al., Cooperativity in Surface Bonding and Hydrogen Bonding of Water and Hydroxyl at Metal Surfaces. J. Phys. Chem. C **114**(22), 2010, 10240-10248.
442. Kundakovic, L., Mullins, D.R., and Overbury, S.H., Adsorption and reaction of H2O and CO on oxidized and reduced Rh/CeOx(111) surfaces. Surf. Sci. **457**(1-2), 2000, 51-62.
443. Senanayake, S.D., Stacchiola, D., Evans, J., Estrella, M., et al., Probing the reaction intermediates for the water-gas shift over inverse CeOx/Au(111) catalysts. J. Catal. **271**(2), 2010, 392-400.
444. Duchon, T., Dvorak, F., Aulicka, M., Stetsovych, V., et al., Ordered Phases of Reduced Ceria As Epitaxial Films on Cu(111). J. Phys. Chem. C **118**(1), 2014, 357-365.
445. Sutara, F., Cabala, M., Sedlacek, L., Skala, T., et al., Epitaxial growth of continuous CeO(2) (111) ultra-thin films on Cu(111). Thin Solid Films **516**(18), 2008, 6120-6124.
446. Hansen, H.A. and Wolverton, C., Kinetics and Thermodynamics of H2O Dissociation on Reduced CeO2(111). J. Phys. Chem. C **118**(47), 2014, 27402-27414.
447. Chueh, W.C., McDaniel, A.H., Grass, M.E., Hao, Y., et al., Highly Enhanced Concentration and Stability of Reactive Ce3+ on Doped CeO2 Surface Revealed In Operando. Chem. Mater. **24**(10), 2012, 1876-1882.
448. Abanades, S. and Flamant, G., Thermochemical hydrogen production from a two-step solar-driven water-splitting cycle based on cerium oxides. Sol Energy **80**(12), 2006, 1611-1623.
449. Chueh, W.C., Falter, C., Abbott, M., Scipio, D., et al., High-Flux Solar-Driven Thermochemical Dissociation of CO2 and H2O Using Nonstoichiometric Ceria. Science **330**(6012), 2010, 1797-1801.

450. Boaro, M., de Leitenburg, C., Dolcetti, G., and Trovarelli, A., The dynamics of oxygen storage in ceria-zirconia model catalysts measured by CO oxidation under stationary and cycling feedstream compositions. J. Catal. **193**(2), 2000, 338-347.
451. Zhou, G., Barrio, L., Agnoli, S., Senanayake, S.D., et al., High Activity of Ce1-xNixO2-y for H-2 Production through Ethanol Steam Reforming: Tuning Catalytic Performance through Metal-Oxide Interactions. Angew Chem Int Edit **49**(50), 2010, 9680-9684.
452. Sun, L.X., Marrocchelli, D., and Yildiz, B., Edge dislocation slows down oxide ion diffusion in doped CeO2 by segregation of charged defects. Nat Commun **6**, 2015.
453. Ackermann, S., Sauvin, L., Castiglioni, R., Rupp, J.L.M., et al., Kinetics of CO2 Reduction over Nonstoichiometric Ceria. J. Phys. Chem. C **119**(29), 2015, 16452-16461.
454. Scheffe, J.R., Jacot, R., Patzke, G.R., and Steinfeld, A., Synthesis, Characterization, and Thermochemical Redox Performance of Hf4+, Zr4+, and Sc3+ Doped Ceria for Splitting CO2. J. Phys. Chem. C **117**(46), 2013, 24104-24114.
455. Szabova, L., Stetsovych, O., Dvorak, F., Camellone, M.F., et al., Distinct Physicochemical Properties of the First Ceria Monolayer on Cu(111). J. Phys. Chem. C **116**(11), 2012, 6677-6684.
456. Dunn, S., Hydrogen futures: toward a sustainable energy system. Int. J. Hydrogen Energy **27**(3), 2002, 235-264.
457. Goldemberg, J., Ethanol for a sustainable energy future. Science **315**(5813), 2007, 808-810.
458. Hemminger, J.C., New Science for a Secure and Sustainable Energy Future. 2008, U.S. Department of Energy.
459. Rostrup-Nielsen, J.R. and Nielsen, R., Fuels and energy for the future: The role of catalysis. Catal Rev **46**(3-4), 2004, 247-270.
460. Momirlan, M. and Veziroglu, T.N., The properties of hydrogen as fuel tomorrow in sustainable energy system for a cleaner planet. Int. J. Hydrogen Energy **30**(7), 2005, 795-802.
461. Muradov, N.Z. and Veziroglu, T.N., "Green" path from fossil-based to hydrogen economy: An overview of carbon-neutral technologies. Int. J. Hydrogen Energy **33**(23), 2008, 6804-6839.
462. Momirlan, M. and Veziroglu, T.N., Current status of hydrogen energy. Renew Sust Energ Rev **6**(1-2), 2002, 141-179.
463. Kotay, S.M. and Das, D., Biohydrogen as a renewable energy resource - Prospects and potentials. Int. J. Hydrogen Energy **33**(1), 2008, 258-263.
464. Nikolaidis, P. and Poullikkas, A., A comparative overview of hydrogen production processes. Renew Sust Energ Rev **67**, 2017, 597-611.
465. Hefner, R.A.I., The Age of Energy Gases. 2007, Oklahoma City, Oklahoma, USA: The GHK Company.
466. Rostrup-Nielsen, J.R., Sehested, J., and Norskov, J.K., Hydrogen and synthesis gas by steam- and CO2 reforming. Adv. Catal. **47**, 2002, 65-139.
467. Gratzel, M., Photoelectrochemical cells. Nature **414**(6861), 2001, 338-344.
468. Armor, J.N., The multiple roles for catalysis in the production of H-2. Appl Catal a-Gen **176**(2), 1999, 159-176.
469. Service, R.F., Profile: Daniel Nocera - Hydrogen economy? Let sunlight do the work. Science **315**(5813), 2007, 789-789.
470. Ngoh, S.K. and Njomo, D., An overview of hydrogen gas production from solar energy. Renew Sust Energ Rev **16**(9), 2012, 6782-6792.
471. Li, Y.D., Li, D.X., and Wang, G.W., Methane decomposition to COx-free hydrogen and nano-carbon material on group 8-10 base metal catalysts: A review. Catal. Today **162**(1), 2011, 1-48.
472. Hou, T.F., Zhang, S.Y., Chen, Y.D., Wang, D.Z., and Cal, W.J., Hydrogen production from ethanol reforming: Catalysts and reaction mechanism. Renew Sust Energ Rev **44**, 2015, 132-148.
473. Mattos, L.V., Jacobs, G., Davis, B.H., and Noronha, F.B., Production of Hydrogen from Ethanol: Review of Reaction Mechanism and Catalyst Deactivation. Chem. Rev. (Washington, DC, U. S.) **112**(7), 2012, 4094-4123.
474. Roudesly, F., Oble, J., and Poli, G., Metal-catalyzed C-H activation/functionalization: The fundamentals. Journal of Molecular Catalysis A-Chemical **426**, 2017, 275-296.

475. Labinger, J.A. and Bercaw, J.E., Understanding and exploiting C-H bond activation. Nature **417**(6888), 2002, 507-514.
476. Ma, Z. and Zaera, F., Organic chemistry on solid surfaces. Surf. Sci. Rep. **61**(5), 2006, 229-281.
477. Rostrup-Nielsen, J.R., Conversion of hydrocarbons and alcohols for fuel cells. Phys. Chem. Chem. Phys. **3**(3), 2001, 283-288.
478. Croy, J.R., Mostafa, S., Liu, J., Sohn, Y.H., et al., Support dependence of MeOH decomposition over size-selected Pt nanoparticles. Catal. Lett. **119**(3-4), 2007, 209-216.
479. Wang, H.L., An, K., Sapi, A., Liu, F.D., and Somorjai, G.A., Effects of Nanoparticle Size and Metal/Support Interactions in Pt-Catalyzed Methanol Oxidation Reactions in Gas and Liquid Phases. Catal. Lett. **144**(11), 2014, 1930-1938.
480. Cordeiro, G.L., de Camargo, E.F., Santos, M.C.L., Pereira, C.V., et al., Improved Pt/CeO2 Electrocatalysts for Ethanol Electro-oxidation. Int. J. Electrochem. Sci. **13**(7), 2018, 6388-6401.
481. Xu, C.W., Zeng, R., Shen, P.K., and Wei, Z.D., Synergistic effect of CeO2 modified Pt/C catalysts on the alcohols oxidation. Electrochim. Acta **51**(6), 2005, 1031-1035.
482. Ou, D.R., Mori, T., Togasaki, H., Takahashi, M., et al., Microstructural and Metal-Support Interactions of the Pt-CeO2/C Catalysts for Direct Methanol Fuel Cell Application. Langmuir **27**(7), 2011, 3859-3866.
483. Matolin, V., Libra, J., Skoda, M., Tsud, N., et al., Methanol adsorption on a CeO2(111)/Cu(111) thin film model catalyst. Surf. Sci. **603**(8), 2009, 1087-1092.
484. Albrecht, P.M. and Mullins, D.R., Adsorption and Reaction of Methanol over CeOx(100) Thin Films. Langmuir **29**(14), 2013, 4559-4567.
485. Mullins, D.R., Robbins, M.D., and Zhou, J., Adsorption and reaction of methanol on thin-film cerium oxide. Surf. Sci. **600**(7), 2006, 1547-1558.
486. Siokou, A. and Nix, R.M., Interaction of methanol with well-defined ceria surfaces: Reflection/absorption infrared spectroscopy, X-ray photoelectron spectroscopy, and temperature-programmed desorption study. J. Phys. Chem. B **103**(33), 1999, 6984-6997.
487. Diekhoner, L., Butler, D.A., Baurichter, A., and Luntz, A.C., Parallel pathways in methanol decomposition on Pt(111). Surf. Sci. **409**(2), 1998, 384-391.
488. Gibson, K.D. and Dubois, L.H., Step Effects in the Thermal-Decomposition of Methanol on Pt(111). Surf. Sci. **233**(1-2), 1990, 59-64.
489. Lykhach, Y., Staudt, T., Lorenz, M.P.A., Streber, R., et al., Microscopic Insights into Methane Activation and Related Processes on Pt/Ceria Model Catalysts. ChemPhysChem **11**(7), 2010, 1496-1504.
490. Campos, C.L., Roldan, C., Aponte, M., Ishikawa, Y., and Cabrera, C.R., Preparation and methanol oxidation catalysis of Pt-CeO2 electrode. J. Electroanal. Chem. **581**(2), 2005, 206-215.
491. Hameed, R.M.A., Amin, R.S., El-Khatib, K.M., and Fetohi, A.E., Preparation and characterization of Pt-CeO2/C and Pt-TiO2/C electrocatalysts with improved electrocatalytic activity for methanol oxidation. Appl. Surf. Sci. **367**, 2016, 382-390.
492. Mori, T., Ou, D.R., Zou, J., and Drennan, J., Present status and future prospect of design of Pt-cerium oxide electrodes for fuel cell applications. Prog Nat Sci-Mater **22**(6), 2012, 561-571.
493. Vaclavu, M., Matolinova, I., Myslivecek, J., Fiala, R., and Matolin, V., Anode Material for Hydrogen Polymer Membrane Fuel Cell: Pt-CeO2 RF-Sputtered Thin Films. J. Electrochem. Soc. **156**(8), 2009, B938-B942.
494. Surnev, S., Fortunelli, A., and Netzer, F.P., Structure-Property Relationship and Chemical Aspects of Oxide-Metal Hybrid Nanostructures. Chem. Rev. (Washington, DC, U. S.) **113**(6), 2013, 4314-4372.
495. Senanayake, S.D., Ramirez, P.J., Waluyo, I., Kundu, S., et al., Hydrogenation of CO2 to Methanol on CeOx/Cu(111) and ZnO/Cu(111) Catalysts: Role of the Metal-Oxide Interface and Importance of Ce3+ Sites. J. Phys. Chem. C **120**(3), 2016, 1778-1784.
496. Netzer, F.P., "Small and beautiful" - The novel structures and phases of nano-oxides. Surf. Sci. **604**(5-6), 2010, 485-489.

497. Luches, P., Pagliuca, F., Valeri, S., and Boscherini, F., Structure of Ultrathin CeO2 Films on Pt(111) by Polarization-Dependent X-ray Absorption Fine Structure. J. Phys. Chem. C **117**(2), 2013, 1030-1036.
498. Stetsovych, O., Dvorak, F., Szabova, L., Fabris, S., et al., Nanometer-Range Strain Distribution in Layered Incommensurate Systems. Phys. Rev. Lett. **109**(26), 2012, Art. # 266102.
499. Rodriguez, J.A., Liu, P., Graciani, J., Senanayake, S.D., et al., Inverse Oxide/Metal Catalysts in Fundamental Studies and Practical Applications: A Perspective of Recent Developments. J Phys Chem Lett **7**(13), 2016, 2627-2639.
500. Graciani, J., Vidal, A.B., Rodriguez, J.A., and Sanz, J.F., Unraveling the Nature of the Oxide-Metal Interaction in Ceria-Based Noble Metal Inverse Catalysts. J. Phys. Chem. C **118**(46), 2014, 26931-26938.
501. Rodriguez, J.A., Graciani, J., Evans, J., Park, J.B., et al., Water-Gas Shift Reaction on a Highly Active Inverse CeOx/Cu(111) Catalyst: Unique Role of Ceria Nanoparticles. Angew Chem Int Edit **48**(43), 2009, 8047-8050.
502. Senanayake, S.D., Stacchiola, D., and Rodriguez, J.A., Unique Properties of Ceria Nanoparticles Supported on Metals: Novel Inverse Ceria/Copper Catalysts for CO Oxidation and the Water-Gas Shift Reaction. Acc. Chem. Res. **46**(8), 2013, 1702-1711.
503. Yang, F., Graciani, J., Evans, J., Liu, P., et al., CO Oxidation on Inverse CeOx/Cu(111) Catalysts: High Catalytic Activity and Ceria-Promoted Dissociation of O-2. J. Am. Chem. Soc. **133**(10), 2011, 3444-3451.
504. Yang, B.X., Luo, Y., and Ye, L.P., CO oxidation on inverse Ce6O12/Cu(111) catalyst: role of copper-ceria interactions. J Mol Model **24**(1), 2018, Art. # 20.
505. Graciani, J., Mudiyanselage, K., Xu, F., Baber, A.E., et al., Highly active copper-ceria and copper-ceria-titania catalysts for methanol synthesis from CO2. Science **345**(6196), 2014, 546-550.
506. Matolin, V., Sedlacek, L., Matolinova, I., Sutara, F., et al., Photoemission spectroscopy study of Cu/CeO2 systems: Cu/CeO2 nanosized catalyst and CeO2(111)/Cu(111) inverse model catalyst. J. Phys. Chem. C **112**(10), 2008, 3751-3758.
507. Rodriguez, J.A., Ma, S., Liu, P., Hrbek, J., et al., Activity of CeOx and TiOx nanoparticles grown on Au(111) in the water-gas shift reaction. Science **318**(5857), 2007, 1757-1760.
508. Zhao, X.E., Ma, S.G., Hrbek, J., and Rodriguez, J.A., Reaction of water with Ce-Au(111) and CeOx/Au(111) surfaces: Photoemission and STM studies. Surf. Sci. **601**(12), 2007, 2445-2452.
509. Ma, T., Surnev, S., and Netzer, F.P., Growth of Ceria Nano-Islands on a Stepped Au(788) Surface. Materials **8**(8), 2015, 5205-5215.
510. Suchorski, Y., Wrobel, R., Becker, S., and Weiss, H., CO Oxidation on a CeOx/Pt(111) Inverse Model Catalyst Surface: Catalytic Promotion and Tuning of Kinetic Phase Diagrams. J. Phys. Chem. C **112**(50), 2008, 20012-20017.
511. Grinter, D.C., Ithnin, R., Pang, C.L., and Thornton, G., Defect Structure of Ultrathin Ceria Films on Pt(111): Atomic Views from Scanning Tunnelling Microscopy. J. Phys. Chem. C **114**(40), 2010, 17036-17041.
512. Hayek, K., Jenewein, B., Klotzer, B., and Reichl, W., Surface reactions on inverse model catalysts: CO adsorption and CO hydrogenation on vanadia- and ceria-modified surfaces of rhodium and palladium. Top. Catal. **14**(1-4), 2001, 25-33.
513. Eck, S., Castellarin-Cudia, C., Surnev, S., Prince, K.C., et al., Adsorption and reaction of CO on a ceria-Rh(111) "inverse model catalyst" surface. Surf. Sci. **536**(1-3), 2003, 166-176.
514. Kaemena, B., Senanayake, S.D., Meyer, A., Sadowski, J.T., et al., Growth and Morphology of Ceria on Ruthenium (0001). J. Phys. Chem. C **117**(1), 2013, 221-232.
515. Grinter, D.C., Yim, C.M., Pang, C.L., Santos, B., et al., Oxidation State Imaging of Ceria Island Growth on Re(0001). J. Phys. Chem. C **117**(32), 2013, 16509-16514.
516. Barrio, L., Estrella, M., Zhou, G., Wen, W., et al., Unraveling the Active Site in Copper-Ceria Systems for the Water-Gas Shift Reaction: In Situ Characterization of an Inverse Powder CeO2-x/CuO-Cu Catalyst. J. Phys. Chem. C **114**(8), 2010, 3580-3587.

517. Mudiyanselage, K., Senanayake, S.D., Feria, L., Kundu, S., et al., Importance of the Metal-Oxide Interface in Catalysis: In Situ Studies of the Water-Gas Shift Reaction by Ambient-Pressure X-ray Photoelectron Spectroscopy. Angew Chem Int Edit **52**(19), 2013, 5101-5105.
518. Rodriguez, J.A., Grinter, D.C., Liu, Z.Y., Palomino, R.M., and Senanayake, S.D., Ceria-based model catalysts: fundamental studies on the importance of the metal-ceria interface in CO oxidation, the water-gas shift, CO2 hydrogenation, and methane and alcohol reforming. Chem. Soc. Rev. **46**(7), 2017, 1824-1841.
519. Li, D., Li, X.Y., and Gong, J.L., Catalytic Reforming of Oxygenates: State of the Art and Future Prospects. Chem. Rev. (Washington, DC, U. S.) **116**(19), 2016, 11529-11653.
520. Guell, B.M., Babich, I., Nichols, K.P., Gardeniers, J.G.E., et al., Design of a stable steam reforming catalyst-A promising route to sustainable hydrogen from biomass oxygenates. Appl Catal B-Environ **90**(1-2), 2009, 38-44.
521. Columbia, M.R. and Thiel, P.A., The Interaction of Formic-Acid with Transition-Metal Surfaces, Studied in Ultrahigh-Vacuum. J. Electroanal. Chem. **369**(1-2), 1994, 1-14.
522. Hu, C.Q., Ting, S.W., Chan, K.Y., and Huang, W., Reaction pathways derived from DFT for understanding catalytic decomposition of formic acid into hydrogen on noble metals. Int. J. Hydrogen Energy **37**(21), 2012, 15956-15965.
523. Senanayake, S.D. and Mullins, D.R., Redox pathways for HCOOH decomposition over CeO2 surfaces. J. Phys. Chem. C **112**(26), 2008, 9744-9752.
524. Trillo, J.M., Criado, J.M., and Munuera, G., Catalytic Decomposition of Formic-Acid on Metal-Oxides. Cataly Rev **7**(1), 1972, 51-&.
525. Gercher, V.A. and Cox, D.F., Formic-Acid Decomposition on Sno2(110). Surf. Sci. **312**(1-2), 1994, 106-114.
526. Avery, N.R., Adsorption of Formic-Acid on Clean and Oxygen Covered Pt(111). Appl Surf Sc **11-2**(Jul), 1982, 774-783.
527. Bandara, A., Kubota, J., Wada, A., Domen, K., and Hirose, C., Adsorption and reactions of formic acid on (2x2)-NiO(111)Ni(111) surface .2. IRAS study under catalytic steady-state conditions. J. Phys. Chem. B **101**(3), 1997, 361-368.
528. Ai, M., Activities for the decomposition of formic acid and the acid-base properties of metal oxide catalysts. J. Catal. **50**(2), 1977, 291-300.
529. Mars, P., Scholten, J.J.F., and Zwietering, P., The Catalytic Decomposition of Formic Acid. Adv. Catal. **14**, 1963, 35-113.
530. Borowiak, L.A., Jamroz, M.H., and Larsson, R., Catalytic decomposition of formic acid on oxide catalysts - III. IOM model approach to bimolecular mechanism. Journal of Molecular Catalysis a-Chemical **152**(1-2), 2000, 121-132.
531. Borowiak, M.A., Jamroz, M.H., and Larsson, R., Catalytic decomposition of formic acid on oxide catalysts - an impulse-oscillation model approach to the unimolecular mechanism. Journal of Molecular Catalysis a-Chemical **139**(1), 1999, 97-104.
532. Mullen, C.A. and Boateng, A.A., Chemical composition of bio-oils produced by fast pyrolysis of two energy crops. Energy Fuels **22**(3), 2008, 2104-2109.
533. Singh, V., Joung, D., Zhai, L., Das, S., et al., Graphene based materials: Past, present and future. Prog Mater Sci **56**(8), 2011, 1178-1271.
534. Allen, M.J., Tung, V.C., and Kaner, R.B., Honeycomb Carbon: A Review of Graphene. Chem. Rev. (Washington, DC, U. S.) **110**(1), 2010, 132-145.
535. Geim, A.K., Graphene: Status and Prospects. Science **324**(5934), 2009, 1530-1534.
536. Tetlow, H., de Boer, J.P., Ford, I.J., Vvedensky, D.D., et al., Growth of Epitaxial Graphene: Theory and Experiment. Physics Reports-Review Section of Physics Letters **542**(3), 2014, 195-295.
537. Castro Neto, A.H., Guinea, F., Peres, N.M.R., Novoselov, K.S., and Geim, A.K., The electronic properties of graphene. Rev. Mod. Phys. **81**(1), 2009, 109-162.
538. Batzill, M., The Surface Science of Graphene: Metal Interfaces, CVD Synthesis, Nanoribbons, Chemical Modifications, and Defects. Surf. Sci. Rep. **67**(3-4), 2012, 83-115.

539. Lang, B., LEED Study of Deposition of Carbon on Platinum Crystal-Surfaces. Surf. Sci. **53**(Dec), 1975, 317-329.
540. Hu, Z.P., Ogletree, D.F., Vanhove, M.A., and Somorjai, G.A., LEED Theory for Incommensurate Overlayers - Application to Graphite on Pt(111). Surf. Sci. **180**(2-3), 1987, 433-459.
541. Land, T.A., Michely, T., Behm, R.J., Hemminger, J.C., and Comsa, G., STM Investigation of Single Layer Graphite Structures Produced on Pt(111) by Hydrocarbon Decomposition. Surf. Sci. **264**(3), 1992, 261-270.
542. Tontegode, A.Y., Carbon on Transition-Metal Surfaces. Prog. Surf. Sci. **38**(3-4), 1991, 201-429.
543. Novoselov, K.S., Geim, A.K., Morozov, S.V., Jiang, D., et al., Electric Field Effect in Atomically Thin Carbon Films. Science **306**(5696), 2004, 666-669.
544. Geim, A.K. and Novoselov, K.S., The rise of graphene. Nat. Mater. **6**(3), 2007, 183-191.
545. Ohta, T., Bartelt, N.C., Nie, S., Thurmer, K., and Kellogg, G.L., Role of carbon surface diffusion on the growth of epitaxial graphene on SiC. Phys. Rev. B **81**(12), 2010.
546. Emtsev, K.V., Bostwick, A., Horn, K., Jobst, J., et al., Towards wafer-size graphene layers by atmospheric pressure graphitization of silicon carbide. Nat. Mater. **8**(3), 2009, 203-207.
547. Dikin, D.A., Stankovich, S., Zimney, E.J., Piner, R.D., et al., Preparation and characterization of graphene oxide paper. Nature **448**(7152), 2007, 457-460.
548. Gilje, S., Han, S., Wang, M., Wang, K.L., and Kaner, R.B., A chemical route to graphene for device applications. Nano Lett. **7**(11), 2007, 3394-3398.
549. Wintterlin, J. and Bocquet, M.L., Graphene on Metal Surfaces. Surf. Sci. **603**(10-12), 2009, 1841-1852.
550. Hamilton, J.C. and Blakely, J.M., Carbon Segregation to Single-Crystal Surfaces of Pt, Pd and Co. Surf. Sci. **91**(1), 1980, 199-217.
551. Seah, C.-M., Chai, S.-P., and Mohamed, A.R., Mechanisms of Graphene Growth by Chemical Vapour Deposition on Transition Metals. Carbon **70**, 2014, 1-21.
552. Li, X.S., Cai, W.W., An, J.H., Kim, S., et al., Large-Area Synthesis of High-Quality and Uniform Graphene Films on Copper Foils. Science **324**(5932), 2009, 1312-1314.
553. Argyle, M.D. and Bartholomew, C.H., Heterogeneous Catalyst Deactivation and Regeneration: A Review. Catalysts **5**(1), 2015, 145-269.
554. Morgan, A.E. and Somorjai, G.A., Low Energy Electron Diffraction Studies of Gas Adsorption on Platinum (100) Single Crystal Surface. Surf. Sci. **12**(3), 1968, 405-425.
555. May, J.W., Platinum Surface LEED Rings. Surf. Sci. **17**(1), 1969, 267-270.
556. Gamo, Y., Nagashima, A., Wakabayashi, M., Terai, M., and Oshima, C., Atomic structure of monolayer graphite formed on Ni(111). Surf. Sci. **374**(1-3), 1997, 61-64.
557. Aizawa, T., Souda, R., Otani, S., Ishizawa, Y., and Oshima, C., Bond Softening in Monolayer Graphite Formed on Transition-Metal Carbide Surfaces. Phys. Rev. B **42**(18), 1990, 11469-11478.
558. Shelton, J.C., Patil, H.R., and Blakely, J.M., Equilibrium Segregation of Carbon to a Nickel (111) Surface - Surface Phase-Transition. Surf. Sci. **43**(2), 1974, 493-520.
559. Oshima, C. and Nagashima, A., Ultra-thin epitaxial films of graphite and hexagonal boron nitride on solid surfaces. J Phys-Condens Mat **9**(1), 1997, 1-20.
560. Land, T.A., Michely, T., Behm, R.J., Hemminger, J.C., and Comsa, G., STM Investigation of the Adsorption and Temperature-Dependent Reactions of Ethylene on Pt(111). Appl. Phys. A Mater. Sci. Process. **53**(5), 1991, 414-417.
561. Land, T.A., Michely, T., Behm, R.J., Hemminger, J.C., and Comsa, G., Direct Observation of Surface-Reactions by Scanning Tunneling Microscopy - Ethylene->Ethylidyne->Carbon Particles->Graphite on Pt(111). J. Chem. Phys. **97**(9), 1992, 6774-6783.
562. Iwasita, T. and Nart, F.C., In situ infrared spectroscopy at electrochemical interfaces. Prog. Surf. Sci. **55**(4), 1997, 271-340.
563. Bligaard, T., Norskov, J.K., Dahl, S., Matthiesen, J., et al., The Bronsted-Evans-Polanyi relation and the volcano curve in heterogeneous catalysis. J. Catal. **224**(1), 2004, 206-217.

564. Bukoski, A., Blumling, D., and Harrison, I., Microcanonical unimolecular rate theory at surfaces. I. Dissociative chemisorption of methane on Pt(111). J. Chem. Phys. **118**(2), 2003, 843-871.
565. Abbott, H.L., Bukoski, A., and Harrison, I., Microcanonical unimolecular rate theory at surfaces. II. Vibrational state resolved dissociative chemisorption of methane on Ni(100). J. Chem. Phys. **121**(8), 2004, 3792-3810.
566. Bukoski, A., Abbott, H.L., and Harrison, I., Microcanonical unimolecular rate theory at surfaces. III. Thermal dissociative chemisorption of methane on Pt(111) and detailed balance. J. Chem. Phys. **123**(9), 2005, Art. # 094707.
567. Tait, S.L., Dohnalek, Z., Campbell, C.T., and Kay, B.D., n-alkanes on Pt(111) and on C(0001)/Pt(111): Chain length dependence of kinetic desorption parameters. J. Chem. Phys. **125**(23), 2006.
568. Barteau, M.A., Linear Free-Energy Relationships for C1-Oxygenate Decomposition on Transition-Metal Surfaces. Catal. Lett. **8**(2-4), 1991, 175-184.
569. Klimes, J., Bowler, D.R., and Michaelides, A., Van der Waals density functionals applied to solids. Phys. Rev. B **83**(19), 2011.
570. Riley, K.E., Pitonak, M., Jurecka, P., and Hobza, P., Stabilization and Structure Calculations for Noncovalent Interactions in Extended Molecular Systems Based on Wave Function and Density Functional Theories. Chem. Rev. (Washington, DC, U. S.) **110**(9), 2010, 5023-5063.
571. Navin, J.K., Donald, S.B., and Harrison, I., Angle-Resolved Thermal Dissociative Sticking of Light Alkanes on Pt(111): Transitioning from Dynamical to Statistical Behavior. J. Phys. Chem. C **118**(38), 2014, 22003-22011.
572. Tromp, R.M. and Reuter, M.C., Imaging with a Low-Energy-Electron Microscope. Ultramicroscopy **50**(2), 1993, 171-178.
573. Tromp, R.M., Low-energy electron microscopy. IBM J. Res. Dev. **44**(4), 2000, 503-516.
574. Enachescu, M., Schleef, D., Ogletree, D.F., and Salmeron, M., Integration of point-contact microscopy and atomic-force microscopy: Application to characterization of graphite/Pt(111). Phys. Rev. B **60**(24), 1999, 16913-16919.
575. Ofner, H. and Zaera, F., Isothermal kinetic measurements for the hydrogenation of ethylene on Pt(111) under vacuum: Significance of weakly-bound species in the reaction mechanism. J. Phys. Chem. B **101**(3), 1997, 396-408.
576. Loginova, E., Bartelt, N.C., Feibelman, P.J., and McCarty, K.F., Evidence for Graphene Growth by C Cluster Attachment. New J. Chem. **10**, 2008, Art. # 093026.
577. Zangwill, A. and Vvedensky, D.D., Novel Growth Mechanism of Epitaxial Graphene on Metals. Nano Lett. **11**(5), 2011, 2092-2095.
578. Wang, B., Konig, M., Bromley, C.J., Yoon, B., et al., Ethene to Graphene: Surface Catalyzed Chemical Pathways, Intermediates, and Assembly. J. Phys. Chem. C **121**(17), 2017, 9413-9423.
579. Handy, R.D. and Shaw, B.J., Toxic effects of nanoparticles and nanomaterials: Implications for public health, risk assessment and the public perception of nanotechnology. Health Risk Soc **9**(2), 2007, 125-144.
580. Singh, S. and Nalwa, H.S., Nanotechnology and health safety - Toxicity and risk assessments of nanostructured materials on human health. J. Nanosci. Nanotechnol. **7**(9), 2007, 3048-3070.
581. Rostrup-Nielsen, J.R., 50 years in catalysis. Lessons learned. Catal. Today **272**, 2016, 2-5.
582. Figueroba, A., Kovacs, G., Bruix, A., and Neyman, K.M., Towards stable single-atom catalysts: strong binding of atomically dispersed transition metals on the surface of nanostructured ceria. Catalysis Science & Technology **6**(18), 2016, 6806-6813.
583. Chen, Y.J., Ji, S.F., Chen, C., Peng, Q., et al., Single-Atom Catalysts: Synthetic Strategies and Electrochemical Applications. Joule **2**(7), 2018, 1242-1264.
584. Zaera, F., The surface chemistry of catalysis: new challenges ahead. Surf. Sci. **500**(1-3), 2002, 947-965.
585. Tao, F. and Salmeron, M., In Situ Studies of Chemistry and Structure of Materials in Reactive Environments. Science **331**(6014), 2011, 171-174.

586. Hunger, M. and Weitkamp, J., In situ IR, NMR, EPR, and UV/Vis spectroscopy: Tools for new insight into the mechanisms of heterogeneous catalysis. Angew Chem Int Edit **40**(16), 2001, 2954-2971.
587. Somorjai, G.A. and Rupprechter, G., Molecular studies of catalytic reactions on crystal surfaces at high pressures and high temperatures by infrared-visible sum frequency generation (SFG) surface vibrational spectroscopy. J. Phys. Chem. B **103**(10), 1999, 1623-1638.
588. Harvey, C.E. and Weckhuysen, B.M., Surface- and Tip-Enhanced Raman Spectroscopy as Operando Probes for Monitoring and Understanding Heterogeneous Catalysis. Catal. Lett. **145**(1), 2015, 40-57.
589. Rasmussen, P.B., Hendriksen, B.L.M., Zeijlemaker, H., Ficke, H.G., and Frenken, J.W.M., The "reactor STM": A scanning tunneling microscope for investigation of catalytic surfaces at semi-industrial reaction conditions. Rev. Sci. Instrum. **69**(11), 1998, 3879-3884.
590. Laegsgaard, E., Osterlund, L., Thostrup, P., Rasmussen, P.B., et al., A high-pressure scanning tunneling microscope. Rev. Sci. Instrum. **72**(9), 2001, 3537-3542.
591. Tao, F., Tang, D., Salmeron, M., and Somorjai, G.A., A new scanning tunneling microscope reactor used for high-pressure and high-temperature catalysis studies. Rev. Sci. Instrum. **79**(8), 2008.
592. Gewirth, A.A. and Niece, B.K., Electrochemical applications of in situ scanning probe microscopy. Chem. Rev. (Washington, DC, U. S.) **97**(4), 1997, 1129-1162.
593. Kouzeki, T., Tatezono, S., and Yanagi, H., Electrochromism of orientation-controlled naphthalocyanine thin films. J. Phys. Chem. **100**(51), 1996, 20097-20102.
594. van Rijn, R., Ackermann, M.D., Balmes, O., Dufrane, T., et al., Ultrahigh vacuum/high-pressure flow reactor for surface x-ray diffraction and grazing incidence small angle x-ray scattering studies close to conditions for industrial catalysis. Rev. Sci. Instrum. **81**(1), 2010.
595. Chenna, S. and Crozier, P.A., Operando Transmission Electron Microscopy: A Technique for Detection of Catalysis Using Electron Energy-Loss Spectroscopy in the Transmission Electron Microscope. Acs Catal **2**(11), 2012, 2395-2402.
596. de Smit, E., Swart, I., Creemer, J.F., Hoveling, G.H., et al., Nanoscale chemical imaging of a working catalyst by scanning transmission X-ray microscopy. Nature **456**(7219), 2008, 222-U39.
597. Zhao, S., Li, Y.Y., Stavitski, E., Tappero, R., et al., Operando Characterization of Catalysts through use of a Portable Microreactor. ChemCatChem **7**(22), 2015, 3683-3691.
598. Tandon, U.S., An Overview of Ion-Beam Lithography for Nanofabrication. Vacuum **43**(3), 1992, 241-251.
599. Watt, F., Bettiol, A.A., van Kan, J.A., Teo, E.J., and Breese, M.B.H., Ion Beam Lithography and Nanofabrication: A Review. Int. J. Nanosci. **4**(3), 2005, 269-286.
600. Chou, S.Y., Krauss, P.R., and Renstrom, P.J., Nanoimprint lithography. J Vac Sci Technol B **14**(6), 1996, 4129-4133.
601. Melngailis, J., Mondelli, A.A., Berry, I.L., and Mohondro, R., A review of ion projection lithography. J Vac Sci Technol B **16**(3), 1998, 927-957.
602. Schreiber, F., Structure and growth of self-assembling monolayers. Prog. Surf. Sci. **65**(5-8), 2000, 151-256.
603. Yang, J., Kim, K., Lee, Y., Kim, K., et al., Self-organized growth and self-assembly of nanostructures on 2D materials. FlatChem **5**, 2017, 50-68.
604. Smith, R.K., Lewis, P.A., and Weiss, P.S., Patterning self-assembled monolayers. Prog. Surf. Sci. **75**(1-2), 2004, 1-68.
605. Julkapli, N.M. and Bagheri, S., Graphene supported heterogeneous catalysts: An overview. Int. J. Hydrogen Energy **40**(2), 2015, 948-979.
606. Joo, S.H., Choi, S.J., Oh, I., Kwak, J., et al., Ordered nanoporous arrays of carbon supporting high dispersions of platinum nanoparticles. Nature **412**(6843), 2001, 169-172.
607. Wang, Y., Angelatos, A.S., and Caruso, F., Template synthesis of nanostructured materials via layer-by-layer assembly. Chem. Mater. **20**(3), 2008, 848-858.
608. Somorjai, G.A., Tao, F., and Park, J.Y., The nanoscience revolution: Merging of colloid science, catalysis and nanoelectronics. Top. Catal. **47**(1-2), 2008, 1-14.

609. Karim, W., Spreafico, C., Kleibert, A., Gobrecht, J., et al., Catalyst support effects on hydrogen spillover. Nature **541**(7635), 2017, 68-+.
610. Kang, Y.J., Ye, X.C., Chen, J., Qi, L., et al., Engineering Catalytic Contacts and Thermal Stability: Gold/Iron Oxide Binary Nanocrystal Superlattices for CO Oxidation. J. Am. Chem. Soc. **135**(4), 2013, 1499-1505.
611. Norskov, J.K., Bligaard, T., Rossmeisl, J., and Christensen, C.H., Towards the computational design of solid catalysts. Nature Chem. **1**(1), 2009, 37-46.
612. Besenbacher, F., Chorkendorff, I., Clausen, B.S., Hammer, B., et al., Design of a surface alloy catalyst for steam reforming. Science **279**(5358), 1998, 1913-1915.
613. Jacobsen, C.J.H., Dahl, S., Clausen, B.S., Bahn, S., et al., Catalyst design by interpolation in the periodic table: Bimetallic ammonia synthesis catalysts. J. Am. Chem. Soc. **123**(34), 2001, 8404-8405.
614. Toulhoat, H. and Raybaud, P., Kinetic interpretation of catalytic activity patterns based on theoretical chemical descriptors. J. Catal. **216**(1-2), 2003, 63-72.
615. Strasser, P., Fan, Q., Devenney, M., Weinberg, W.H., et al., High throughput experimental and theoretical predictive screening of materials - A comparative study of search strategies for new fuel cell anode catalysts. J. Phys. Chem. B **107**(40), 2003, 11013-11021.
616. Starrost, F. and Carter, E.A., Modeling the full monty: baring the nature of surfaces across time and space. Surf. Sci. **500**(1-3), 2002, 323-346.
617. Hammer, B. and Norskov, J.K., Theoretical surface science and catalysis - Calculations and concepts. Adv. Catal. **45**, 2000, 71-129.
618. Stoltze, P., Microkinetic simulation of catalytic reactions. Prog. Surf. Sci. **65**(3-4), 2000, 65-150.
619. Kang, H.C. and Weinberg, W.H., Modeling the Kinetics of Heterogeneous Catalysis. Chem. Rev. (Washington, DC, U. S.) **95**(3), 1995, 667-676.
620. Deutschmann, O., ed. Modeling and Simulation of Heterogeneous Catalytic Reactions: From the Molecular Process to the Technical System. 2011, Wiley-VCH.
621. van Santen, R.A. and Sautet, P., eds. Computational Methods in Catalysis and Materials Science. 2009, Wiley-VCH.
622. Czarniecki, J. and Jaroniec, M., Studies of adsorption kinetics by means of the stochastic numerical simulation. Surf. Sci. Rep. **3**(6), 1983, 301-353.
623. Gross, A., The virtual chemistry lab for reactions at surfaces: Is it possible? Will it be useful? Surf. Sci. **500**(1-3), 2002, 347-367.
624. Hafner, J., Ab-initio simulations of materials using VASP: Density-functional theory and beyond. J. Comput. Chem. **29**(13), 2008, 2044-2078.
625. Koch, W. and Holthausen, M.C., A Chemist's Guide to Density Functional Theory, Second Edition. 2001: Wiley-VCH.
626. Kohanoff, J. and Gidopoulos, N.I., Density Functional Theory: Basics, New Trends and Applications, in Handbook of Molecular Physics and Quantum Chemistry, S. Wilson, Editor. 2003, John Wiley & Sons, Ltd: Chichester.
627. Parr, R.G. and Yang, W., Density-Functional Theory of Atoms and Molecules. 1994: Oxford University Press. 352.
628. Balbuena, P. and Seminario, J., eds. Molecular Dynamics: From Classical to Quantum Methods, 1st Edition. Vol. 7. 1999, Elsevier Science. 945.

9 List of Abbreviations

2D..... Two-dimensional
3D..... Three-dimensional
AES..... Auger Electron Spectroscopy
AFM..... Atomic Force Microscopy
AR-QMS ..... Angle Resolved Quadrupole Mass Spectrometry
ATR-FTIR ..... Attenuated Total Reflectance Fourier-Transform Infrared Spectroscopy
BE ..... Binding Energy
CNT..... Carbon Nanotube
CVD..... Chemical Vapor Deposition
DFT ..... Density Functional Theory
DPF..... Diesel Particulate Filter
DRIFTS..... Diffuse Reflectance Infrared Fourier Transform Spectroscopy
EMSI..... Electronic Metal-Support Interaction
fcc..... Face Centered Cubic
FTIR ..... Fourier-Transform Infrared Spectroscopy
FWHM ..... Full Width at Half Maximum
GCA..... Glass Capillary Array
HC..... Hydrocarbon
hcp..... Hexagonal Close-Packed
HOPG ..... Highly Oriented Pyrolytic Graphite
IR..... Infrared
IRAS..... Infrared Absorption Spectroscopy (equivalent to RAIRS)
ISS ..... Ion Scattering Spectroscopy (equivalent to LEIS)
KE..... Kinetic Energy
LEED ..... Low-Energy Electron Diffraction
LEEM..... Low-Energy Electron Microscopy
LEIS..... Low-Energy Ion Scattering Spectroscopy (equivalent to ISS)
LH ..... Langmuir-Hinshelwood
LT..... Low Temperature
MB..... Molecular Beam
MBE..... Molecular Beam Epitaxy
MC..... Monte-Carlo
ML..... Monolayer
μLEED..... Low-Energy Electron Microdiffraction
MSI..... Metal-Support Interaction
MURT..... Microcanonical Unimolecular Rate Theory
MvK..... Mars–van Krevelen
MWCNT ..... Multiwall Carbon Nanotube
NAP-XPS..... Near-ambient Pressure X-ray Photoelectron Spectroscopy
NIL ..... Nanoimprint Lithography
NP ..... Nanoparticle, Nanometer-sized Particle
PES ..... Photoelectron Spectroscopy
PLD..... Pulsed Laser Deposition
PVD ..... Physical Vapor Deposition
QMS..... Quadrupole Mass Spectrometry, Quadrupole Mass Spectrometer
PEEM..... Photoemission Electron Microscopy
RAIRS..... Reflection Absorption Infrared Spectroscopy (equivalent to IRAS)
RPES..... Resonance Photoelectron Spectroscopy
RT..... Room Temperature
SAM ..... Self-assembled Monolayer
SCR ..... Selective Catalytic Reduction

SEM..... Scanning Electron Microscopy
SFG ..... Sum Frequency Generation Laser Spectroscopy
SIMS..... Secondary Ion Mass Spectrometry
SMSI..... Strong Metal-Support Interaction
SPA-LEED ..... Spot Profile Analysis Low Energy Electron Diffraction
SPEM..... Scanning Photoemission Microscopy (a.k.a. X-ray Spectromicroscopy)
SPM..... Scanning Probe Microscopy
SRPES..... Synchrotron Radiation Photoelectron Spectroscopy
STM..... Scanning Tunneling Microscopy
SXRD..... Surface X-ray Diffraction
TDS..... Thermal Desorption Spectroscopy (equivalent to TPD)
TMP ..... Turbomolecular Pump
TOF..... Turnover Frequency; Time-of-Flight Spectrometry
TPD..... Temperature-Programmed Desorption (equivalent to TDS)
TPG..... Temperature-Programmed Growth
TPR ..... Temperature-Programmed Reaction
TR-FTIR..... Time-resolved Fourier-Transform Infrared Spectroscopy
TR-RAIRS..... Time-resolved Reflection Absorption Infrared Spectroscopy
TWC..... Three-Way Catalyst
UHV..... Ultra-High Vacuum
WGS..... Water-Gas Shift
XANES..... X-ray Absorption Near Edge Structure
XAS..... X-ray Absorption Spectroscopy
XPEEM..... X-ray Photoemission Electron Microscopy
XPS..... X-ray Photoelectron Spectroscopy

Appendices – Selected presented publications

1. Matolin, V., Stara, I., Tsud, N., and Johanek, V., *XPS and TDS study of CO interaction with Pd-AlOx systems.* Prog. Surf. Sci. **67**(1-8), 2001, 167-181
   DOI: 10.1016/S0079-6816(01)00022-3.

2. Laurin, M., Johanek, V., Grant, A.W., Kasemo, B., Libuda, J., and Freund, H.J., *Local reaction rates and surface diffusion on nanolithographically prepared model catalysts: Experiments and simulations.* J. Chem. Phys. **122**(8), 2005, Art. # 084713
   DOI: 10.1063/1.184622.

3. Happel, M., Myslivecek, J., Johanek, V., Dvorak, F., Stetsovych, O., Lykhach, Y., Matolin, V., and Libuda, J., *Adsorption sites, metal-support interactions, and oxygen spillover identified by vibrational spectroscopy of adsorbed CO: A model study on Pt/ceria catalysts.* J. Catal. **289**, 2012, 118-126
   DOI: 10.1016/j.jcat.2012.01.022.

4. Lykhach, Y., Kozlov, S.M., Skala, T., Tovt, A., Stetsovych, V., Tsud, N., Dvorak, F., Johanek, V., Neitzel, A., Myslivecek, J., Fabris, S., Matolin, V., Neyman, K.M., and Libuda, J., *Counting electrons on supported nanoparticles.* Nat. Mater. **15**(3), 2016, 284-289
   DOI: 10.1038/NMAT4500.

5. Johánek, V., Václavů, M., Matolínová, I., Khalakhan, I., Haviar, S., and Matolín, V., *High low-temperature CO oxidation activity of platinum oxide prepared by magnetron sputtering.* Appl. Surf. Sci. **345**, 2015, 319-328
   DOI: 10.1016/j.apsusc.2015.03.108.

6. Johanek, V., Laurin, M., Grant, A.W., Kasemo, B., Henry, C.R., and Libuda, J., *Fluctuations and bistabilities on catalyst nanoparticles.* Science **304**(5677), 2004, 1639-1644
   DOI: 10.1126/science.1097513.

7. Johanek, V., Schauermann, S., Laurin, M., Gopinath, C.S., Libuda, J., and Freund, H.J., *On the role of different adsorption and reaction sites on supported nanoparticles during a catalytic reaction: NO decomposition on a Pd/alumina model catalyst.* J. Phys. Chem. B **108**(38), 2004, 14244-14254
   DOI: 10.1021/Jp031371f.

8. Matolin, V., Matolinova, I., Dvorak, F., Johanek, V., Myslivecek, J., Prince, K.C., Skala, T., Stetsovych, O., Tsud, N., Vaclavu, M., and Smid, B., *Water interaction with CeO2(111)/Cu(111) model catalyst surface.* Catal. Today **181**(1), 2012, 124-132
   DOI: 10.1016/j.cattod.2011.05.032.

9. Dvorak, F., Szabova, L., Johanek, V., Camellone, M.F., Stetsovych, V., Vorokhta, M., Tovt, A., Skala, T., Matolinova, I., Tateyama, Y., Myslivecek, J., Fabris, S., and Matolin, V., *Bulk Hydroxylation and Effective Water Splitting by Highly Reduced Cerium Oxide: The Role of O Vacancy Coordination.* Acs Catal **8**(5), 2018, 4354-4363
   DOI: 10.1021/acscatal.7b04409

10. Schauermann, S., Hoffmann, J., Johanek, V., Hartmann, J., and Libuda, J., *Adsorption, decomposition and oxidation of methanol on alumina supported palladium particles.* Phys. Chem. Chem. Phys. **4**(15), 2002, 3909-3918
    DOI: 10.1039/B203250n.

11. Matolin, V., Johanek, V., Skoda, M., Tsud, N., Prince, K.C., Skala, T., and Matolinova, I., *Methanol Adsorption and Decomposition on Pt/CeO2(111)/Cu(111) Thin Film Model Catalyst.* Langmuir **26**(16), 2010, 13333-13341
DOI: 10.1021/La101936b.

12. Ostroverkh, A., Johanek, V., Kus, P., Sediva, R., and Matolin, V., *Efficient Ceria-Platinum Inverse Catalyst for Partial Oxidation of Methanol.* Langmuir **32**(25), 2016, 6297-6309
DOI: 10.1021/acs.langmuir.6b01316.

13. Lykhach, Y., Happel, M., Johanek, V., Skala, T., Kollhoff, F., Tsud, N., Dvorak, F., Prince, K.C., Matolin, V., and Libuda, J., *Adsorption and Decomposition of Formic Acid on Model Ceria and Pt/Ceria Catalysts.* J. Phys. Chem. C **117**(24), 2013, 12483-12494
DOI: 10.1021/Jp311008v.

14. Neitzel, A., Lykhach, Y., Johanek, V., Tsud, N., Skala, T., Prince, K.C., Matolin, V., and Libuda, J., *Decomposition of Acetic Acid on Model Pt/CeO2 Catalysts: The Effect of Surface Crowding.* J. Phys. Chem. C **119**(24), 2015, 13721-13734
DOI: 10.1021/acs.jpcc.5b03079.

15. Johanek, V., De la Ree, A.B., and Hemminger, J.C., *Scanning Tunneling Microscopy Investigation of the Conversion of Ethylene to Carbon Clusters and Graphite on Pt(111).* J. Phys. Chem. C **113**(11), 2009, 4441-4444
DOI: 10.1021/Jp810298w.

16. Cushing, G.W., Navin, J.K., Donald, S.B., Valadez, L., Johanek, V., and Harrison, I., *C-H Bond Activation of Light Alkanes on Pt(111): Dissociative Sticking Coefficients, Evans-Polanyi Relation, and Gas-Surface Energy Transfer.* J. Phys. Chem. C **114**(40), 2010, 17222-17232
DOI: 10.1021/Jp105073g.
Cushing, G.W., Navin, J.K., Donald, S.B., Valadez, L., Johanek, V., and Harrison, I., *C-H Bond Activation of Light Alkanes on Pt(111): Dissociative Sticking Coefficients, Evans-Polanyi Relation, and Gas-Surface Energy Transfer (vol 114, pg 17222, 2010).* J. Phys. Chem. C **114**(51), 2010, 22790-22790
DOI: 10.1021/Jp1112119.

17. Cushing, G.W., Johánek, V., Navin, J.K., and Harrison, I., *Graphene Growth on Pt(111) by Ethylene Chemical Vapor Deposition at Surface Temperatures near 1000 K.* J. Phys. Chem. C **119**(9), 2015, 4759-4768
DOI: 10.1021/jp508177k.

18. Johánek, V., Nehasil, V., Skála, T., and Tsud, N., *Carbon Chain Length Dependence of Graphene Formation via Thermal Decomposition of Alkenes on Pt(111).* J. Phys. Chem. C, 2018, in press (published online)
DOI: 10.1021/acs.jpcc.8b07165.